

THESIS FOR THE DEGREE OF DOCTOR OF PHILOSOPHY

**Voyage Planning Framework for Autonomous Inland Waterway Vessels:  
Ship Performance Modelling and Operational Analysis**

CHENGQIAN ZHANG



Department of Mechanics and Maritime Sciences  
CHALMERS UNIVERSITY OF TECHNOLOGY  
Gothenburg, Sweden, 2026

**Voyage Planning Framework for Autonomous Inland Waterway Vessels:  
Ship Performance Modelling and Operational Analysis**

CHENGQIAN ZHANG

ISBN: 978-91-8103-339-7

© CHENGQIAN ZHANG, 2026

Doktorsavhandlingar vid Chalmers tekniska högskola

Series number: 5796

ISSN: 0346-718X

Chalmers University of Technology

Department of Mechanics and Maritime Sciences

Division of Marine Technology

SE-412 96, Gothenburg

Sweden

Telephone: + 46 (0)31-772 1000

[www.chalmers.se](http://www.chalmers.se)

Printed by Chalmers Reproservice

Gothenburg, Sweden, 2026

*To my beloved wife, Xue*



# **Voyage Planning Framework for Autonomous Inland Waterway Vessels: Ship Performance Modelling and Operational Analysis**

CHENGQIAN ZHANG

Chalmers University of Technology

Department of Mechanics and Maritime Sciences

Division of Marine Technology

## **Abstract**

Inland waterway transport offers substantial potential to mitigate greenhouse gas emissions and congestion from road freight transport. The development of advanced inland vessels equipped with clean energy systems and a high degree of automation represents a promising direction for future transport networks. Nevertheless, inland waterways are often restricted by shallow water and limited manoeuvring space. Hence, the deployment of full-scale autonomous vessels requires careful consideration of environmental and operational challenges to ensure safety and energy efficiency. To enhance the automation of inland shipping, this thesis provides an in-depth analysis of how shallow and confined water affects ship resistance, manoeuvring, control implementation, and energy efficiency. The aim of this thesis is to develop a holistic simulation framework for ship performance prediction and operational analysis.

The development of such a comprehensive framework requires modelling of vessel characteristics with hydrodynamic and river hydraulic effects. Firstly, this thesis develops a novel ship energy performance model explicitly tailored for resistance and energy consumption prediction of inland waterway vessels. It aims to generate fast and accurate predictions based on a collection of purely empirical methods. Secondly, this thesis develops a Manoeuvring Modelling Group-based manoeuvring model for motion prediction under shallow water and bank effects. Building upon this, a systematic control design was conducted with consideration of ship hydrodynamic characteristics in confined waterways. A comparison of a conventional controller and an advanced model predictive control was performed to evaluate their performance and robustness in tackling path-following tasks under complex environments with various disturbances. With these models and control methods, an integrated voyage planning framework (VPF) is proposed for analysing vessel operations. It captures a vessel's dynamic performance with energy consumption analysis under coupled interactions between ship hydrodynamics, river hydraulics, and motion control. Based on the analysis of ship energy performance, this thesis proposes a particle swarm optimisation (PSO) module for fuel optimisation in inland waterways.

Validation studies with full-scale trial measurements revealed that the energy performance prediction model achieved promising accuracy, ensuring a mean absolute error below 10% based on finite input parameters. It was also observed that disturbances in inland waterways, such as currents and bank effects, significantly affect a vessel's course stability, which should be carefully considered in the control system development of autonomous vessels operating in narrow channels. A series of case studies showcased the VPF's capabilities for enabling a wide range of applications, such as route assessment, evaluation of control design, and operational energy efficiency analysis. It was shown that the PSO-based optimisation achieved an average of 5.7% fuel savings in shallow water operations with water depth-aware speed initialisation methods.

**Keywords:** autonomous vessels, control design, energy efficiency, inland waterways, operational analysis, voyage planning.



## Preface

This thesis presents research work performed from March 2022 to December 2025 at the Division of Marine Technology, Department of Mechanics and Maritime Sciences, Chalmers University of Technology, Sweden. Financial support was provided by AUTOBarge, the European Union's Framework Programme for Research and Innovation Horizon 2020 under Grant 955768.

First of all, I would like to sincerely thank my main supervisor, Full Professor Jonas Ringsberg. Your enduring patience since the beginning of my PhD study has always given me the courage to approach you whenever I faced challenges. To me, you are not only an academic mentor but also a senior friend who has always offered invaluable guidance and heartfelt support throughout my doctoral study. I will cherish our discussions as one of the most valuable assets in my path towards becoming an independent researcher.

I would like to extend my appreciation to my co-supervisor, Professor Wengang Mao, for consistently providing constructive feedback and insightful guidance. I still remember your valuable advice, especially during the early period when I felt uncertain, which greatly helped me identify my research direction. I have gained much inspiration from your broad expertise and perspective, and I am sincerely grateful for your help and supervision throughout these years.

I am also profoundly grateful to my other co-supervisor, Dr Fabian Thies. I sincerely appreciate your solid knowledge as an excellent naval architect, which has supported me greatly whenever I faced challenges. Those insightful discussions have contributed significantly to the progress of my doctoral study.

I would also like to thank all my friends in the AUTOBarge project, especially Abhishek, for friendship and efficient collaboration. Thank you, Yanyun, Lingyu, Amir, Dhanika, Hoang, Martin, and other fellows for the joyful chats and fun activities during NWEs. My sincere thanks go to Professor Rudy Negenborn, Dr Vasso Reppa, and Mr Ehab El Amam for their kind hospitality and for offering me the opportunity to experience both academia and industry in the Netherlands.

Moreover, I would like to extend my appreciation to the friends and colleagues in our Division of Marine Technology. Thank you, Yuhan, for being a good friend since we took the same flight to start this PhD journey. Thank you, Chi, for the nice memories and valuable collaborations. I also appreciate Heng, Xiao, Mohammad, Daniel, Stephan, Oweis, Malik and other friends for the joyful moments, and I would like to thank Professor Huadong Yao, Associate Professor Arash Eslamdoost, Rui, and Qais for their excellent help with the CFD study, even though this part was not included in this thesis. Thank you, Azim, for being a good roommate.

Beyond Chalmers, I am also grateful to all my friends and mentors whom I met during my master's studies in Southampton. I would like to thank Dr Xiaowen Bi and Dr Siqi Zhang for their friendship and continued encouragement in pursuing doctoral studies. Thanks to Hao and Juntao for being lifelong friends, and I will cherish these joyful memories. I would also like to thank my master's thesis supervisor, Professor Blair Thornton. You helped me broaden my view with a multidisciplinary perspective, and those skills remain essential assets for pursuing

my doctoral studies. My appreciation also goes to my dear friends in China, Yucong and Jianan, and I wish you all the best in Beijing. Thank you, Dr Xiaodong Chen, for the warm support and friendship when I was in Dalian.

I would like to commemorate my grandfather, who passed away in 2024. You always exemplified what it means to be an excellent engineer, and it was you who showed me how to retain curiosity and passion for the scientific world. You are a scientist and will remain a star shining brightly above me. I will keep your love and guidance in mind as I move forward.

I wish to express my profound gratitude to my parents. Your kindness, patience, and unwavering encouragement have not only supported me but have also shaped the person I am today.

Last but not least, I would like to express my thanks and appreciation to my beloved wife, Xue. Thank you for always bringing happiness, love, and support, and for being the best part of my life. This journey could not have been completed without your devotion and encouragement.

Chengqian Zhang, 张承乾  
Gothenburg, December 2025

# Contents

Abstract .....	i
Preface .....	iii
List of appended papers.....	vii
Authors' contributions (CRediT) .....	viii
List of other papers by the author.....	ix
Nomenclature .....	xi
Original features .....	xv
1 Introduction.....	1
1.1 Background.....	1
1.2 Motivation and objectives .....	3
1.3 Assumptions and limitations .....	4
1.4 Outline of the thesis .....	5
2 Literature review.....	7
2.1 Navigational challenges in inland waterways .....	7
2.2 Resistance prediction.....	7
2.2.1 Experimental tests .....	9
2.2.2 Numerical simulations .....	9
2.3 Manoeuvring modelling .....	11
2.4 Control design.....	12
2.5 Energy performance analysis.....	13
3 Methodology: development of the voyage planning framework.....	15
3.1 Overview of the voyage planning framework .....	15
3.2 Ship energy performance model.....	15
3.2.1 Resistance in shallow and confined waters.....	16
3.2.2 Propeller design.....	18
3.2.3 Power and energy consumption prediction.....	19
3.3 Manoeuvring model in confined waterways .....	20
3.3.1 Rigid body dynamics .....	20
3.3.2 Equations of motion .....	20
3.3.3 Hydrodynamic forces on the ship hull .....	21
3.3.4 Propeller force.....	21
3.3.5 Rudder model.....	22
3.3.6 Mathematical model for bank effect .....	23
3.3.7 Water currents .....	26

3.4	Control system design for inland vessels .....	27
3.4.1	Guidance system in confined water .....	27
3.4.2	Classical PID controller .....	28
3.4.3	Incremental PID controller.....	28
3.4.4	Model predictive control .....	29
3.5	River hydraulics modelling .....	31
3.5.1	Cross-sectional shift modelling.....	31
3.5.2	Current modelling .....	32
3.6	Energy optimisation.....	33
3.6.1	Particle swarm algorithm .....	33
3.6.2	Energy optimisation in inland waterways .....	34
3.7	System integration of the voyage planning framework.....	35
4	Summary of appended papers.....	37
4.1	Paper I – Energy performance modelling of IWV .....	37
4.1.1	Resistance prediction and validation.....	37
4.1.2	Operational analysis .....	39
4.2	Paper II – Manoeuvring modelling.....	41
4.2.1	Turning test validation .....	41
4.2.2	Bank effect simulation .....	42
4.2.3	Course-keeping control simulation .....	43
4.3	Paper III – Control design with PID.....	45
4.3.1	Operation at the waterway confluence.....	47
4.4	Paper IV – Improved path-following with NMPC .....	48
4.4.1	Path following control in straight channels.....	48
4.4.2	Path-following control in a waterway confluence .....	49
4.4.3	Path following control in river bends.....	51
4.5	Paper V – VPF development and operational analysis.....	54
4.5.1	Model validation .....	54
4.5.2	Operational analysis .....	56
4.5.3	Energy optimisation .....	60
5	Conclusions .....	63
6	Future work.....	67
	References .....	69

## List of appended papers

- Paper I**     **Zhang, C.,** Ringsberg, J. W., & Thies, F. (2023). Development of a ship performance model for power estimation of inland waterway vessels. *Ocean Engineering*, 287, 115731. DOI: 10.1016/j.oceaneng.2023.115731
- Paper II**     **Zhang, C.,** Ma, Y., Thies, F., Ringsberg, J. W., & Xing, Y. (2025). Towards autonomous inland shipping: A manoeuvring model in confined waterways. *Ships and Offshore Structures*, 20(6), 767–779.  
DOI: 10.1080/17445302.2024.2358284
- Paper III**    **Zhang, C.,** Dhyani, A., Ringsberg, J. W., Thies, F., Reppa, V., & Negenborn, R. R. (2024). Manoeuvring modelling and control design of autonomous vessels on inland waterways. In *Proceedings of the ASME 2024 43rd International Conference on Ocean, Offshore and Arctic Engineering*. OMAE 2024, 9-14 June 2024, Singapore. (Vol. 87820, p. V05AT06A046). American Society of Mechanical Engineers.  
DOI: 10.1115/OMAE2024-126580
- Paper IV**    **Zhang, C.,** Dhyani, A., Ringsberg, J. W., Thies, F., Negenborn, R. R., & Reppa, V. (2025). Nonlinear model predictive control for path following of autonomous inland vessels in confined waterways. *Ocean Engineering*, 334, 121592.  
DOI: 10.1016/j.oceaneng.2025.121592
- Paper V**     **Zhang, C.,** Zhang, C., Thies, F., Mao, W., & Ringsberg, J. W. (2025). A voyage planning framework for energy performance analysis of autonomous inland waterway vessels. *Energy*, 335, 137906.  
DOI: 10.1016/j.energy.2025.137906

## Authors' contributions (CRediT)

Authors are listed in the order in which they appear in Papers I–V:

**Chengqian Zhang (all papers):** Conceptualisation, Methodology, Writing – original draft, Writing – review and editing, Investigation, Validation, Visualisation, Programming.

**Jonas W. Ringsberg (all papers):** Conceptualisation, Validation, Writing – review and editing, Supervision, Funding acquisition.

**Fabian Thies (all papers):** Conceptualisation, Methodology, Validation, Writing – review and editing, Supervision.

**Yucong Ma (Paper II):** Writing – original draft, Conceptualisation, Investigation, Methodology, Visualisation.

**Yihan Xing (Paper II):** Investigation, Validation, Supervision.

**Abhishek Dhyani (Papers III and IV):**

- Paper III: Methodology, Writing – original draft, Writing – review and editing, Investigation, Validation.
- Paper IV: Conceptualisation, Methodology, Writing – original draft, Writing – review and editing, Investigation, Validation.

**Vasso Reppa (Papers III and IV):** Methodology, Validation, Supervision, Funding acquisition.

**Rudy R. Negenborn (Papers III and IV):** Methodology, Validation, Supervision.

**Chi Zhang (Paper V):** Methodology, Writing – review and editing, Investigation, Validation, Visualisation.

**Wengang Mao (Paper V):** Methodology, Writing – review and editing, Validation, Supervision, Funding acquisition.

## List of other papers by the author

- Paper A**     **Zhang, C.**, Ringsberg, J. W., & Thies, F. (2025). Hydrologic riverbed generation and operational analysis for autonomous vessels in meandering inland waterways. *Proceedings of the 35th International Ocean and Polar Engineering Conference (ISOPE 2025)*, 1-6 June 2025, Seoul/KINTEX, Korea. Paper No. ISOPE-I-25-442.
- Paper B**     Dhyani, A., Mojaveri, A. H., **Zhang, C.**, Mahipala, D., Tran, H. A., Zhang, Y. Y., Luo, Z., & Reppa, V. (2025). AUTOBargeSim: MATLAB (R) toolbox for the design and analysis of the guidance and control system for autonomous inland vessels. *Proceedings of the 16th IFAC Conference on Control Applications in Marine Systems, Robotics and Vehicles (CAMS 2025)*, August 25-28, 2025, Wuhan, China.
- Paper C**     Saha, R., Zhang, Y., Baerveldt, M., Luo, Z., Tran, H., Mojaveri, A., Mahipala, D., **Zhang, C.**, Dhyani, A., Wang, Y., Amien, D., Orzechowski, S., Domenighini, C., & Reppa, V. (2025). Autonomous inland waterway transport for a safer and sustainable tomorrow: The AUTOBarge Project. *Societal Impacts*, 7, 100161. DOI:10.1016/j.socimp.2025.100161
- Paper D**     **Zhang, C.**, Zhu, H., Yao, H., & Ringsberg, J. W. (2025). Unsteady Numerical Investigations of Shallow Water Effect on the Resistance of Inland Waterway Vessels. *To be submitted for journal publication*.
- Paper E**     **Zhang, C.**, Chen, X., & Ji, S. (2022). Semantic image segmentation for sea ice parameters recognition using deep convolutional neural networks. *International Journal of Applied Earth Observation and Geoinformation*, 112, 102885. DOI:10.1016/j.jag.2022.102885



# Nomenclature

## *Greek notations*

$\alpha$	Constant that determines the direction of the segment curvature [-]
$\alpha_H$	Rudder force increase factor [-]
$\beta_m$	Drift angle at midship [rad]
$\beta_P$	Inflow angle to rudder during manoeuvring [rad]
$\gamma$	Skewing factor in river meanders [-]
$\delta$	Rudder angle [rad]
$\varepsilon$	Ratio of wake fraction at rudder to propeller [-]
$\eta_H$	Hull efficiency [-]
$\eta_o$	Propeller open water efficiency [-]
$\eta_R$	Relative rotative efficiency [-]
$\theta$	Angle of curved waterway segment [rad]
$\Lambda$	Rudder aspect ratio [-]
$\rho_{FW}$	Freshwater density [kg/m <sup>3</sup> ]
$\psi$	Heading angle [rad]
$\psi^{ref}$	Reference heading angle [rad]
$\omega$	Inertia weight in PSO algorithm [-]

## *Latin notations*

$A_c$	Cross-sectional area of waterway [m <sup>2</sup> ]
$A_R$	Rudder area [m <sup>2</sup> ]
$A_s$	Cross-sectional area of the ship [m <sup>2</sup> ]
$A_{WP}$	Ship waterplane area [m <sup>2</sup> ]
$B$	Ship beam [m]
$b$	Half-width of the channel [m]
$C$	Duct chord length [m]
$C_B$	Block coefficient [-]
$c_F$	Frictional resistance coefficient [-]
$c_W$	Wave resistance coefficient [-]
$D_P$	Propeller diameter [m]
$d$	Distance between vessel and bank [m]
$F_N$	Rudder normal force [kN]
$Fr$	Froude number [-]
$Fr_h$	Depth Froude number [-]
$Fr_{hd}$	Depth Froude number (deep water) [-]
$g$	Gravitational constant [m/s <sup>2</sup> ]

$H$	Water depth [m]
$H_{max}$	Maximum cross-sectional water depth [m]
$J$	Propeller advance ratio [-]
$K_p$	Controller proportional gain [-]
$K_T$	Propeller thrust coefficient [-]
$k$	Ship form factor [-]
$L$	Ship length overall [m]
$n$	Propeller revolution speed [r/min]
$n_{Prop}$	Number of propellers [-]
$P_D$	Delivered power [kW]
$P_E$	Effective power [kW]
$P_S$	Service power [kW]
$P_{max}$	Engine limit [kW]
$q$	Vessel's states in MPC
$R_{AW}$	Added wave resistance [kN]
$R_{BANK}$	Bank-induced resistance [kN]
$Re$	Reynolds number [-]
$R_s$	Squat-induced resistance [kN]
$R_T$	Total resistance [kN]
$R_W$	Wind resistance [kN]
$r$	Yaw speed [rad/s]
$r'$	Non-dimensional yaw rate [-]
$SFOC$	Specific fuel oil consumption [g/kWh]
$S_W$	Wetted surface area [m <sup>2</sup> ]
$s$	Propeller slip ratio [-]
$T$	Ship draught [m]
$T_d$	PID derivative constant [-]
$T_i$	PID integral time constant [-]
$T_s$	Time constant for sampling period [-]
$T_P^P$	Propeller thrust force from portside [kN]
$T_P^S$	Propeller thrust force from starboard [kN]
$t$	Thrust deduction factor [-]
$U$	Ship speed [m/s]
$U_C$	River current speed [m/s]
$U_R$	Total inflow speed at rudder [m/s]
$u$	Longitudinal ship speed [m/s]
$u_R$	Longitudinal rudder inflow speed [m/s]
$u_r$	Relative surge speed under currents [m/s]

$u$	MPC control input vector (rudder angle $\delta_c$ [rad] and shaft speed $n_c$ [r/s])
$V_c$	Critical ship speed in confined waterways [m/s]
$V_T$	Reference velocity in bank effects [m/s]
$v$	Lateral ship speed at centre of gravity [m/s]
$v_m$	Lateral ship speed at midship [m/s]
$v_R$	Lateral rudder inflow speed [m/s]
$v_{rm}$	Relative sway speed under currents [m/s]
$W_C$	Channel width [m]
$w_E$	Effective wake [-]
$w_P$	Wake fraction at propeller [-]
$w_R$	Wake fraction at rudder [-]
$X_B, X_H, X_P, X_R$	Surge force components from bank effect, ship hull, propellers, and rudders [kN]
$Y_B, Y_H, Y_R$	Sway force components from bank effect, ship hull, and rudders [kN]
$y_{infl}$	Influence distance of bank effect [m]
$y_p$	Ship–bank distance from portside [m]
$y_s$	Ship–bank distance from starboard [m]

### *Abbreviations*

CFD	Computational fluid dynamics
CoG	Centre of gravity
DoF	Degree of freedom
ETA	Estimated time of arrival
EU	European Union
GHG	Greenhouse gas
GNC	Guidance, navigation, and control
IWT	Inland waterway transport
IWV	Inland waterway vessel
ML	Machine learning
MPC	Model predictive control
MMG	Manoeuvring Modelling Group
NMPC	Nonlinear model predictive control
PID	Proportional–integral–derivative
PSO	Particle swarm optimisation
RPM	Revolutions per minute
UKC	Under keel clearance
VPF	Voyage planning framework



## Original features

This thesis aims to enhance the automation and digitalisation of inland water transport by developing a novel simulation framework for evaluating the operational performance of inland vessels in confined waterways. This integrated framework includes vessel hydrodynamics, control responses, and ship–waterway interactions to quantify energy consumption during dynamic operations in meandering inland waterways. The results provide an innovative digital testbed for assessing route feasibility, control performance, and energy efficiency under hydrodynamic and hydraulic disturbances. The originality and contributions of this thesis are presented below:

1. A dedicated ship energy performance model for inland vessels is developed for providing fast and accurate predictions of power and energy consumption in shallow and confined waters (Paper I). The model's accuracy is validated using experimental data (Paper I) and actual measurements of inland vessels (Paper V).
2. A manoeuvring model is developed for vessel motion dynamics and trajectory prediction in confined waterways. The simulation reveals that bank effects have a significant impact on the ship's course stability, which is critical for vessel operations in narrow fairways (Paper II).
3. Comprehensive control systems design is conducted for evaluating the ship's path following performance with the consideration of environmental disturbances in curved and constrained fairways (Papers III and IV).
4. A novel hydraulic modelling approach is introduced for bathymetry, cross-sectional shifts, and current generation. The model enables physically consistent river environments for simulation (Paper V).
5. An integrated voyage planning framework (VPF) is established, combining energy modelling, manoeuvring modelling, motion control, and river hydraulic effects into a single digital testbed. Case studies illustrate its applicability for route feasibility assessment, near-bank operation analysis, and energy prediction under spatially varying bathymetry. In addition, a depth-awareness speed optimisation strategy is proposed to reduce energy consumption (Paper V).



# 1 Introduction

This chapter introduces the research background of this thesis. Subsequently, the aims and objectives are presented, along with the study’s scope, assumptions, and limitations.

## 1.1 Background

With the increasing number of industrial and engineering activities, the transport sector is one of the largest sources of greenhouse gas (GHG) emissions. According to the European Commission (2025a), freight transport contributes over 10% of total GHG emissions, with road transport accounting for the largest share (Figure 1.1). Under the Paris Agreement, the EU set a long-term goal to become climate-neutral by 2050, including a target of a 55% reduction in CO<sub>2</sub> emissions by 2030 (European Commission, 2015). Achieving this strategy requires practical solutions to reduce GHG emissions, particularly in the road transport sector.

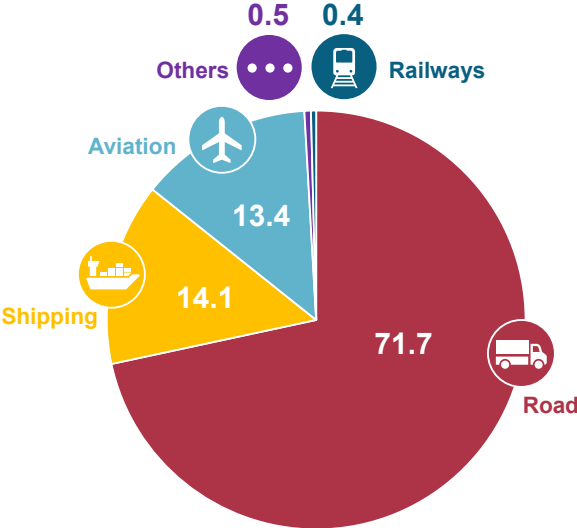


Figure 1.1. Emissions by transport mode in the European Union (European Environment Agency, 2023).

Considering the growing environmental challenges and road traffic congestion, inland waterway transport (IWT) is seen as a promising solution for shifting goods transport from road to waterways. Compared to other modes of transport, particularly road and rail, IWT offers unique advantages in terms of capacity, energy efficiency, and safety. Its inherently lower navigation speed contributes to a strong safety record, with accident rates significantly lower than those in road transport. For instance, an inland cargo vessel of approximately 3,000 deadweight tonnage (DWT) can carry the equivalent load of nearly 60 railway wagons of 50 tons each or more than 100 trucks. Combined with the absence of congestion on IWT, such a high capacity per transport unit offers significant potential to reduce pressure on road traffic.

As worldwide transport volumes continue to rise, innovation across transport modes is essential to improve cargo flows and logistics and minimise operational costs. IWT, characterised by safety, affordability, and reliability, provides a strong basis for such development. However, the share of inland waterways in total freight transport has remained relatively low over the past

decade (Figure 1.2). According to the European Commission (2025b), European IWT reached its lowest level between 2022 and 2023, accounting for only 1.6% of total freight transport (116 billion tonne-km). According to the Central Commission for the Navigation of the Rhine’s (CCNR) action plan, even the GHG emissions due to inland navigation are insignificant compared to the total amount of emissions from the transport sector, actions should be taken to improve its energy efficiency and to retain its competitiveness since the other modes of transport are making advances in reducing their greenhouse gas emissions (CCNR, 2025). Accordingly, coherent policy measures are required to accelerate the transition of IWT and maintain its competitiveness. One practical approach is to establish legal requirements and regulatory frameworks to support the decarbonisation of inland transport, such as measures promoting the use of alternative fuels and batteries in vessel construction (Christodoulou Raftis et al., 2023).

In line with these decarbonisation efforts, the European Commission released the action programme, ‘Navigation and Inland Waterway Action and Development in Europe’ (NAIADES), to enhance the role of IWT in mobility and logistics systems (European Commission, 2021). Its main objective is to shift more cargo transport onto rivers and canals. Furthermore, the adoption of autonomous shipping is regarded as a critical solution to strengthen the competitiveness of inland shipping through high levels of digitalisation and automation (European Commission, 2020).

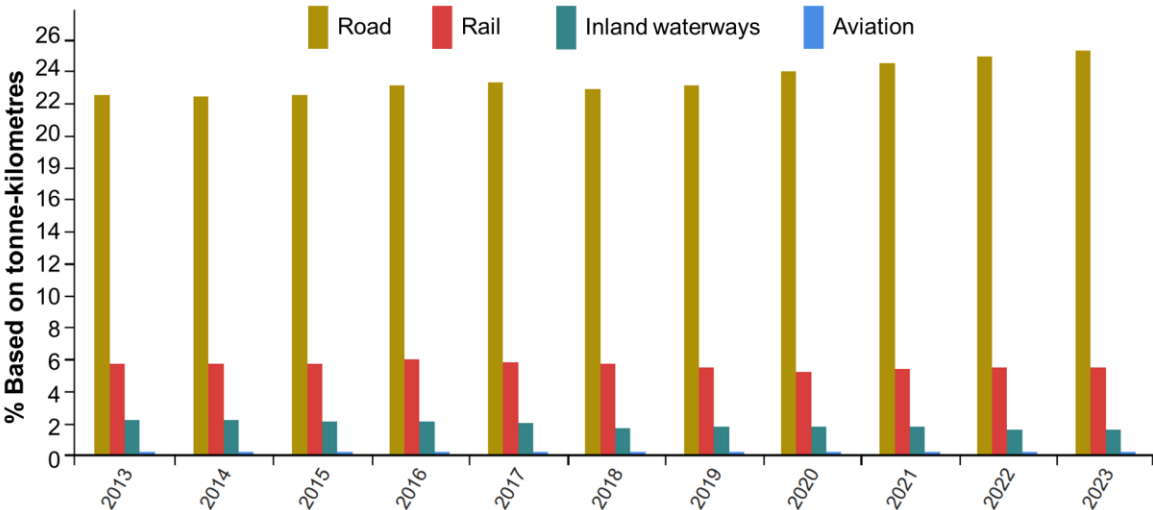


Figure 1.2. Freight transport split by sector in the EU, 2013–2023 (European Commission, 2025b).

However, due to the confined operational environments of these rivers and canals, the implementation of autonomous vessels in inland waterways faces multiple challenges. Bathymetry constraints and varying currents strongly influence vessel dynamics, while effective course-keeping and autonomous navigation require precise control in confined waterways. These environmental and operational complexities pose significant challenges to navigational safety and energy efficiency. In this context, the central objective of this doctoral research is to develop a holistic simulation framework for autonomous inland vessels that incorporates hydrodynamics, river hydraulics, motion control, and energy predictions, enabling systematic analysis and performance evaluation under realistic inland waterway conditions.

## **1.2 Motivation and objectives**

A key limitation of existing studies is the lack of systematic analysis of inland vessel operational performance, particularly considering the coupled effects of ship hydrodynamics and river hydraulics. Previous research in confined waters has primarily focused on specific aspects. For example, studies on hydrodynamic performance are often limited to shallow water (Mucha et al., 2018; Raven, 2016; Zeng et al., 2019) without lateral confinement, or on sophisticated control design with oversimplified waterways and vessel dynamics (Chen et al., 2018; Du et al., 2022). In reality, the operational performance of an inland vessel involves the integration of motion control, energy consumption analysis, and accurate predictions of interactions with the surrounding environment, such as bathymetry and currents. Regarding confined water, many existing studies rely on idealised straight channels with simplified cross-sectional geometries (Du et al., 2020; Sano et al., 2014; Zou & Larsson, 2013). In contrast, natural rivers are typically characterised by curved fairways, irregular bathymetry, and spatially varying current fields, which significantly affect ship manoeuvrability and energy efficiency depending on the navigational area. These limitations highlight the need for a comprehensive framework that combines hydrodynamic modelling, vessel control, and energy assessment in realistic inland waterways.

This thesis aims to address these challenges by developing a comprehensive simulation framework that enhances autonomous inland shipping, considering both safety (route feasibility assessment) and energy efficiency for vessel operations in shallow and confined waterways. The primary focus is to propose a digital testbed that facilitates the performance evaluation of autonomous inland vessels from early design to the operational stage. The objectives are divided into the following aspects.

### **Developing a ship energy performance model for inland vessels**

This aspect develops a comprehensive ship energy performance model for rapid and accurate analysis of inland vessel operations in confined waterways. The model integrates a newly proposed resistance prediction formula that accounts for shallow-water and bank-induced effects, along with propeller characteristics and engine dynamics. Building on these components, the model aims to generate rapid, relatively accurate estimates of power and energy consumption under dynamic inland water conditions.

### **Proposing a manoeuvring model in shallow and confined water**

This aspect focuses on capturing the vessel's motion dynamics and kinematics (trajectories) in confined waters by developing an improved manoeuvring model that includes the hydrodynamic effects of varying water depth and ship–bank distance. It provides a quantitative assessment of how waterway restrictions affect turning performance and overall course stability.

### **Developing control systems under environmental disturbances**

This aspect implements a systematic path-following control design that accounts for hydrodynamic and hydraulic effects across various inland water scenarios. The performance of conventional proportional–integral–derivative (PID) and model-based controllers is compared under

complex disturbances, providing insights for the integration of advanced control strategies into ship automation systems.

### **Conducting systematic operational analysis under river hydraulics effects**

This aspect establishes a holistic ship voyage planning framework (VPF) that integrates ship hydrodynamics, motion control, and energy performance prediction. A hydraulic model is proposed to capture bathymetric and current variations in curved inland waterways. Systematic case studies are conducted under various operational modes to demonstrate the capability of the VPF in achieving robust path-following control, dynamic energy estimation, and fuel consumption optimisation.

### **1.3 Assumptions and limitations**

Overall, the VPF is designed for conventional inland vessels with standard propeller–rudder systems powered by diesel engines. Other types of propulsion and steering systems, such as azimuth thrusters, water jets, tunnel thrusters, or Voith Schneider propellers, are not considered in this thesis. The characteristics of hybrid or electric engines are also excluded. The assumptions and limitations are outlined below.

The ship energy performance model aims to capture the speed–power relationship and provide energy consumption predictions for ships operating in shallow and confined waters. The applicable water depth ranges from deep to extremely shallow conditions, where the water depth to ship draught ratio follows a critical range ( $H/T \geq 1.2$ ). The bank-induced drag force is accounted for using a minimum ship–bank distance equivalent to one ship beam. In addition, this model only considers ship hydrodynamics in the normal waterways, where ice-infested rivers or canals are not included.

The manoeuvring model is limited to two-dimensional ship motion with three degrees of freedom (3-DoF), considering surge, sway, and yaw motions. Vertical motions of inland vessels are relatively small, as they typically operate in calm waters without significant ocean waves, and are therefore not included. The model assumes equal propeller thrust and rudder forces on both sides, disregarding the asymmetrical flow generated during steering. Manoeuvring simulations are conducted for single-vessel scenarios, meaning that the effects of ship–ship interactions, such as head-on encounters or overtaking, are not considered. Although ship–ship interactions are essential for close-quarters manoeuvring, their explicit modelling lies outside the present scope of this thesis. Recent studies, such as the Fourier-based ship–ship interaction model by Yang and el Moctar (2025), demonstrate that accurately predicting dynamic interaction forces during overtaking in deep and shallow waters requires CFD-calibrated, scenario-dependent surrogate models that depend strongly on encounter geometry, ship types, speed combinations, lateral distance, and water depth. Integrating such multi-ship models would require a dedicated traffic and encounter-management module, high-frequency closed-loop control simulations, and markedly smaller time steps, which is inconsistent with the aim of maintaining a computationally efficient, route-scale energy assessment framework. In addition, ship–ship interaction effects are local and short-lived, making them more critical for control and collision-avoidance functions than for the voyage-level energy analysis considered in this thesis.

In the control design, the primary objective is to achieve effective path-following using rudder control. Speed control is considered only in specific scenarios where the ship operates near infrastructure, such as bridge passes or locks, and speed must be reduced for safety.

The hydraulic model generates a series of meandering waterways with bathymetric variations and currents that reflect the characteristics of natural rivers. Nevertheless, the complex phenomena of river dynamics, including sediment transport, riverbed morphological changes, and secondary flows, cannot be captured by the present model.

In operational simulation and analysis, an enhanced PID controller is employed to ensure tracking performance and computational efficiency. The model predictive control (MPC) developed in Paper IV was not used due to its high computational demand for long-duration voyages. The ship's operational performance was evaluated from both a safety perspective, focusing on trajectory tracking, and an energy efficiency perspective, focusing on fuel consumption. Emissions were not included in the evaluation metrics. Energy consumption optimisation was simplified as an offline problem based on the given route and corresponding speeds. The interaction between real-time ship motion and dynamic speed optimisation is not considered in this thesis.

This thesis primarily focuses on the simulation-based investigation of autonomous inland vessel motion, control, and energy responses. The waterways were generated using a hydraulic modelling approach, rather than relying on statistical or measurement-based data. The available full-scale trial data were used only for model validation simulations. Therefore, a systematic study on uncertainty analysis is not included in this thesis. Regarding model sensitivity, Papers I and II involve the parameter sensitivity analyses of the energy performance model and the manoeuvring model, respectively. The global impacts on ship energy consumption and manoeuvrability, resulting from variations in individual parameters, were quantified.

## **1.4 Outline of the thesis**

This thesis presents a summary of the research contributing to the development of the VPF, and the connections between the included papers are illustrated in Figure 1.3. Papers I and II focus on model development for capturing energy performance and manoeuvrability, while Papers III and IV present the path-following control design and assessment. Paper V presents a systematic operational simulation and analysis using the developed model.

The remainder of the thesis is structured as follows: chapter 2 presents a literature review on ship performance in confined waterways, focusing on hydrodynamics, motion control, and energy efficiency analysis. Chapter 3 introduces the primary methodology for developing an integrated simulation framework for autonomous inland vessels. Chapter 4 presents the main findings and results from the appended publications. Chapter 5 summarises the conclusions of this thesis, and chapter 6 discusses insights for future studies.

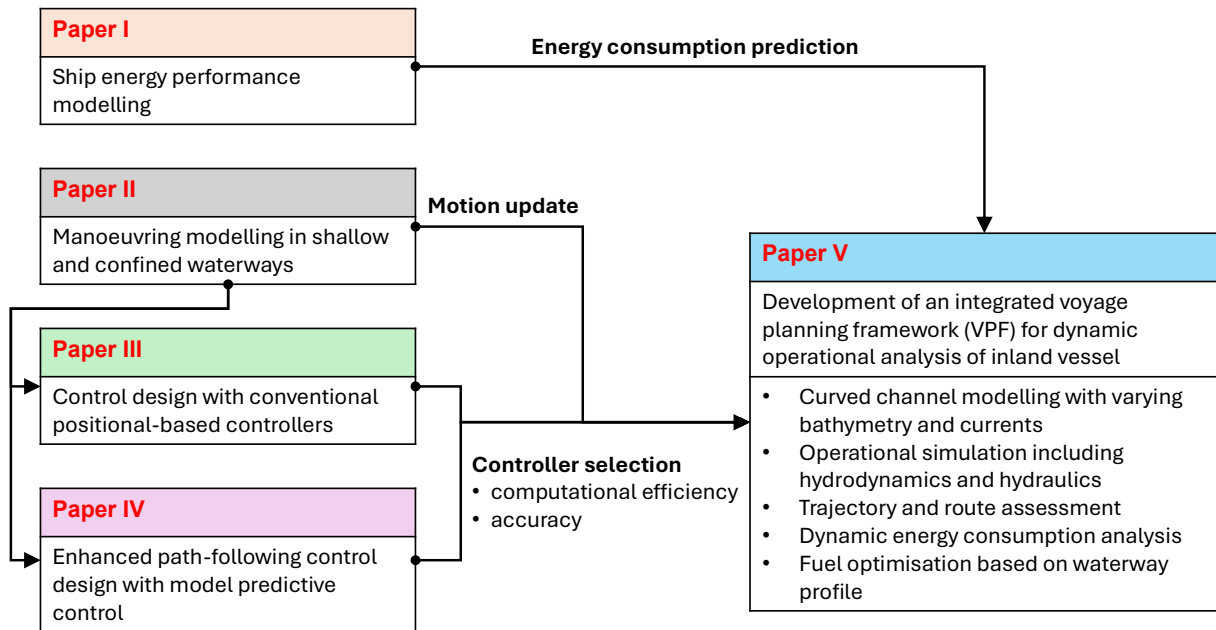


Figure 1.3. Outline of the thesis with appended papers.

## 2 Literature review

This chapter presents a systematic literature review and highlights the main gap in current studies, which motivates the contribution of the work presented in this thesis.

### 2.1 Navigational challenges in inland waterways

Due to the distinct nature of inland waterways, vessels operating in rivers and canals face unique navigational challenges, as the fairways are usually restricted both vertically and horizontally. Confined water affects vessel performance in various aspects, including resistance and propulsion, manoeuvrability, control behaviour, and overall energy efficiency.

When a vessel sails on inland waters, a decreasing under-keel clearance (UKC) results in strong flow interactions in the gap, leading to additional drag on the hull (Aztjushkov, 1968; Millward, 1989; Raven, 2016). The accelerated flow under the hull induces a pressure difference, causing additional sinkage and trim, so-called squat effects (Eloot et al., 2008; Lataire et al., 2012; Pompée, 2015; Raven, 2012). In conditions of low UKC, shallow water amplifies the squat effect due to the greater restriction of water flow.

In addition to the increased resistance, the shallow water effect also alters the manoeuvrability of vessels operating in confined waters (Kijima & Nakiri, 1990; Liu et al., 2015; Yasukawa & Kobayashi, 1995; Yoshimura, 1986). The turning ability of a vessel is influenced by both water depth and hull form, with the variation trends of tactical diameter depending on different ship geometries (Liu et al., 2015; Yoshimura, 1986). For instance, it has been observed that the tactical diameter becomes smaller in shallow water for wide-beam ships, while slender vessels display completely different turning characteristics as the tactical diameter increases with decreasing water depth (Yasukawa & Kobayashi, 1995).

Beyond vertical constraints, operational space on narrow rivers or canals is also limited laterally. A decreased ship–bank distance alters the flow in the gap, leading to additional sway forces and yaw moments on the vessel, commonly referred to as the bank effect. Moreover, Yang et al. (2022) highlighted that a vessel’s hydrodynamic performance becomes more complex in curved channels, as ship manoeuvrability can be strongly affected by channel geometry and flow conditions. At river bends, secondary flows erode the outer bank while depositing sediments along the inner bank, producing point bars and riverbed migration. This creates an asymmetric operational environment in which vessels face greater demands on steering forces on the outer side and increased grounding risks on the inner side due to reduced water depth.

These disturbances affect course stability and impose additional energy costs on vessel operations. For inland vessels, especially autonomous ones, accounting for these influences in onboard automation system design is vital to enhance operational efficiency, improve navigational safety, and optimise energy usage.

### 2.2 Resistance prediction

When a vessel operates in restricted waterways, the resistance pattern can differ substantially from that in open water, depending on water depth and channel width restrictions. To distinguish between different levels of confinement, Pompée (2015) suggests critical thresholds

based on the relative dimensions of the waterway and the vessel (Table 2.1), where  $A_c$  and  $A_s$  are the cross-sectional areas of the waterway and the vessel,  $H$  is the water depth,  $T$  is the ship draught, and  $W_c$  and  $B_s$  represent the channel width and ship beam, respectively.

Table 2.1. Thresholds for determining the confinement effect (Pompée, 2015).

Parameters	Start of confinement	Important confinement	Highly confined
$A_c/A_s$	50	7–8	4
$H/T$	15	3–4	1.5
$W_c/B_s$	50–100	10–15	4

According to a series of studies on ship hydrodynamics in confined waters (Aztjushkov, 1968; Constantine, 1960; Lackenby, 1963; Schlichting, 1934), changes in resistance can be classified according to vessel speed and water depth into subcritical, critical, and supercritical regimes, as shown in Figure 2.1.

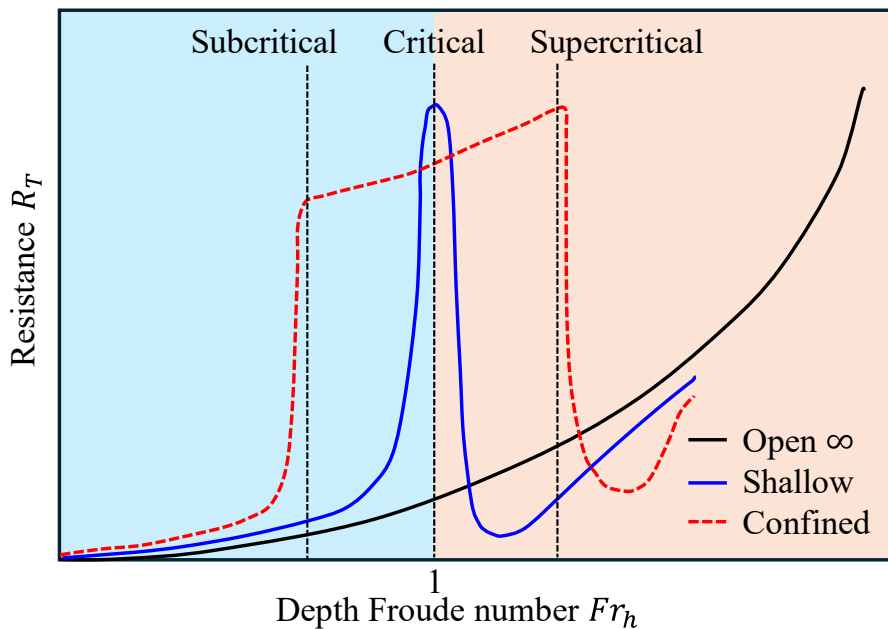


Figure 2.1. Resistance profile in open, shallow, and fully confined water, adapted from Du et al. (2020).

In shallow water, resistance increases significantly when the depth Froude number ( $Fr_h = V/\sqrt{gH}$ ) is around 1, corresponding to a critical ship speed of  $V_c \approx \sqrt{gH}$  (Schlichting, 1934). For shallow-water conditions without lateral restriction, the undulatory effect dominates, producing a resistance curve with a single peak at the critical speed. When confinement occurs in both width and depth, hydraulic effects arise alongside the undulatory effect, leading to a dramatic change in resistance around the subcritical limit and an M-shaped resistance curve. Conversely, during the transition around the supercritical range, the vessel experiences an increase in resistance, while lighter vessels show resistance reduction due to a significant change in wetted surface area (Constantine, 1960). For heavy vessels, such as displacement vessels, there is a limiting speed that should not be exceeded due to the risk of grounding.

Over the past decades, research on vessel resistance has been active, with a primary focus on shallow-water conditions, which can be broadly categorised into: (i) experimental studies and (ii) numerical simulations.

### **2.2.1 Experimental tests**

Experimental tests are the most direct method for capturing resistance patterns under various shallow or confined water conditions. Jiang (2001) conducted extensive model tests with an inland vessel and a container ship at different water depths in the Shallow Water Towing Tank Duisburg. Based on these experiments, a new method was proposed for predicting a vessel's resistance and propulsion performance from deep to moderately shallow water ( $H/T \geq 1.5$ ). To address shallower conditions, Zeng et al. (2018) performed a benchmark test to quantify the resistance of an inland ship model in extremely shallow water. The measurements include resistance, sinkage, and trim, serving as validation for numerical methods. Mucha et al. (2017) carried out an experimental study to analyse the effect of shallow water on the resistance and propulsion of a self-propelled inland vessel model. Building on this test, Mucha et al. (2018) conducted a more comprehensive benchmark study, evaluating the vessel's resistance and propulsion performance in confined waters across a wide range of water depths, ship–bank distances, and speeds.

In addition to self-propelled vessels, Du et al. (2020) conducted towing tank experiments to evaluate the resistance and wave patterns of two pusher–barge convoys in fully confined waterways. Ship hydrodynamics were examined under varying conditions, including channel dimensions, water depth, ship draught, and velocity. Building on this research, Du et al. (2021) quantified the impact of passing bridge piers in a confined waterway on ship resistance and squat. Similarly, Zentari et al. (2022) conducted systematic experimental tests on pusher–barge convoys with different barge configurations and in varying shallow-water conditions. The results showed that convoy arrangement significantly affects resistance and transport efficiency, due to strong flow separations in the gap between the barges and the pusher. More recently, Zentari et al. (2023) further quantified the effects of gap flow through continuous experimental testing on a convoy with a single barge, finding that covering the gap to suppress flow interaction reduced resistance by 6.5%.

These experimental studies provide essential validation references for numerical investigations of ship hydrodynamics in shallow and confined waters. However, most tests remain vessel-specific, which limits their applicability at the early design stage, when ship details are scarce. In addition, towing-tank tests are costly and time-consuming, and their scope is constrained by facility dimensions, making it extremely expensive and difficult to achieve comprehensive coverage of conditions such as varying bank distances, channel depths, and operational speeds. Building such databases for model regression requires a large number of tests and reduces applicability to other vessel types.

### **2.2.2 Numerical simulations**

With advances in turbulence modelling and computational resources, computational fluid dynamics (CFD) simulations have become a reliable and efficient method for analysing ship hydrodynamics. In resistance prediction for shallow water, extensive numerical studies have been conducted over the past decades. Linde (2017) carried out a series of CFD simulations on an

inland cargo vessel to investigate ship resistance and squat in a restricted channel, with results that aligned well with model test data in shallow water. Rotteveel et al. (2017) used CFD for stern optimisation of an inland vessel from deep to shallow water. The Parnassos RANS Solver was applied to determine the flow pattern for a series of hull forms. The findings suggested that a V-shaped ship bottom minimises power requirements in shallow water, while an idealised bottom transitions to an S-shape in deep-water conditions. Zeng (2019) performed systematic CFD simulations to propose an integrated formula for predicting ship resistance in shallow water, including viscous resistance correction (Zeng et al., 2019) and wave-making resistance correction (Zeng et al., 2020). Kaidi et al. (2018) conducted a numerical analysis of hull–propeller–rudder interactions for an inland container vessel, with simulations covering depths from deep to extremely shallow waters. The results showed that among parameters such as: (i) rudder deflection, (ii) the  $H/T$  ratio, and (iii) the advance coefficients of the propellers, water depth had the dominant influence on overall interactions. Islam et al. (2021) performed extensive simulations to investigate the resistance and propulsion performance of an inland container vessel from calm open waters to confined channels. The results suggested that full-scale simulations are necessary to determine the vessel’s required power.

Beyond single-vessel simulations, numerous numerical studies on vessel convoys have also been conducted. A series of CFD simulations (Zentari et al., 2022) investigated the hydrodynamic performance of pusher–barge convoys under varying shallow-water conditions and quantified the impact of gap flow in the convoy (Zentari et al., 2023). The effect of turbulence models was systematically discussed, and it was found that, compared with the standard  $k - \varepsilon$  model (Launder & Sharma, 1974) and the  $k - \omega$  SST model (Menter, 1992), a more advanced, improved delayed detached eddy simulation (IDDES) model (Gritskevich et al., 2012) produced the best agreement with experiments, particularly for capturing complex flows in extremely shallow water. Similarly, Du et al. (2020) reported good agreement between CFD simulations and model tests for resistance prediction of different pusher–barge convoys in a highly confined waterway with trapezoidal cross-sections. In a follow-up study, ship–ship interactions were evaluated through head-on simulations between a tanker and a convoy, and ship–structure interactions were examined in simulations of a convoy passing bridge piers (Li et al., 2021).

It can be concluded that with high-fidelity turbulence models, numerical simulations can yield accurate predictions of a ship’s hydrodynamic performance. However, a common limitation is their high computational cost. In addition, the simulations are usually restricted to fixed operational conditions such as constant speed or water depth. To capture the operational range of an inland vessel in dynamic flows in rivers or canals, regression model development requires extensive, costly simulations across a wide range of conditions. While parametric models enable resistance prediction for multiple hull geometries, developing such models requires substantial simulation efforts across numerous vessel configurations. The difficulty of conducting such extensive simulations in early-stage design motivates the development of a more efficient, empirically driven alternative. To address this gap, Paper I proposes a generic model based on empirical methods for a ship’s hydrodynamic performance prediction in shallow and confined water.

## 2.3 Manoeuvring modelling

Ship manoeuvring has long been a critical research topic due to its significance for safety, efficiency, and operational performance. Existing research can be broadly divided into two categories: (i) direct experimental or numerical free-running tests with propeller and rudder in action, and (ii) mathematical models for solving a vessel's equations of motion. Given the high cost and complexity of the environmental setup required for direct free-running trials, most studies focus on manoeuvring models for fast and accurate prediction of vessel motions. Classical models, such as the linear Nomoto model (Nomoto et al., 1957), the whole-ship model (Abkowitz, 1964), and the modular manoeuvring model (Ogawa & Kasai, 1978; Yasukawa & Yoshimura, 2015), have been widely applied in research and ship design. However, these models were originally developed for conventional sea-going vessels operating in deep, open water, so their applicability to confined waterways is questionable due to the distinct nature of the operating conditions. Beyond the differences in hydrodynamic derivatives between inland and sea-going ships, shallow-water and bank-induced forces introduce additional forces and moments that can substantially alter a vessel's manoeuvring behaviour (Lataire et al., 2009; Vantorre et al., 2003).

To enhance manoeuvring prediction in shallow and confined waters, a series of studies have been undertaken to improve the applicability of manoeuvring models by incorporating confinement effects. Yoshimura (1986) applied the Manoeuvring Modelling Group (MMG) model to predict the manoeuvring of a car carrier under various shallow-water conditions. The predicted trajectories agreed well with experimental measurements, but the results also highlighted the limitations of using vessel-specific hydrodynamic derivatives. Kijima and Nakiri (1990) proposed a widely used formula for correcting hydrodynamic derivatives in shallow water based on experimental data from merchant vessels. Research indicates that under shallow-water conditions, a ship's manoeuvrability also depends on its hull type (Liu et al., 2015; Yasukawa & Kobayashi, 1995; Yoshimura, 1986). For conventional vessels with single or twin propellers, turning behaviour typically deteriorates with decreasing water depth. However, wide-beam ships show the opposite trend, with even better turning ability in shallow water than in deep water due to the increased rudder force and moment (Koh & Yasukawa, 2012; Yoshimura, 1986). This highlights that, unlike mathematical models for conventional ships in open water, manoeuvring models for inland vessels must incorporate shallow-water effects as well as vessel type and steering configuration.

To improve manoeuvring prediction for inland vessels, Liu et al. (2017) proposed an integrated manoeuvring model specifically for inland vessels, incorporating an enhanced rudder lift and drag prediction formula derived from extensive 2D CFD simulations (Liu et al., 2016). However, the model was applied only in deep water, where confined-water effects were neglected. More recently, Yang and el Moctar (2024) extended the Abkowitz-based model by incorporating shallow-water corrections to hydrodynamic derivatives derived from extensive numerical captive model tests with an inland vessel at varying water depths. The manoeuvring model was successfully validated through full-scale trials of an inland barge. Nevertheless, the model remains limited to a vessel with a specific hull type and does not account for lateral effects, such as the bank effect.

While certain advances have been made in manoeuvring modelling in inland waterways, current applications are often limited to the validation phase, such as turning circle comparisons. In

addition, their application scenarios remain limited to relatively deep, open fairways or to shallow waters without lateral disturbances (Yang & el Moctar, 2024). To enhance the practical relevance and accuracy of manoeuvring prediction for inland vessels, a dedicated manoeuvring model that captures ship characteristics in shallow, confined waters must be developed. Moreover, such a model should be more extensively applied to vessel operational analyses under complex river bathymetries. Therefore, Paper II introduces the manoeuvring modelling for inland vessels, including the effects of shallow water, currents, and bank effects. The shallow-water correction implemented here focuses on resistance. The hydrodynamic derivatives under different water depths follow established experimental formulations reported in the literature (Koh & Yasukawa, 2012). It should be noted that for newly designed vessels, the correction formula (Kijima & Nakiri, 1990) provides a practical approximation for shallow water derivatives, although measured coefficients remain preferable when available.

## 2.4 Control design

Control design is a critical task for autonomous inland vessels, where accurate path-following is essential to ensure safety in constrained environments (He et al., 2024; Paulig & Okhrin, 2024; Waltz et al., 2025). Navigating river bends requires continual heading adjustments and drift compensation. Robust controllers are therefore crucial for counteracting disturbances from currents and hydrodynamic loads, ensuring effective course-keeping along curved paths.

Sano et al. (2014) employed a conventional proportional–derivative (PD) controller to investigate the course stability of a container vessel model near channel walls. The results highlighted that rudder control is essential for maintaining heading during near-bank operations, particularly in shallow-water conditions. Chen et al. (2021a) applied a conventional PID controller to an LNG carrier model in a confined channel, investigating the effects of water depth and speed on ship manoeuvring and motion control across varying operating conditions. Reduced water depth was found to significantly affect propulsion efficiency, and cross-track error increased markedly. These results indicate the importance of incorporating shallow-water effects in control design. However, the study was limited to straight channels with path-following on zig-zag courses in calm water, neglecting the influence of curved channels and currents. In a subsequent study, a fuzzy-based tracking controller (FuzzyTC) was developed for rapid heading control under realistic inland-water conditions with current effects (Chen et al., 2021b). The trajectory showed significant improvement with FuzzyTC in terms of computational speed and tracking performance compared with a conventional prescience model-based tracking controller.

Chen et al. (2018) proposed a distributed MPC method for vessel platooning, demonstrating promising performance in deep-water port navigation. Tao et al. (2022) extended this concept to inland waterways, but their framework relied on simplified vessel dynamics and environmental forces. Xu et al. (2023) developed an improved heading control design for large inland vessels in confined waters using MPC, with vessel dynamics calculated from a simplified MMG model and experimentally derived hydrodynamic coefficients. Nevertheless, the application scenario was limited to straight channels, and shallow-water resistance was not considered during the modelling process. Zheng et al. (2016) introduced an integrated time-awareness controller for path-following of an autonomous cargo vessel in port operations. Low-level tracking control was achieved with MPC, while a mixed-integer quadratic programming problem was solved at a higher level to generate timing-aware and energy-optimal reference trajectories over

the MPC horizon. Simulations demonstrated good tracking performance and energy efficiency using this mixed control strategy.

Existing research indicates that model-based control algorithms (Chen et al., 2018; Du et al., 2022; Mahipala & Johansen, 2023; Zheng et al., 2016) perform well in congested waterways. However, a common limitation is that these studies often rely on overly simplified ship manoeuvring models, which cannot fully capture actual vessel dynamics. In addition, their applications primarily focus on ports or straight channels, with limited consideration of waterway bathymetry, raising concerns about their suitability for natural rivers. In complex inland waterways, such as river meanders or curved canals, non-linear disturbances (e.g. shallow-water effects, bank effects, and currents) encountered during long voyages pose significant challenges to MPC efficiency due to high computational demands. Linear MPC can reduce this burden, but linearising vessel dynamics in curved waterways is difficult and requires comprehensive system identification. To improve tracking performance in curved inland waterways, reinforcement learning methods (Paulig & Okhrin, 2024; Waltz et al., 2025) have been developed to enhance control robustness, although their simulation involves costly training and implementation processes. To conduct robust, effective, and computationally efficient control design with considerations of environmental disturbances in confined fairways, Papers III and IV showcase comprehensive control systems development with a combination of classical and advanced MPC controllers, tailored to autonomous inland vessels.

## 2.5 Energy performance analysis

Given the confined nature of rivers and canals, ship energy efficiency is a key metric for sustainable transport and logistics on inland waterways (Fan et al., 2021; Wang et al., 2016; Yan et al., 2018; Zheng et al., 2024). With increasingly strict environmental regulations and rising fuel costs, reducing energy consumption has become both an economic and ecological priority for enhancing the competitiveness of inland shipping.

Current research on ship energy predictions can be divided into: (a) physics-based, or white box, methods (Calleya, 2014; Mermiris et al., 2011; Tillig et al., 2017), (b) data-driven methods (Hu et al., 2019; Karagiannidis & Themelis, 2021; Parkes et al., 2018; Zhang et al., 2025b), and (c) physics-informed (grey-box) models (Haranen et al., 2016; Lang et al., 2024). These models have demonstrated satisfactory accuracy in speed–power modelling and energy consumption predictions for vessels operating in open waters. However, they were developed for conventional merchant vessels, focusing on the influence of wind and ocean waves while neglecting the effects of shallow water and confined channels.

For inland vessels, Fan et al. (2020) proposed a novel energy performance prediction model specifically for inland vessels, based on measurements from a bulk carrier operating on the Yangtze River, China. However, the critical shallow-water effect was oversimplified using a speed-correction method. Using onboard sensor data from an inland ship, Yuan et al. (2021) developed a regression model for real-time fuel consumption prediction based on a long short-term memory (LSTM) neural network. More recently, Fan et al. (2024) evaluated several machine learning models for predicting ship energy consumption using onboard sensor data from an inland bulk carrier, concluding that Random Forest and XGBoost provided the most accurate predictions.

With the development of various energy prediction methods, studies on energy-efficiency optimisation have been actively conducted. Wang et al. (2016) integrated a wavelet neural network with a real-time engine speed optimisation model for short-term prediction on a river cruise vessel. Yan et al. (2018) applied big-data analytics with distributed k-means clustering to segment inland ship routes and determine optimal engine speeds under varying conditions. Yuan et al. (2021) employed a heuristic algorithm to optimise engine speed and reduce operational costs of inland ships, based on a machine learning model. Similarly, Perera and Mo (2017) developed a machine-intelligence framework combining onboard data pre-processing with shore-based analysis to enhance energy-efficiency management. Together, these studies provide a foundation for inland vessel energy optimisation, highlighting the importance of accurate prediction to support decision-making across varying operating environments.

However, existing research on inland vessel energy efficiency remains fragmented. Data-driven methods rely heavily on operational measurements, which are typically unavailable during the early design stages, limiting their generalisability across vessel types and waterways. As discussed in Sections 2.2, 2.3, and 2.4, most physics-based (white-box) models focus on ship hydrodynamics in shallow water in isolation, neglecting the combined effects of ship resistance, propulsion, manoeuvring, and motion control, and their overall impact on energy performance. These limitations have motivated the development of a novel voyage-planning framework in this thesis, capable of evaluating the performance of arbitrary inland vessels from the design stage through to operations. Based on the models and methods developed, Paper V introduces the development of such a holistic simulation framework for a vessel's energy performance prediction and dynamic operational analysis.

### 3 Methodology: development of the voyage planning framework

This chapter presents the primary methods used in the VPF, which involve energy performance modelling, manoeuvring modelling, control design, and system integrations.

#### 3.1 Overview of the voyage planning framework

The overall architecture of the VPF developed in this thesis is shown in Figure 3.1. It consists of several modules with key models and components that capture vessel dynamics, including interactions between the hull and the surrounding environment. The ship simulation modules include: (a) a ship energy performance model for predicting power and fuel consumption according to the vessel’s state and relevant environmental factors, such as water depth, ship–bank distance, and the speed and direction of water currents, and (b) a manoeuvring model to predict the vessel’s motion based on control output.

The environment module features a novel hydraulic model for generating waterway maps, including bathymetry and current profiles. These models are integrated into a voyage planning module. Once the route and engine mode are defined, operational simulations are conducted. The results are presented in the route analysis module, which includes vessel trajectory assessment and energy consumption analysis. Based on dynamic fuel consumption data from historical states, an energy optimisation module is developed to adjust vessel speed to minimise fuel consumption according to waterway conditions.

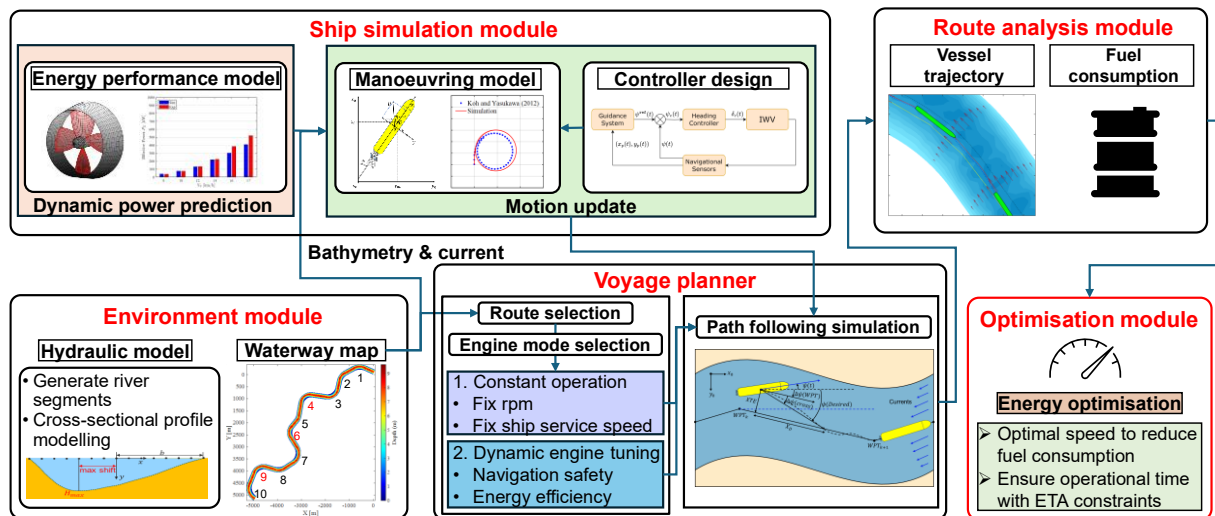


Figure 3.1. Overview of the voyage planning framework (Zhang et al., 2025c).

#### 3.2 Ship energy performance model

A ship energy system model enables rapid estimation of energy consumption by establishing the speed–power relationship, which is essential for autonomous inland navigation, where dynamic energy demand must be accurately monitored for efficient fuel or energy use. However, energy prediction is particularly challenging at the design stage due to the limited availability of data, which restricts the performance and applicability of data-driven models (Fan et al., 2024; Yuan et al., 2021).

Therefore, Paper I applied the architecture of the physics-based ship performance model ShipCLEAN (Tillig et al., 2017), originally developed for sea-going vessels, and modified its main methodology to account for ship hydrodynamics in shallow and confined water. This adaptation established a dedicated model for inland vessels, named ShipCLEAN-IWV (Zhang et al., 2023). The overall model structure is shown in Figure 3.2. It consists of several modules for ship geometry modelling, resistance prediction, propeller design, and power prediction. The detailed model development is presented in the remainder of this section.

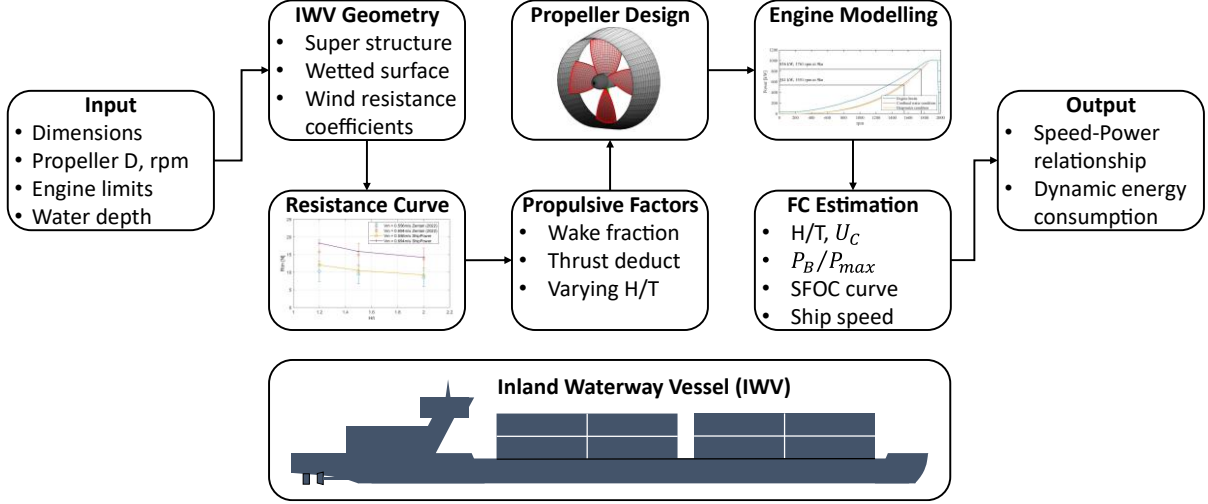


Figure 3.2. Overview of the ship performance model ShipCLEAN-IWV (Zhang et al., 2023).

### 3.2.1 Resistance in shallow and confined waters

Because inland vessels operate under relatively calm conditions with minimal influence from wind and waves, the resistance formula developed in this study focuses on inland waterway effects. It incorporates the influence of water depth and channel width (ship–bank distance). The total resistance in ShipCLEAN-IWV is determined as follows:

$$R_T = 0.5\rho_{FW}V_S^2S_W C_T + R_S + R_{BANK} \quad (1)$$

where  $\rho_{FW}$  is the freshwater density,  $R_S$  is the additional resistance due to squat effects in shallow water (Raven, 2016),  $R_{BANK}$  is the additional resistance induced by bank effects, and  $C_T$  is the total resistance coefficient. The estimation of  $C_T$  is based on the methods proposed by Millward (1989) and Zeng (2019), and is given by:

$$C_T = \left(1 + (k_{deep} + \Delta k)\right) C_F^* + C_W \quad (2)$$

where  $k_{deep}$  is the form factor from deep water,  $\Delta k$  is the form factor correction for shallow water, and  $C_F^*$  is the frictional resistance coefficient. The  $k_{deep}$  and  $C_F^*$  are calculated using the method proposed by Zeng (2019). A generic method for form factor correction (Millward, 1989) is applied:

$$\Delta k = 0.644 \left( \frac{H}{T} \right)^{-1.72} \quad (3)$$

where  $H$  is water depth and  $T$  is the ship draught. The equation for calculating  $C_F^*$  is given as:

$$C_F^* = \frac{0.08468}{(\log_{10} Re - 1.631)^2} \left( 1 + \frac{c_1}{\log_{10} Re + c_2} \left( \frac{H}{T} \right)^{c_3} \right) \quad (4)$$

where  $Re$  is the Reynolds number, and  $c_1$ ,  $c_2$ , and  $c_3$  are parameters determined by ship type, as shown in Table 3.1. In shallow water, frictional resistance depends on both the Reynolds number and the water depth-to-draught ratio, which deviates from the conventional ITTC '57 correlation line. Zentari et al. (2022) observed a similar increase in frictional resistance with decreasing UKC, particularly when  $H/T$  is below 2.

Table 3.1. Vessel-specific parameters from reference hull models (Zeng, 2019).

Vessel	$C_B$	$c_1$	$c_2$	$c_3$
Wigley hull	0.445	0.3466	-0.4909	-1.461
KCS	0.651	1.2050	-0.5406	-1.451
Rhine Ship 86	0.860	1.1680	-0.5238	-1.472

As indicated by Raven (2016), the additional squat effect in shallow water is incorporated to account for its contribution to the total resistance. Developed from towing tank tests, this formulation depends on ship fullness and the depth Froude number  $Fr_h$ , and is expressed as:

$$\Delta_{sinkage}/L = c_z \frac{\nabla}{L^3} \left[ \frac{Fr_h^2}{\sqrt{1 - Fr_h^2}} - \frac{Fr_{hd}^2}{\sqrt{1 - Fr_{hd}^2}} \right] \quad (5)$$

where  $c_z$  is a parameter that depends on the hull shape and fullness, with an average value of 1.46 (Raven, 2016), and  $Fr_{hd}$  is the depth Froude number in deep-water conditions, given by  $Fr_{hd} = V_S/\sqrt{0.3gL}$ .

The additional resistance from the squat ( $R_S$ ) can be calculated based on the increased wetted surface:

$$R_S/R_T = (\Delta_{sinkage} A_{WP}/\nabla)^{2/3} \quad (6)$$

where  $A_{WP}$  represents the ship's waterplane area and  $\nabla$  is the ship's displacement (in  $m^3$ ). It is important to note that, apart from shallow-water effects, inland vessels often operate in confined waterways, where fairways are restricted both vertically (by water depth) and laterally (by ship-bank distance). As the vessel approaches the bank, the channel wall induces additional drag on the hull (Lataire et al., 2009; Zou & Larsson, 2013). The additional resistance induced by bank effects was derived from a regression model based on experimental measurements and CFD simulations (Du et al., 2020; Linde et al., 2017; Mucha et al., 2018).

According to data reported in the literature, a marked increase in resistance occurs as the ship-bank distance-to-beam ratio ( $d/B$ ) decreases from around 2.5 to 1.0. Figure 3.3 presents the

regression model of the additional resistance as a function of the speed–depth relationship ( $Fr_h$ ) and the relative ship–bank distance ( $d/B$ ). The data indicate that channel walls may cause up to a 30% increase in resistance when a vessel travels close to shore at high speeds in confined waterways. Conversely, when the lateral distance exceeds a certain threshold, the bank effect becomes negligible. This threshold is defined by the influential transversal distance  $y_{infl}$  (Lataire et al., 2009), expressed as:

$$y_{infl} = 5B(Fr_h + 1) \quad (7)$$

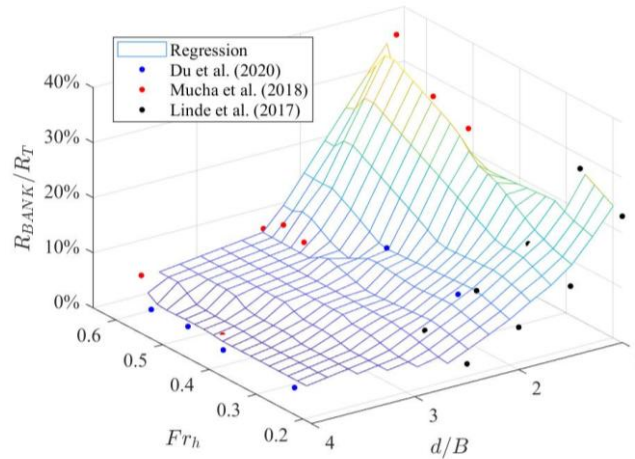


Figure 3.3. Regression surface for bank-induced resistance, derived from a collection of model test measurements and computational fluid dynamics simulations.

In the simulations, the additional bank-induced resistance is obtained by interpolating this regression surface using the vessel’s speed and the local water depth relationship ( $Fr_h$ ), and the instantaneous ship–bank distance. In this thesis, the bank-effect resistance model is applied to subcritical depth Froude numbers ( $Fr_h < 0.7$ ), as high-speed in shallow-water operations near the river bank markedly increases the vessel’s resistance and risk of grounding or loss of manoeuvrability (Du et al., 2020; Lataire, 2014).

### 3.2.2 Propeller design

In ShipCLEAN, propellers are designed using a standard propeller series and the open-source tool OpenProp (Epps et al., 2009). Because the baseline blade geometries are primarily intended for conventional commercial vessels, the module was adapted with a new standard series to better represent inland vessel characteristics, such as ducted propellers. Blade sections were based on the classical Ka-470 type. For duct design, OpenProp offers only a limited selection of airfoil profiles; therefore, the NACA 4315 mean line, which has a geometry similar to the classical N19A nozzle, was incorporated as an example, as shown in Figure 3.4.

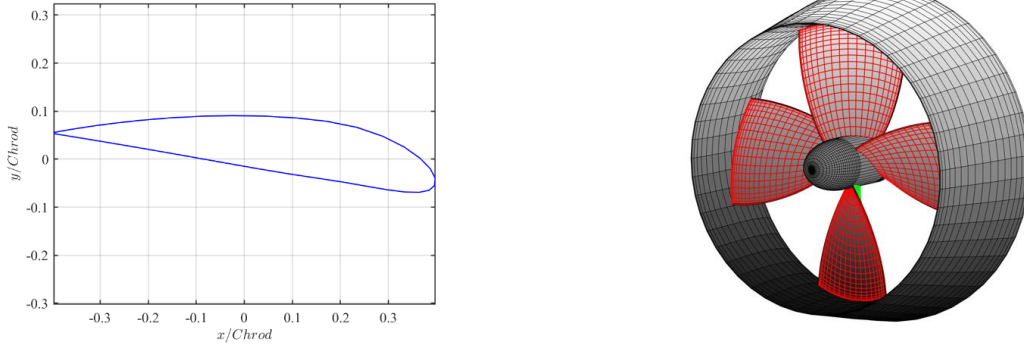


Figure 3.4. Ducted propeller design in ShipCLEAN-IWV.

With the resistance and propeller design analysis, the required shaft power ( $P_S$ ) can be calculated as follows:

$$P_S = \frac{R_T V_S}{\eta_H \eta_O \eta_R \eta_S} \quad (8)$$

where  $\eta_H$  is the hull efficiency ( $\eta_H = (1 - t)/(1 - w_E)$ ),  $\eta_O$  is the open-water efficiency obtained from the propeller curve,  $\eta_R$  is the relative rotative efficiency (assumed constant at 1.0), and  $\eta_S$  is the transmission efficiency, including shaft and gearbox loss, set to 0.97 in Papers I and V.

### 3.2.3 Power and energy consumption prediction

ShipCLEAN-IWV uses an engine module derived from regression analysis of engine curves from major suppliers and marine engine manufacturers (Hidouche et al., 2015), including Cummins, MAN, Caterpillar, and Wärtsilä, covering a broad operational load spectrum (Table 3.2). The formulation allows straightforward, load-dependent estimation of *SFOC* based on the rated power ( $P_{max}$ ) and the load ratio ( $P_S/P_{max}$ ).

Table 3.2. Engine regression model based on load ratio ( $P_S/P_{max}$ ).

$P_{max}$ [kW]	$X = P_S/P_{max}$ [%]	$SFOC = f(X)$ [g/kW/h]	Error [%]
100–300	0–20	$398.89X^{-0.1987} + 8.945$	10
	20–100	$242.51 - 0.810X + 0.0065X^2$	7
300–500	0–20	$342.077X^{-0.1361}$	10
	20–100	$237.84 - 0.5957X + 0.0040X^2$	7
500–1,000	0–20	$327.708X^{-0.1262} + 1.984$	15
	20–100	$230.192 - 0.4496X + 0.0033X^2$	10
1,000–2,000	0–20	$296.346X^{-0.0963} - 1.06$	10
	20–100	$236.786 - 0.7577X + 0.0064X^2$	10
2,000–10,000	0–20	$265.583X^{-0.0570} - 1.743$	7
	20–100	$240.204 - 0.9639X + 0.0064X^2$	5
>10,000	0–20	$218.92X^{-0.0570} - 1.4368$	-
	20–100	$198 - 0.7945X + 0.0053X^2$	5

This approach is particularly effective for estimating fuel consumption when an inland vessel is at an early design stage with limited data. As more data becomes available after the early

design stage, this model can be easily adapted to incorporate more detailed engine characteristics.

### 3.3 Manoeuvring model in confined waterways

To capture ship motion dynamics in inland waterways, Paper II presents a manoeuvring model that accounts for shallow-water and bank effects. The model development, equations, and characteristics are described in this section.

#### 3.3.1 Rigid body dynamics

The coordinate systems used in this thesis are shown in Figure 3.5. Because inland vessels typically operate in relatively calm water, the manoeuvring model focuses on two-dimensional (2D) planar ship motion (surge, sway, and yaw), where vertical motion is neglected. As depicted in the coordinate systems,  $o_0 - x_0y_0z_0$  represents the earth-fixed frame, and  $o - xyz$  is the body-fixed frame located at midship.  $G$  is the centre of gravity (CoG), and  $u$  and  $v_m$  denote the surge and sway speeds at midship, respectively. Note that  $u$  and  $v_m$  must be adjusted to account for the speed and direction of the water current.

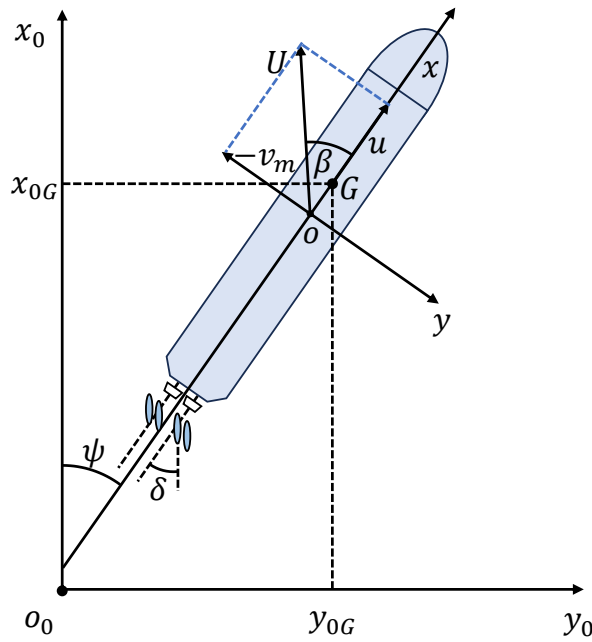


Figure 3.5. Coordinate system of an inland vessel.

#### 3.3.2 Equations of motion

The manoeuvring model for predicting vessel motion in inland waterways is based on the original MMG formulation, modified to account for shallow water and bank effects. The governing equations are expressed as:

$$\left. \begin{aligned} (m+m_x)\dot{u} - (m+m_y)v_m r - x_G m r^2 &= X_H + X_P + X_R + X_B \\ (m+m_x)\dot{v}_m + (m+m_x)ur + x_G m \dot{r} &= Y_H + Y_R + Y_B \\ (I_z + x_G^2 m + J_z)\dot{r} + x_G m(\dot{v}_m + ur) &= N_H + N_R + N_B \end{aligned} \right\} \quad (9)$$

where  $m$  is the ship's mass,  $m_x$  and  $m_y$  are the added masses in the  $x$ - and  $y$ -directions, respectively,  $x_G$  is the longitudinal coordinate of the CoG,  $I_z$  is the moment of inertia, and  $J_z$  is the added moment of inertia for yaw motion. On the right-hand side,  $X$ ,  $Y$ , and  $N$  represent the surge force, sway force, and yaw moment, respectively. The subscripts  $H$ ,  $P$ , and  $R$  denote the contributions from the ship's hull, propeller, and rudder, respectively, as in the original MMG formulation, and  $B$  represents additional contributions from bank effects.

### 3.3.3 Hydrodynamic forces on the ship hull

The forces and moments acting on the ship's hull are calculated using:

$$\left. \begin{aligned} X_H &= 0.5\rho LTU^2 X'_H \\ Y_H &= 0.5\rho LTU^2 Y'_H \\ N_H &= 0.5\rho L^2 TU^2 N'_H \end{aligned} \right\} \quad (10)$$

where  $\rho$  is the freshwater density,  $L$  is the ship's length,  $T$  is the draught, and  $U$  is the ship's speed.  $X'_H$ ,  $Y'_H$ , and  $N'_H$  are the non-dimensional surge force, sway force, and yaw moment, calculated as:

$$\left. \begin{aligned} X'_H &= -R'_0 + X'_{\beta\beta}\beta_m^2 + X'_{\beta r}\beta_m r' + X'_{rr}r'^2 + X'_{\beta\beta\beta}\beta_m^3 \\ Y'_H &= Y'_\beta\beta_m + Y'_r r' + Y'_{\beta\beta\beta}\beta_m^3 + Y'_{\beta\beta r}\beta_m^2 r' + Y'_{\beta rr}\beta_m r'^2 + Y'_{rrr}r'^3 \\ N'_H &= N'_\beta\beta_m + N'_r r' + N'_{\beta\beta\beta}\beta_m^3 + N'_{\beta\beta r}\beta_m^2 r' + N'_{\beta rr}\beta_m r'^2 + N'_{rrr}r'^3 \end{aligned} \right\} \quad (11)$$

In these equations,  $R'_0$  is the non-dimensional total resistance coefficient, including a correction for shallow water and bank-induced resistance, as presented in subsection 3.2.1. The terms  $X'_{\beta\beta}$ ,  $X'_{\beta r}$ , ...,  $N'_{rrr}$  are the hydrodynamic derivatives, where the coefficients were taken from the experimental test of an inland vessel in Koh and Yasukawa (2012).  $\beta_m$  is the mid-ship drift angle, computed as  $\beta_m = -\tan^{-1}(v_m/u)$ , and  $r'$  is the non-dimensional yaw rate,  $r' = rL/U$ . For different inland vessels, Koh et al. (2008) conducted systematic experimental tests in eight different pusher-barge arrangements. However, the coefficients are only applicable to deep-water conditions and were therefore not considered for vessel manoeuvring simulation in shallow water in this thesis.

### 3.3.4 Propeller force

For a twin-propeller configuration, the surge force is given by:

$$X_p = (1-t)(T_p^P + T_p^S) \quad (12)$$

where  $t$  is the thrust deduction factor, and  $T_p^P$  and  $T_p^S$  are the propeller thrusts from the portside and starboard, respectively, calculated as:

$$T_p^P = T_p^S = \rho n_p^2 D_p^4 K_T \quad (13)$$

Here,  $n_p$  is the propeller speed,  $D_p$  is the propeller diameter, and  $K_T$  is the thrust coefficient, expressed as:

$$K_T = k_2 J^2 + k_1 J + k_0 \quad (14)$$

where  $k_1$  and  $k_2$  are regression parameters from open-water curves, and  $J$  is the advance ratio:

$$J = u(1-w_p)/(n_p D_p) \quad (15)$$

In Eq. (15),  $u$  is the ship surge velocity, and  $w_p$  is the wake fraction during ship steering, calculated as:

$$w_p/w_{p0} = \exp(-4\beta_p^2) \quad (16)$$

where  $w_{p0}$  is the wake fraction during straight-ahead motion (Koh & Yasukawa, 2012), and  $\beta_p$  is the propeller inflow angle during manoeuvring, defined as  $\beta_p = \beta - (x_p/L) r'$ , depending on the relative coordinate of the propeller  $x_p$ . Notably, propellers can be developed using the model in Paper I to facilitate manoeuvring simulation and assessment if the open water data is not available at the early design stage.

For model simplification, the parameters of the propeller on each side, such as  $t$  and  $w_{p0}$ , are assumed to be identical. Accurately analysing unsymmetrical inflow for twin propellers during steering would require experimental flow-field measurement or detailed CFD simulations, which are beyond the scope of this model.

### 3.3.5 Rudder model

The rudder forces and moment are calculated as:

$$\left. \begin{aligned} X_R &= -(1-t_R)(F_N^P + F_N^S)\sin\delta \\ Y_R &= -(1+\alpha_H)(F_N^P + F_N^S)\cos\delta \\ N_R &= -(x_R + \alpha_H x_H)(F_N^P + F_N^S)\cos\delta \end{aligned} \right\} \quad (17)$$

where  $t_R$  is the steering resistance deduction factor,  $\alpha_H$  is the rudder force increase factor,  $F_N$  is the rudder normal force,  $x_R$  is the relative longitudinal coordinate of the rudders (identical on each side), and  $x_H$  is the longitudinal coordinate of the location where the additional lateral force acts.

The rudder normal force is computed as:

$$F_N = 0.5\rho A_R U_R^2 C_N \quad (18)$$

where  $A_R$  is the rudder area,  $U_R = \sqrt{u_R^2 + v_R^2}$  is the flow velocity at the rudder, and  $C_N$  is the rudder normal force coefficient based on the original MMG model:

$$C_N = \frac{6.13\Lambda}{\Lambda + 2.25} \sin\alpha_R \quad (19)$$

where  $\Lambda$  is the rudder aspect ratio ( $\Lambda = B_R/C_R$ , with  $B_R$  the rudder span and  $C_R$  the chord length), and  $\alpha_R$  is the effective rudder inflow angle:

$$\alpha_R = \delta - \tan^{-1} \left( \frac{v_R}{u_R} \right) \quad (20)$$

Here,  $u_R$  and  $v_R$  are the longitudinal and transverse rudder inflow speeds, calculated as:

$$u_R = \frac{\varepsilon u_P}{1-s} \sqrt{1 - 2(1-\eta\kappa)s + \{1-\eta\kappa(2-\kappa)\}s^2} \quad (21)$$

$$v_R = U\gamma_R(\beta - l'_R r')$$

where  $\gamma_R$  is the flow straightening coefficient,  $l'_R$  is a constant defining the acting point of  $v_R$  from model tests (Koh & Yasukawa, 2012), and  $\varepsilon$  is the ratio of the rudder wake fraction to the propeller wake fraction,  $\varepsilon = (1 - w_R)/(1 - w_P)$ . In the equation for  $u_R$ ,  $s$  is the propeller slip ratio,  $\eta = D_P/B_R$  is the relative ratio of propeller diameter to rudder span, and  $\kappa$  is an experimental constant. Detailed parameters and coefficients are provided in Paper II.

### 3.3.6 Mathematical model for bank effect

When a vessel operates near channel walls, the accelerated flow in the gap creates pressure differences, producing a combination of longitudinal force (increased resistance), lateral force, and yaw moment on the hull (Figure 3.6). This phenomenon is referred to as the bank effect, which has a crucial influence on the vessel's manoeuvrability. However, the existing studies on inland-vessel manoeuvring modelling often neglect this essential factor (Liu et al., 2017; Yang & el Moctar, 2024). This thesis presents a comparison of the three most well-known bank effects models (Ch'Ng et al., 1993; Norrbin, 1976; Vantorre et al., 2003), and incorporates them to enhance manoeuvring prediction for inland vessels. The detailed equations of these models are shown below.

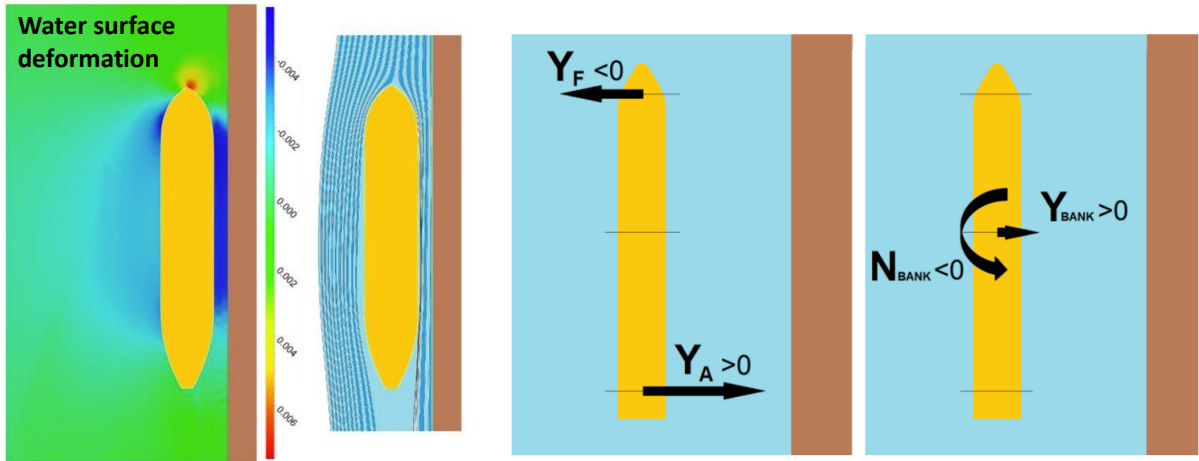


Figure 3.6. Schematics of bank effects, adapted from Lataire et al. (2018).

Based on extensive model tests of ship manoeuvring in confined waterways with vertical banks (Norrbin, 1976, 1985), Norrbin developed an empirical model using rectangular channels (Figure 3.7) to calculate the hydrodynamic forces and yaw moment for varying ship-bank distances and water depths:

$$Y_B = \rho C_B B T u^2 \eta_0 \left( 0.0926 + 0.372 \left( \frac{T}{H} \right)^2 \right) \quad (22)$$

$$N_B = -\rho C_B L B T u^2 \eta_0 \left( 0.0025 + 0.0755 \left( \frac{T}{H} \right)^2 \right)$$

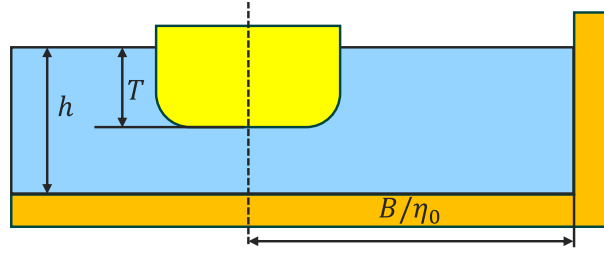


Figure 3.7. Bank configuration from Norrbin (1976).

Similarly, Ch'Ng et al. (1993) proposed an empirical formula based on model tests using three merchant vessels with different hull forms. The nondimensional lateral force and yaw moment are calculated as:

$$\begin{aligned} \frac{1000Y_B}{0.5\rho U^2 L^2} &= a_5 y_{B3} |y_{B3}| Fr + a_7 \frac{y_{B3}}{F} + a_9 \frac{y_{B3} Fr}{F} \\ &\quad + a_{13} \frac{y_{B3}}{F^2} + 0.11 \frac{y_B}{F} C_T + 0.0006 \frac{y_B}{F^2} C_T^2 \\ \frac{1000N_B}{0.5\rho U^2 L^3} &= b_8 \frac{y_{B3} |y_{B3}|}{F} + b_{13} \frac{y_{B3}}{F^2} + b_{14} \frac{y_{B3} |y_{B3}|}{F} + b_{16} \frac{y_{B3} Fr^2}{F^2} \\ &\quad + 0.0009 \frac{y_B}{F} C_T^2 - 0.0044 \frac{y_B |y_B|}{F} C_T^2 \end{aligned} \quad (23)$$

where  $a_5, a_7, \dots, b_{16}$  are regression coefficients (Ch'Ng et al., 1993),  $F$  is the ratio of UKC to water depth  $H$ , and  $y_B$  and  $y_{B3}$  are nondimensional ship–bank distances in a trapezoidal channel (Figure 3.8), defined as:

$$\begin{aligned} y_B &= \frac{1}{2} B \left( \frac{1}{y_p} + \frac{1}{y_s} \right) \\ y_{B3} &= \frac{1}{2} B \left( \frac{1}{y_{p3}} + \frac{1}{y_{s3}} \right) \\ F &= \frac{H - T}{T} \end{aligned} \quad (24)$$

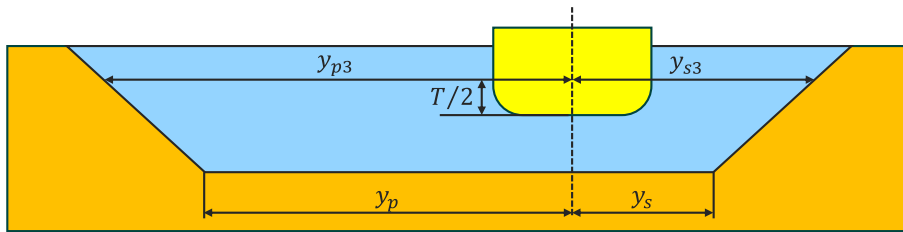


Figure 3.8. Ship–bank configuration in Ch'Ng et al. (1993).

Building upon these previous models, Flanders Hydraulics (Vantorre et al., 2003) developed an empirical formula for modelling the bank effect, based on systematic captive model tests using three vessels under varying water depth, ship–bank distance, and speed conditions. The model is expressed as:

$$\left. \begin{aligned}
Y_B^H &= 0.5\rho L T u^2 \sum_{i=1}^2 \sum_{k=0}^2 \alpha_{ik}^H y_B^i \left(\frac{T}{H-T}\right)^k \\
N_B^H &= 0.5\rho L^2 T u^2 \sum_{i=1}^2 \sum_{k=0}^2 \beta_{ik}^H y_B^i \left(\frac{T}{H-T}\right)^k \\
Y_B^P &= 0.5\rho L T V_T^2 \sum_{i=1}^2 \sum_{k=0}^2 \alpha_{ik}^P y_{B3}^i \left(\frac{T}{H-T}\right)^k \\
N_B^P &= 0.5\rho L^2 T V_T^2 \sum_{i=1}^2 \sum_{k=0}^2 \beta_{ik}^P y_{B3}^i \left(\frac{T}{H-T}\right)^k \\
Y_B^{HP} &= 0.5\rho L T V_T^2 Fr \sum_{i=1}^2 \sum_{k=0}^2 \alpha_{ik}^{HP} y_{B3}^i \left(\frac{T}{H-T}\right)^k \\
N_B^{HP} &= 0.5\rho L^2 T V_T^2 Fr \sum_{i=1}^2 \sum_{k=0}^2 \beta_{ik}^{HP} y_{B3}^i \left(\frac{T}{H-T}\right)^k
\end{aligned} \right\} \quad (25)$$

where the superscripts  $H$ ,  $P$ , and  $HP$  denote the individual effects of hull (pure speed), propulsion, and the coupled effect, respectively;  $V_T$  is the reference velocity that depends on the propeller's thrust and dimension ( $V_T = \sqrt{8 T_p / (\rho \pi D_p^2)}$ );  $Fr$  is the Froude number; and  $\alpha_{ik}^H$ ,  $\beta_{ik}^H$ ,  $\alpha_{ik}^P$ ,  $\beta_{ik}^P$ ,  $\alpha_{ik}^{HP}$ , and  $\beta_{ik}^{HP}$  are regression coefficients.  $y_B$  and  $y_{B3}$  are nondimensional ship-bank distances, following the configurations in Ch'Ng et al. (1993). Detailed parameters are provided in Vantorre et al. (2003).

For the sake of model comparisons, the lateral force  $Y_B$  and yaw moment  $N_B$  predicted by the three bank models (Ch'Ng et al., 1993; Norrbin, 1976; Vantorre et al., 2003) are visualised in Figure 3.9. The three methods produce similar lateral attraction forces until the ship-bank distance to beam ratio ( $d/B$ ) drops below approximately 2, at which point the model by Vantorre et al. (2003) predicts a repulsion force. As shown in Figure 3.9(c, d) for a speed of 4 knots, a clear attraction force occurs as the vessel nears the bank. Lataire (2014) indicated that repulsion arises when the gap distance falls below a critical threshold.

It should be noted that in Papers II, III, and IV, only the model by Vantorre et al. (2003) was used for manoeuvring model development and control simulations. In Paper V, the average value of the three models is applied for moderate distances, providing a comprehensive analysis of bank effects. However, when a repulsion force is detected, the value from Vantorre et al. (2003) is used.

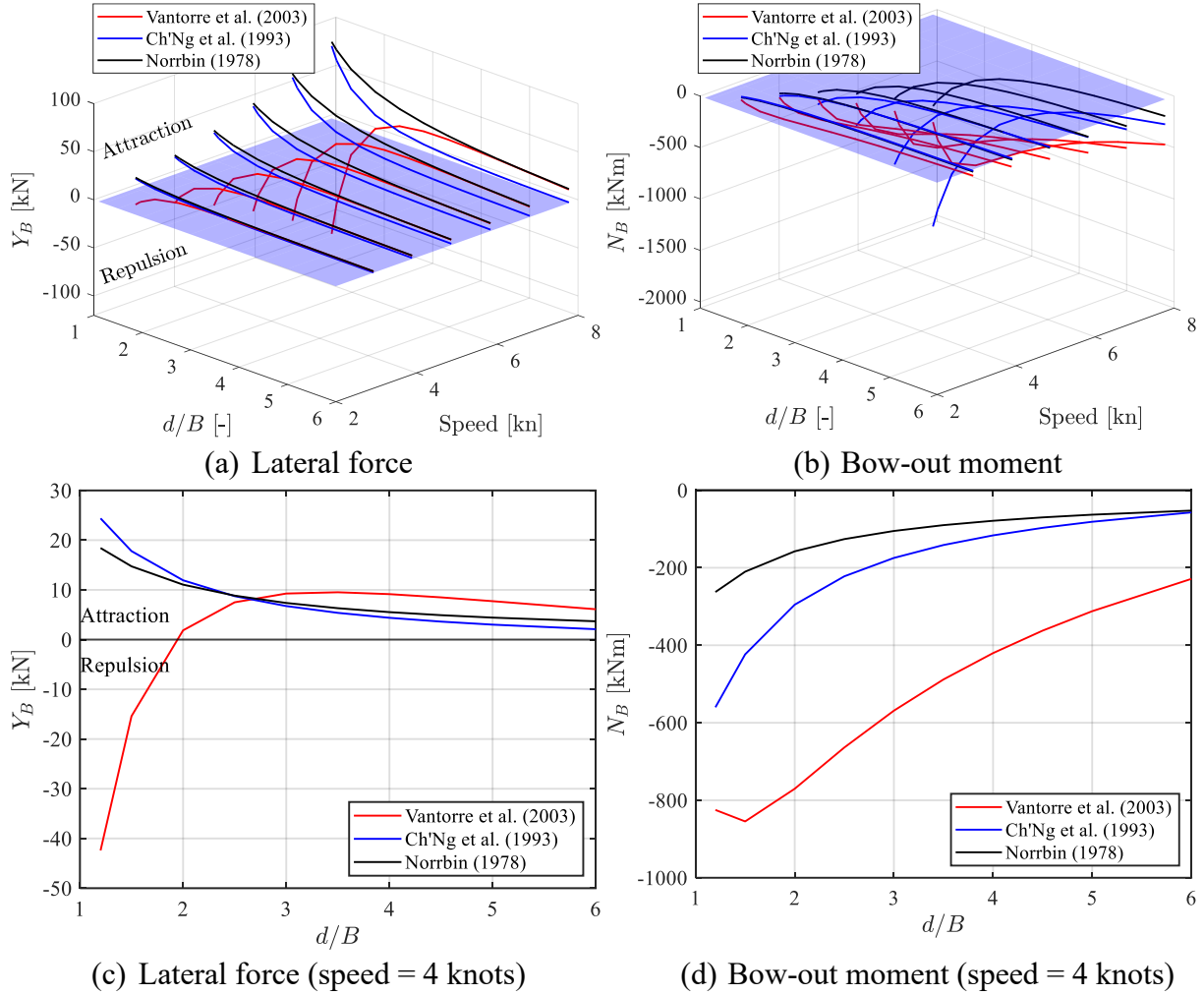


Figure 3.9. Comparison of bank-effect models under a depth-to-draught ratio of  $H/T = 1.5$ : (a) overall lateral force as a function of ship–bank distance  $d/B$  and speed; (b) bow-out moment; (c) cross-sectional view of lateral force at 4 knots, showing the transition between attraction and repulsion zones; (d) cross-sectional view of bow-out moment at 4 knots.

### 3.3.7 Water currents

Currents are a critical factor in inland waterways, affecting vessel dynamics. In sharp river bends or narrow fairways, currents make manoeuvring more complex. In this work, currents follow a near-parabolic distribution along the lateral direction, meaning that flow speeds are higher near the waterway centre and close to zero near the banks. The equations are given as:

$$\begin{aligned} u_r &= u - U_c \cos(\beta_c - \psi) \\ v_{rm} &= v_m - U_c \sin(\beta_c - \psi) \end{aligned} \quad (26)$$

where  $\beta_c$  is the incoming current angle in the earth-fixed coordinate system. The drift angle at midship, which accounts for the difference between the vessel's course and heading, is calculated as  $\beta_m = -\tan^{-1}(v_{rm}/u_r)$ . The total ship speed is given by  $U = \sqrt{u_r^2 + v_{rm}^2}$ . Note that the equations of motion are updated using the vessel's speed through the water.

### 3.4 Control system design for inland vessels

This section introduces the design of guidance and control systems for vessel path-following. The control design includes a comparison of several methods, such as conventional PID and advanced MPC.

#### 3.4.1 Guidance system in confined water

Inland vessels require precise control systems to ensure safe operation in confined waterways, where shallow water effects and river currents can disrupt course stability. To address these challenges, the guidance, navigation, and control (GNC) module developed in this thesis explicitly accounts for such disturbances. The schematic of the path-following GNC module under current conditions is shown in Figure 3.10.

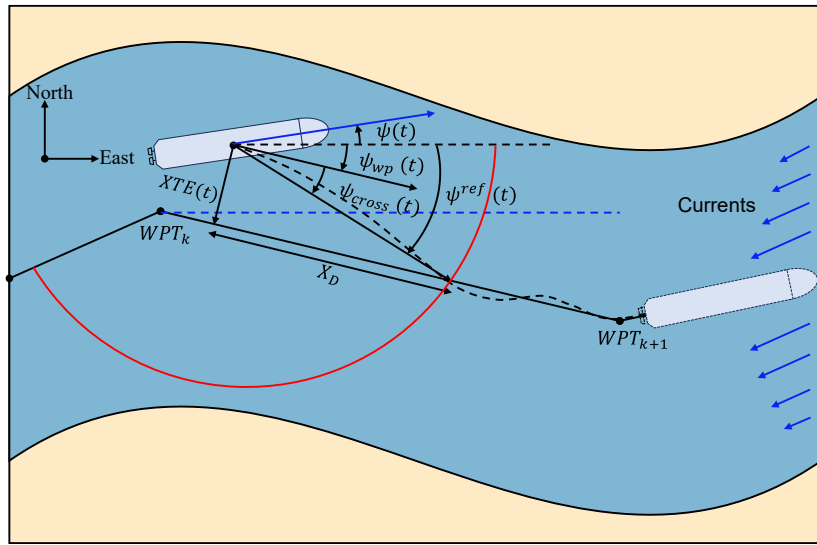


Figure 3.10. Guidance system for path-following control on an inland waterway.

Its main objective is to maintain the vessel's heading along predefined waypoints while minimising cross-track error (XTE) through effective rudder control. Using the vessel's current position and the positions of the waypoints, the reference heading is computed as:

$$\psi^{ref}(t) = \psi_{wp}(t) - \psi_{cross}(t) \quad (27)$$

where  $\psi_{wp}(t)$  represents the reference heading angle, calculated from two consecutive waypoints:

$$\psi_{wp}(t) = \text{atan2}(y_{wp(k+1)} - y_{wp(k)}, x_{wp(k+1)} - x_{wp(k)}) \quad (28)$$

$\psi_{cross}(t)$  is the reference heading component that minimises the cross-track error  $XTE(t)$ , given by:

$$\psi_{cross}(t) = \text{atan2}(SXTE(t), X_D) \quad (29)$$

where  $X_D$  is a predefined lookahead distance corresponding to the reaction distance of the inland water vessel (IWV), depending on the vessel type and dimensions. As noted by Fossen (2011), the lookahead distance can be constant or time-varying. In Papers II, III, and IV, a constant lookahead distance was used, whereas in Paper V, an arc-based varying lookahead

distance was applied to improve trajectory tracking in complex, meandering waterways, as shown in Figure 3.10.

### 3.4.2 Classical PID controller

Figure 3.11 shows the block diagram of the closed-loop heading control using a PID controller. The rudder angle is adjusted at each time step to control the vessel's heading for path-following. The overall equation is given by:

$$\delta_c(t) = K_p \left( \psi_e(t) + T_d(\psi_e(t) - \psi_e(t-1)) + \frac{1}{T_i} \left( \sum_{l=0}^t \psi_{e_l} \right) \right) \quad (30)$$

where  $\psi_e(t)$  is the heading error at the time step  $t$ ,  $K_p$  is the proportional gain, and  $T_d$  and  $T_i$  are the derivative and integral time constants, respectively. The Ziegler–Nichols method (Ziegler & Nichols, 1942) was used to determine optimal values for the control parameters.

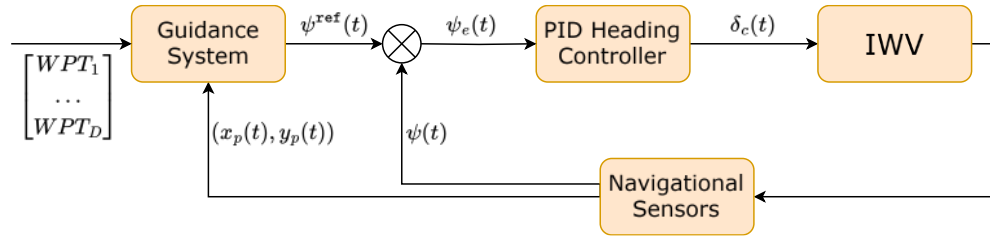


Figure 3.11. Block diagram of the proportional–integral–derivative heading control.

### 3.4.3 Incremental PID controller

In addition to the conventional PID control, an incremental PID controller is introduced to update the rudder angle  $\delta_c$  for complex waterways. The rudder angle is given by:

$$\delta_c(t) = K_p \left( (\psi_e(t) - \psi_e(t-1)) + \frac{T_d}{T_s} (\psi_e(t) - 2\psi_e(t-1) + \psi_e(t-2)) + \frac{T_s}{T_i} \psi_e(t) \right) \quad (31)$$

where  $\psi_e(t)$  is the heading error at the current time step  $t$ ,  $K_p$  is the proportional gain, and  $T_d$  and  $T_i$  are the derivative and integral time constants, same as in the conventional PID.  $T_s$  is the sampling period.

The incremental PID updates the rudder command by adding an increment computed from changes in the error, whereas conventional (positional) PID computes the absolute command directly from the error and its integral/derivative terms. This approach provides improved numerical stability and reduced sensitivity to integral windup, which is particularly beneficial in nonlinear dynamic environments (Åström & Hägglund, 1995).

In Papers III and IV, conventional PID control was used for relatively simplified scenarios, while Paper II employed a further simplified PD-only version for straight-channel conditions. In Paper V, the performance of traditional and incremental PID methods was assessed under river conditions with non-uniform bathymetry and varying currents. Due to its better

adaptability to such complex inland features, incremental PID was implemented in the final simulation framework.

### 3.4.4 Model predictive control

To formulate the nonlinear model predictive control (NMPC) design problem, the IWV dynamics are presented in the state-space notation as:

$$\dot{q}(t) = f(q(t)) + g_1(q(t), u(t)) + g_2(q(t)) \quad (32)$$

where  $q(t)$  denotes the vessel's states and  $u(t)$  is the control input, given by:

$$\begin{aligned} q(t) &= [q_1(t) \quad q_2(t) \quad q_3(t) \quad q_4(t) \quad q_5(t) \quad q_6(t)]^T \\ &= [x_p(t) \quad y_p(t) \quad \psi(t) \quad u(t) \quad v_m(t) \quad r(t)]^T \\ u(t) &= \delta(t) \end{aligned} \quad (33)$$

The function of the vessel states  $f(q(t))$ ,  $g_2(q(t))$ , and of the states and control input are given by:

$$\begin{aligned} f(q(t)) &= \begin{bmatrix} R(q_3(t))v(t) \\ -M^{-1}(D - \tau_e) \end{bmatrix} \\ g_1(q(t), u(t)) &= \begin{bmatrix} \mathbf{0} \\ M^{-1}\tau_c \end{bmatrix} \\ g_2(q(t)) &= \begin{bmatrix} \mathbf{0} \\ M^{-1}\tau_o \end{bmatrix} \end{aligned} \quad (34)$$

where  $M$  denotes the mass matrix,  $D$  is the damping matrix,  $\tau_e$  denotes the forces and moments on the hull and from bank effects,  $\tau_c$  represents the rudder forces and moments, and  $\tau_o$  is the propeller force with a constant rotation speed, given as:

$$\begin{aligned} M &= \begin{bmatrix} (m + m_x) & 0 & 0 \\ 0 & (m + m_x) & x_G m \\ 0 & x_G m & (I_z + x_G^2 m + J_z) \end{bmatrix} \\ D &= \begin{bmatrix} -(m + m_y)q_5(t)q_6(t) - x_G m q_6(t)^2 \\ (m + m_x)q_4(t)q_6(t) \\ x_G m q_4(t)q_6(t) \end{bmatrix} \end{aligned} \quad (35)$$

$$\tau_e = \begin{bmatrix} X_H + X_B \\ Y_H + Y_B \\ N_H + N_B \end{bmatrix}, \tau_c = \begin{bmatrix} X_R \\ Y_R \\ N_R \end{bmatrix}, \tau_o = \begin{bmatrix} X_P \\ 0 \\ 0 \end{bmatrix}, R(q_3(t)) = \begin{bmatrix} \cos(q_3(t)) & -\sin(q_3(t)) & 0 \\ \sin(q_3(t)) & \cos(q_3(t)) & 0 \\ 0 & 0 & 1 \end{bmatrix}$$

In addition,  $v$  represents the generalised velocity vectors, given by:

$$v(t) = [q_4(t) \quad q_5(t) \quad q_6(t)]^T = [u(t) \quad v_m(t) \quad r(t)]^T \quad (36)$$

Equation (32) is discretised using the specified sampling time to serve as the prediction model in NMPC, resulting in the following discrete-time IWV dynamics:

$$q_c(k+1) = f_c(q_c(k)) + g_{1c}(q_c(k), u_c(k)) + g_{2c}(q_c(k)) \quad (37)$$

where the subscript  $(\cdot)_c$  represents the variables used in the vessel's prediction model, and  $k$  is the discrete time step. Hence, the constraints on the state variables and the control inputs are given as follows:

$$\begin{aligned} \psi_{min} &\leq q_{3c}(k) \leq \psi_{max} \\ u_{min} &\leq q_{4c}(k) \leq u_{max} \\ v_{min} &\leq q_{5c}(k) \leq v_{max} \\ r_{min} &\leq q_{6c}(k) \leq r_{max} \\ \delta_{min} &\leq u_c(k) \leq \delta_{max} \end{aligned} \quad (38)$$

As shown in Figure 3.12, the NMPC optimal control problem is formulated as a nonlinear programming problem with multiple shooting over a finite horizon  $N_h$ . At every time step  $k$ , the controller solves the following optimisation problem:

$$\begin{aligned} NMPC(q_{3c}(k), \psi^{ref}(k)) &= \underset{q_{3c}, u_c}{arg\ min} \left( q_{3c}(N_h|k) - \psi^{ref}(N_h|k) \right)^2 p_m \\ &+ \sum_{h=0}^{N_h-1} \frac{1}{2} \left( q_{3c}(h|k) - \psi^{ref}(h|k) \right)^2 q_m + u_c^2(h|k) r_m \end{aligned} \quad (39)$$

where the scalar values  $p_m$ ,  $q_m$ , and  $r_m$  are the controller weights;  $h$  is the time step over the prediction horizon, with  $0 \leq h \leq N_h - 1$ ; and  $h|k$  refers to the prediction at the step  $h$ , performed at the global time step  $k$ . The objective function consists of a running cost and a terminal cost that minimise the heading error. The running cost also minimises control efforts.

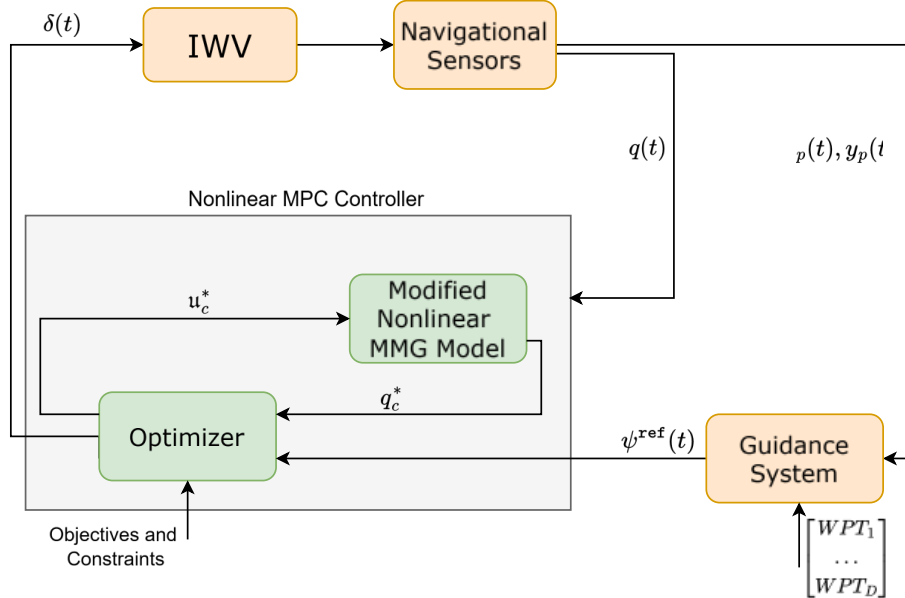


Figure 3.12. Block diagram of model predictive control-based heading control (Zhang et al., 2025a).

Therefore, the solution of the NMPC at the  $k^{\text{th}}$  time step is the sequence of optimal rudder angles and the corresponding vessel states, given as:

$$(u_c^*, q_{3c}^*) = \text{NMPC} \left( q_{3c}(k), \psi^{\text{ref}}(k) \right) \quad (40)$$

The development of the NMPC is presented in Paper IV, with comparisons against conventional PID control in terms of tracking error and control effort. Some selected results are showcased and discussed in chapter 4.

### 3.5 River hydraulics modelling

Accurate hydraulics modelling is essential for analysing vessel motion and energy use in constrained inland waterways. Such models incorporate bathymetric data and varying currents, all of which influence manoeuvring performance and control strategy development (Odgaard, 1989; Rhoads, 2020). To generate a simulation environment that captures the physical characteristics of natural inland waterways, Paper V proposes a novel hydraulic model for the rapid generation of meandering waterways, including predictions of cross-sectional (bathymetric) changes.

#### 3.5.1 Cross-sectional shift modelling

A meandering river can be constructed by combining straight and curved sections of varying sizes (Fossen, 2011; Paulig & Okhrin, 2024). The model follows this approach: the waterway is generated using a sequence of segments, as illustrated in Figure 3.13.

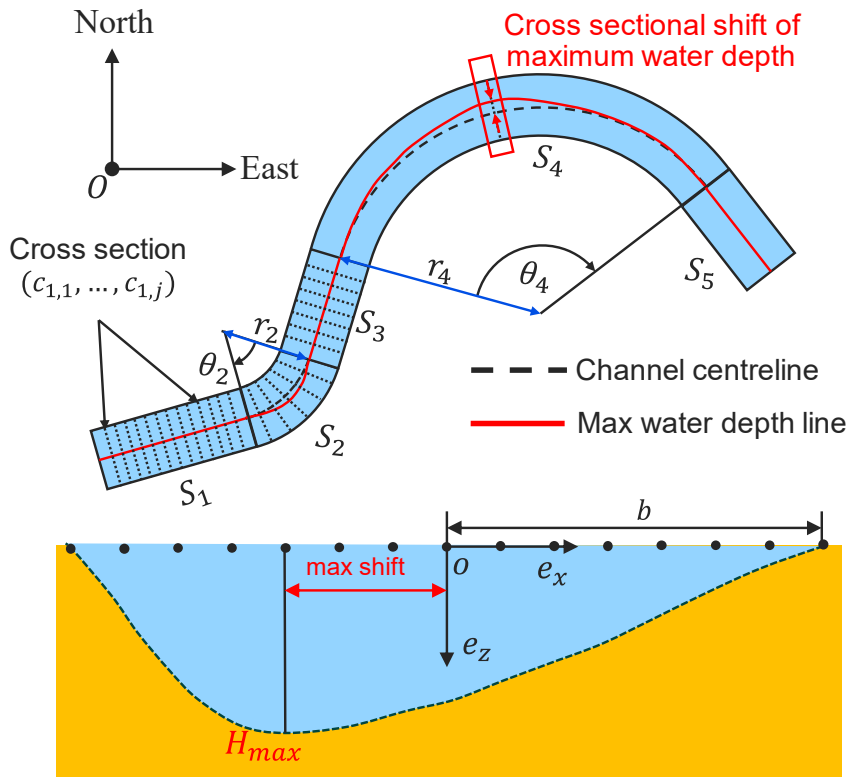


Figure 3.13. Schematics of waterway generation with cross-sectional shift modelling.

Each segment is discretised into cross-sections ( $S_1, S_2, \dots, S_i$ ), with grid points uniformly distributed according to the local geometry. Straight segments are parameterised by their length, with the initial segment additionally defined by a starting orientation. Curved sections are determined by the radius  $r_i$  and segmental angle  $\theta_i$ . Each new segment is transformed to attach to and align with the end cross-section of the previous segment, maintaining continuity and geometric consistency.

To represent the morphological changes of riverbeds, a new parametric formula is proposed as a function of curvature, bend radius, and segment location. The depth profile is modelled using the following equation:

$$h_{i,j} = (1 + \varepsilon_h)H_{max} \left( \frac{e_z}{\min(e_z)} \right) \quad (41)$$

where  $h_{i,j}$  represents the water depth of the cross-section  $j$  in the  $i^{\text{th}}$  segment,  $\varepsilon_h$  is a random perturbation following a normal distribution with a standard deviation of 0.1,  $H_{max}$  is the maximum depth of the cross-section, and  $e_z$  is the shape function of the riverbed in the vertical direction (see Figure 3.13). It is calculated as:

$$e_z = - \left( 1 - \left( \frac{e_x}{b} \right)^2 \right) \left( 1 + \gamma_{i,j} \left( \frac{e_x}{b} \right) \right) \quad (42)$$

where  $e_x$  is the lateral coordinate in the local frame of each cross-section,  $b$  is the half-width of the channel, and  $\gamma_{i,j}$  is a skewing factor that calculates the cross-sectional shift depending on the waterway shape:

$$\gamma_{i,j} = \alpha \left( \frac{\theta_i}{\max(\theta)} \right) \left( 1 - \left( \frac{\Delta i,j}{(r_i \cdot \theta_i)/2} \right)^2 \right) \quad (43)$$

Here,  $\alpha$  is a constant determining the segment curvature direction ( $\alpha \in [-1,0,1]$ ), with 0 for straight segments,  $-1$  for leftward curves, and 1 for rightward curves. Further,  $\theta_i$  is the segment angle,  $\Delta i,j$  is the arc distance between cross-section  $j$  and the segment's mid-section (see red box), and  $r_i$  is the segment radius. The equation indicates that the maximum bathymetric shift occurs at the middle of a curved segment.

### 3.5.2 Current modelling

In river meanders, the distribution of depth-averaged current velocity across a cross-section generally follows the corresponding water depth (Odgaard, 1989). Using a similar approach to the cross-sectional modelling, the current velocity is formulated to align with the depth profile, allowing a simplified representation of flow asymmetry near inner and outer bends. The current velocity is expressed as:

$$u_{c_{i,j}} = (1 + \varepsilon_c)u_{max} \frac{\left( - \left( 1 - \left( \frac{e_x}{b} \right)^2 \right) \left( 1 + \gamma_{i,j} \left( \frac{e_x}{b} \right) \right) \right)}{\min(e_z)} \quad (44)$$

where,  $u_{max}$  is the maximum flow velocity and  $\varepsilon_c$  is a random disturbance representing uncertainties in flow speed. In straight segments, the current distribution along the transverse direction is nearly parabolic. In curved segments, the maximum flow speed is determined by the depth profile. The flow direction is assumed perpendicular to each cross-section, meaning vortex or secondary flows are not modelled and are therefore neglected.

### 3.6 Energy optimisation

Energy-efficient operation is critical for inland vessels, especially for future autonomous vessels that may rely on battery power. Adjusting vessel speed according to environmental and navigational conditions can yield substantial energy savings in constrained waterways. This section describes the energy optimisation module developed within the VPF framework, which supports automated onboard decision-making.

#### 3.6.1 Particle swarm algorithm

Given the geographical limitations of inland waterways, vessel routes are generally fixed. Consequently, optimisation efforts focus on operational strategies, such as adjusting speed profiles along predefined tracks based on environmental conditions. In this thesis, a particle swarm optimisation (PSO) algorithm is applied to determine the energy-efficient speed profile. PSO is a population-based method that iteratively improves candidate solutions by simulating collective behaviour within a search space (Kennedy & Eberhart, 1995).

Figure 3.14 illustrates the optimisation process of the PSO algorithm. During optimisation, each particle records two key elements: its best-found position (personal best,  $pbest_i^t$ ) and the global best position identified by the swarm (global best,  $gbest^t$ ) at time  $t$ . Each particle updates its velocity and position using this information. The velocity is influenced by both individual experience and swarm knowledge, while the new position is computed relative to the personal and global bests. The update equations are:

$$\begin{aligned} v_i^{t+1} &= \omega v_i^t + c_1 r_1 (pbest_i^t - x_i^t) + c_2 r_2 (gbest^t - x_i^t) \\ x_i^{(t+1)} &= x_i^t + v_i^{(t+1)} \end{aligned} \quad (45)$$

where  $\omega$  is the inertia weight,  $c_1$  and  $c_2$  are the particle cognition and social acceleration coefficients,  $r_1$  and  $r_2$  are random values between 0 and 1, and  $x_i^{(t+1)}$  is the updated particle position.

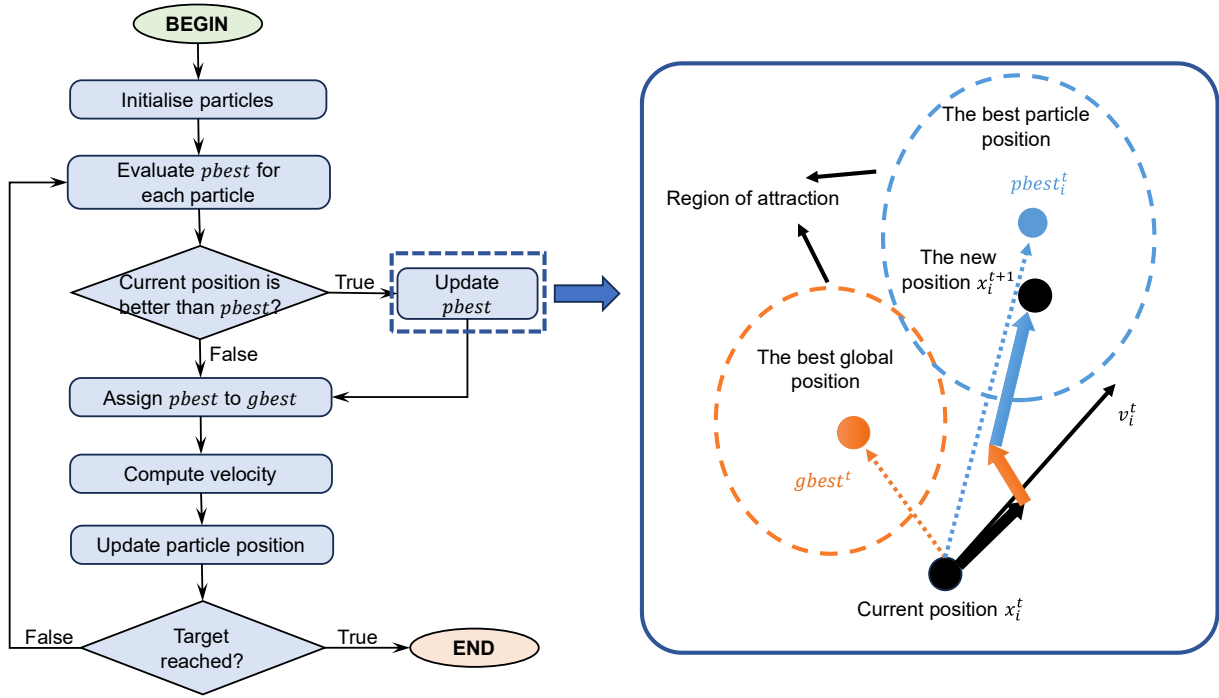


Figure 3.14. Schematic of the particle swarm optimisation process.

The route is discretised into sequential waypoints, and a swarm is initialised, with each particle representing a candidate speed profile along the route. The objective is to minimise fuel consumption while satisfying the estimated time of arrival (ETA) constraint. A dynamic inertia weight is applied to improve convergence towards the global optimum during iterations:

$$\omega = \omega_{max} - t((\omega_{max} - \omega_{min})/T) \quad (46)$$

### 3.6.2 Energy optimisation in inland waterways

Using the PSO algorithm, the schematics of energy optimisation for inland vessels are illustrated in Figure 3.15. The waypoints are mapped into the solution space, incorporating local factors that influence fuel consumption, such as water depth, ship–bank distance, and current velocity. With ship speeds specified at each waypoint and the engine model incorporated, the fuel cost function for each leg ( $FC_{leg}$ ) is established. The objective of the PSO algorithm is to adjust the ship speed at each waypoint to: (a) minimise total energy consumption ( $FC_{sum}$ ) over the entire route, and (b) ensure the total sailing time satisfies the ETA constraints, calculated based on a fixed reference ship speed.

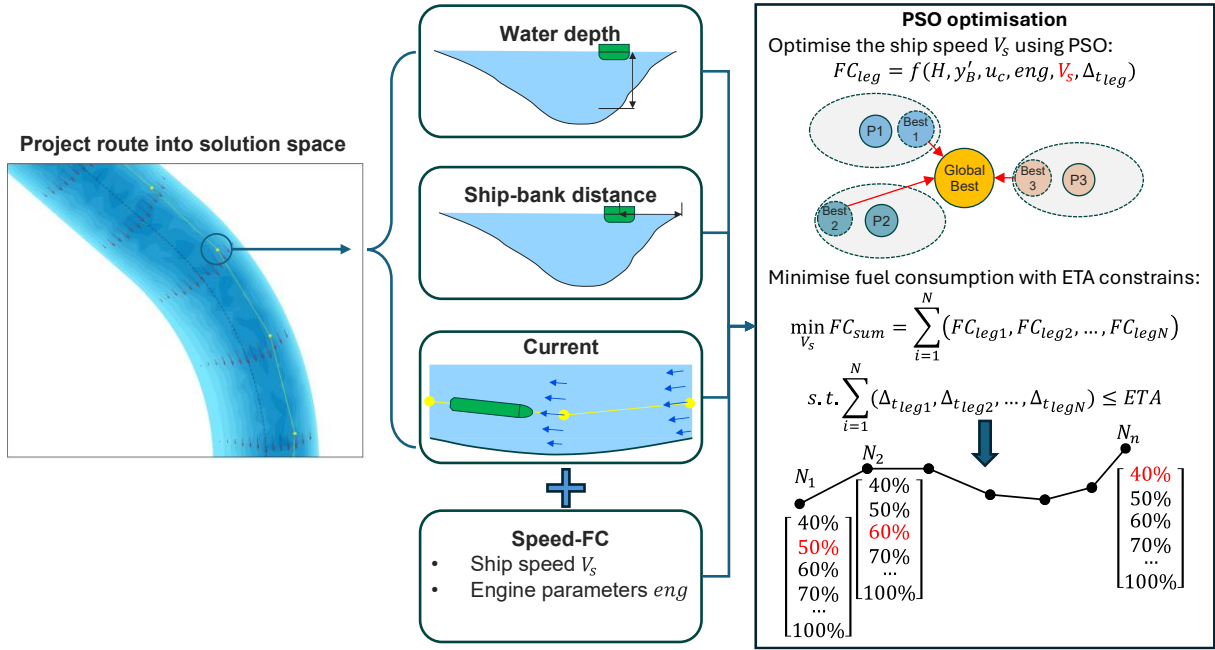


Figure 3.15. Illustration of the particle swarm optimisation algorithm for ship energy optimisation in inland waterways.

The performance of swarm-based algorithms is sensitive to initialisation. To assess this effect, the initial speed profile is generated based on the water depth along the route. Ship speeds are selected within 60–90% of the maximum speed and reduced according to an exponential function:

$$V_i = \begin{cases} 0.6 \cdot V_{MAX} & (r_i \leq 1.2) \\ 0.6 \cdot V_{MAX} \cdot (0.6 + 0.3 \cdot (1 - e^{-\alpha \cdot (r_i - 1.2)})) & (1.2 < r_i \leq 3.0) \\ 0.9 \cdot V_{MAX} & (r_i > 3) \end{cases} \quad (47)$$

where  $r_i$  is the depth-to-draft ratio at waypoint  $i$  ( $r_i = H_i/T$ ), and  $\alpha$  is a factor controlling the rate of speed reduction with respect to water depth (assumed to be 1 in this study). The detailed initialisation process is presented in Paper V.

### 3.7 System integration of the voyage planning framework

Figure 3.16 presents the overall diagram of the VPF, illustrating the integration and interaction of its sub-models and modules. The process begins with the hydraulic model, which generates a waterway map incorporating bathymetry and current profiles to serve as the simulation environment. Once the route and operational mode are defined, path-following control is performed. Based on the control commands, the vessel's state is updated using the manoeuvring model that developed for confined waterways. Upon reaching the endpoint or destination, the vessel's operational data that including trajectory and a sequence of historical states is recorded, enabling the calculation of dynamic energy consumption. The vessel's performance is then evaluated through analysis of tracking accuracy and energy use. Finally, the route and corresponding energy data are used to conduct the optimisation process.

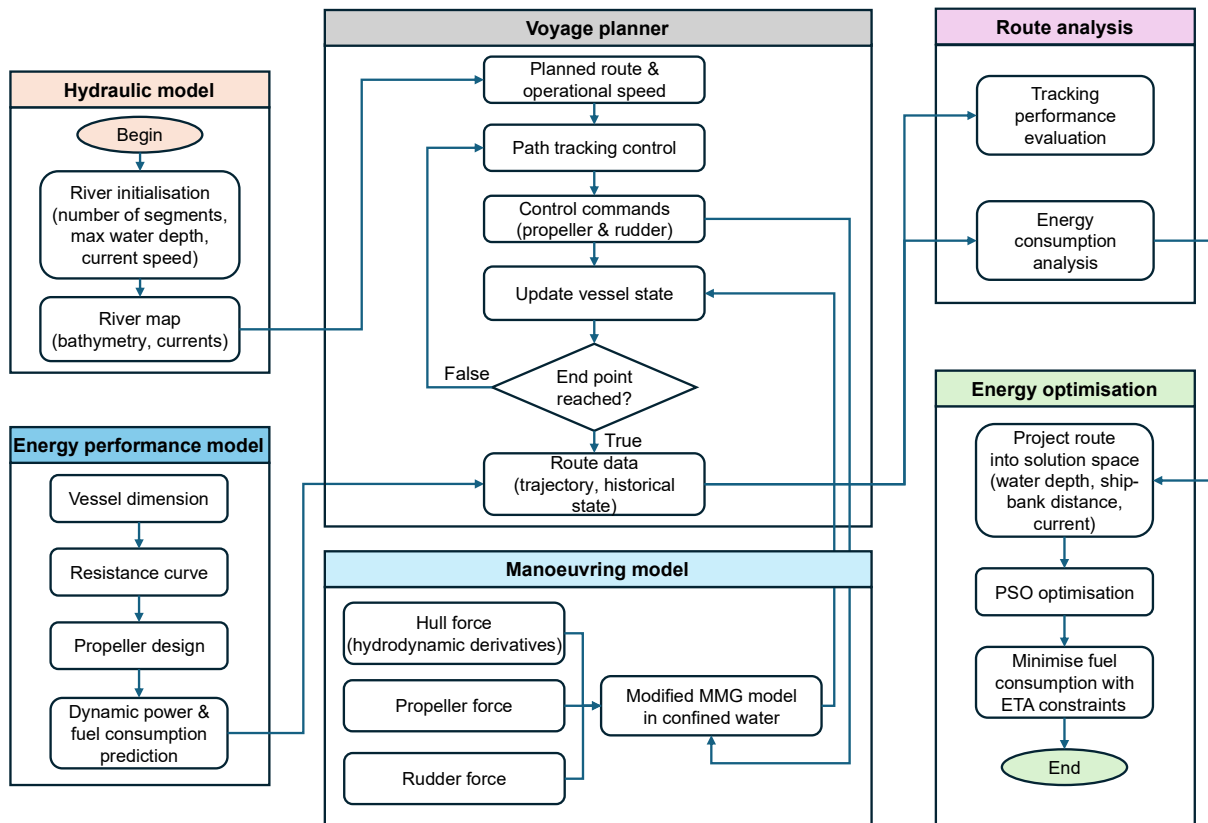


Figure 3.16. Overall block diagram showing the interactions between the sub-models in the voyage planning framework.

## 4 Summary of appended papers

This chapter summarises the main results and findings from the research presented in the appended papers.

### 4.1 Paper I – Energy performance modelling of IWV

Paper I presents the development of ShipCLEAN-IWV, an extended version of the ShipCLEAN energy performance model tailored for inland vessels, with the model structure summarised in section 3.2. The main contribution of this study is to propose a physics-based ship energy-prediction model for rapid, accurate analysis of resistance, power, and energy consumption in shallow and confined waters, particularly useful in the early design stage with limited inputs.

While retaining the modular architecture originally designed for sea-going applications in ShipCLEAN, the modified ShipCLEAN-IWV model incorporates dedicated methods to account for confined waterway effects and vessel-specific characteristics relevant to inland navigation. The resistance module was refined using empirical formulations to capture shallow water influences, and the results showed strong agreement with experimental measurements. Power prediction was validated against published data to ensure modelling accuracy. To demonstrate the model’s applicability under realistic operational conditions, a case study was conducted using data from inland waterway segments of the Seine River with varying water depths and widths. The analysis highlights how vessel loading and ship–bank distances influence energy consumption.

#### 4.1.1 Resistance prediction and validation

The accuracy of resistance prediction plays a key role in reliable power estimations. The proposed resistance formula combines a modified calm-water resistance formulation, primarily addressing the viscous component, with additional terms accounting for squat and bank-induced drag. A validation study based on experimental data from a scaled self-propelled vessel (Mucha et al., 2018) is shown in Figure 4.1.

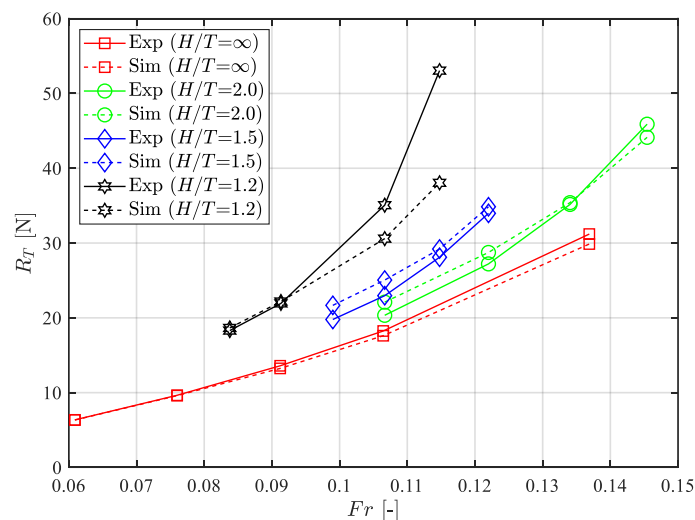


Figure 4.1. Resistance results of a 135 m inland vessel, adapted from Zhang et al. (2023).

The results indicate that the model predictions align well with the test data and capture the changes in resistance across different water depths. Some deviations are observed at high speeds

in very shallow water ( $H/T = 1.2$ ), due to the absence of a correction for wave-making resistance. Nevertheless, such conditions are typically avoided in practice, as inland vessels tend to reduce speed in low water levels to mitigate grounding risks associated with squat. The resistance characteristics of another classical inland vessel type – pusher–barge systems – were evaluated using towing tank data from convoys with varying barge arrangements (Zentari et al., 2022), as shown in Figure 4.2.

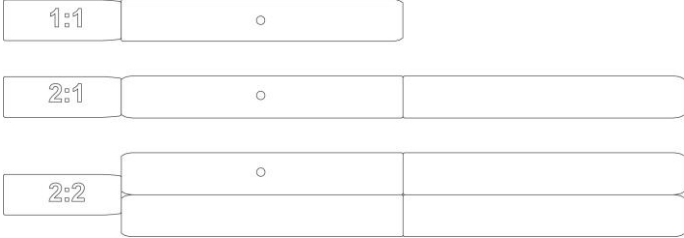


Figure 4.2. Configuration of pusher–barge convoys, adapted from (Zentari et al., 2022).

As shown in Figure 4.3, the model predictions align well with the experimental range. Resistance increases as water depth decreases, with a significant rise observed under extremely shallow conditions.

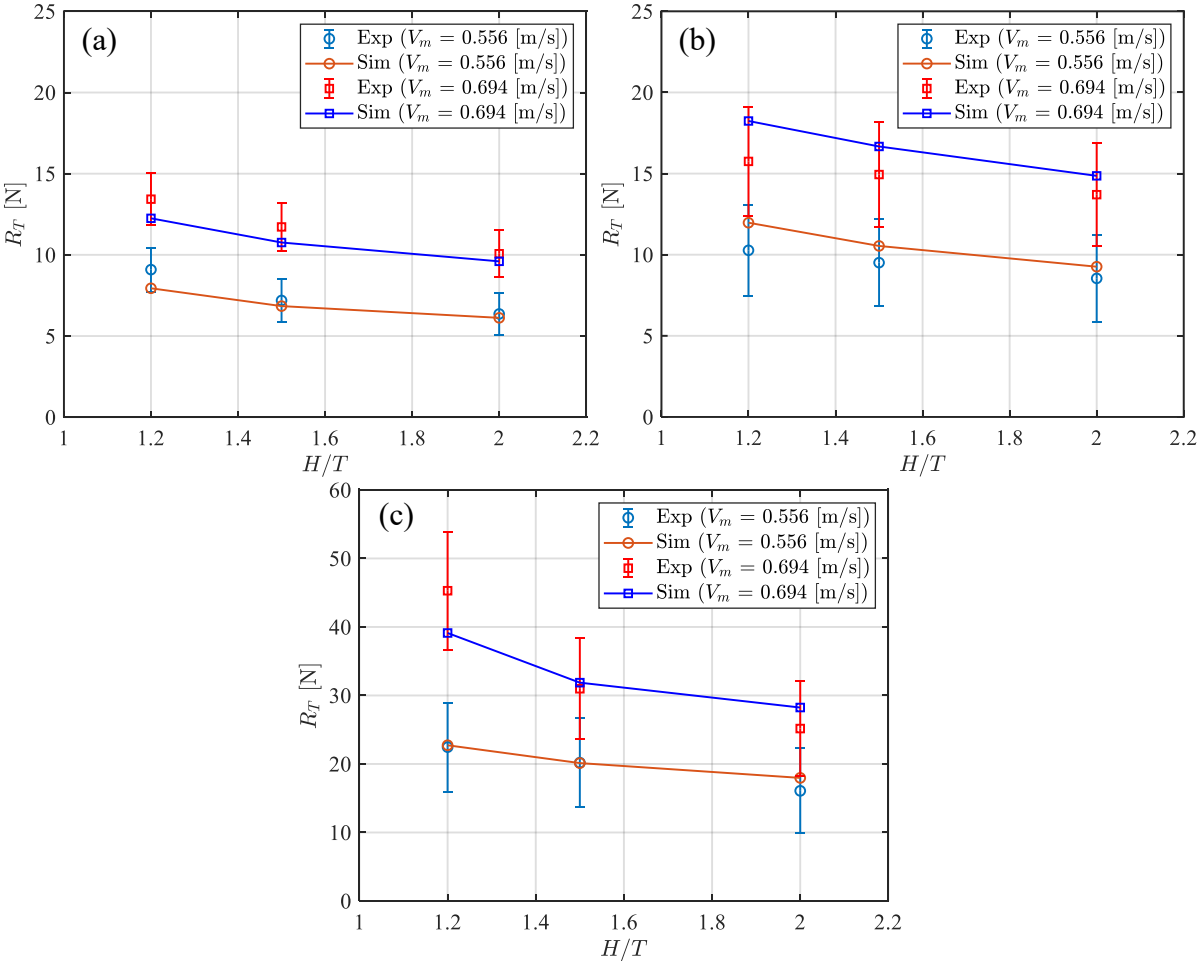


Figure 4.3. Resistance prediction of the pusher–barge convoy in three configurations.

In this case, additional drag results from complex interactions and gap effects between units; the gap between a pusher and a single barge alone can contribute up to 6% of total resistance (Zentari et al., 2023). However, an accurate prediction of these effects is strongly influenced by the hull form of both the pusher and barges connected, and depending on operating speed and water depth, which are beyond the scope and capacity of the current model.

#### 4.1.2 Operational analysis

The dynamic operational analysis was conducted using an inland cargo vessel with a length of 135 m, a beam of 11.45 m, and a design draft of 3.2 m at 90% loading. Water depth values ( $H$ ) were derived from sectional measurements of the Seine River based on data reported by Linde (2017), while the corresponding channel widths ( $W_C$ ) were obtained from the MERIT Hydro database (Yamazaki et al., 2019). Using these waterway profiles, current speeds along the route were estimated from recorded discharge rates, as shown in Figure 4.4.

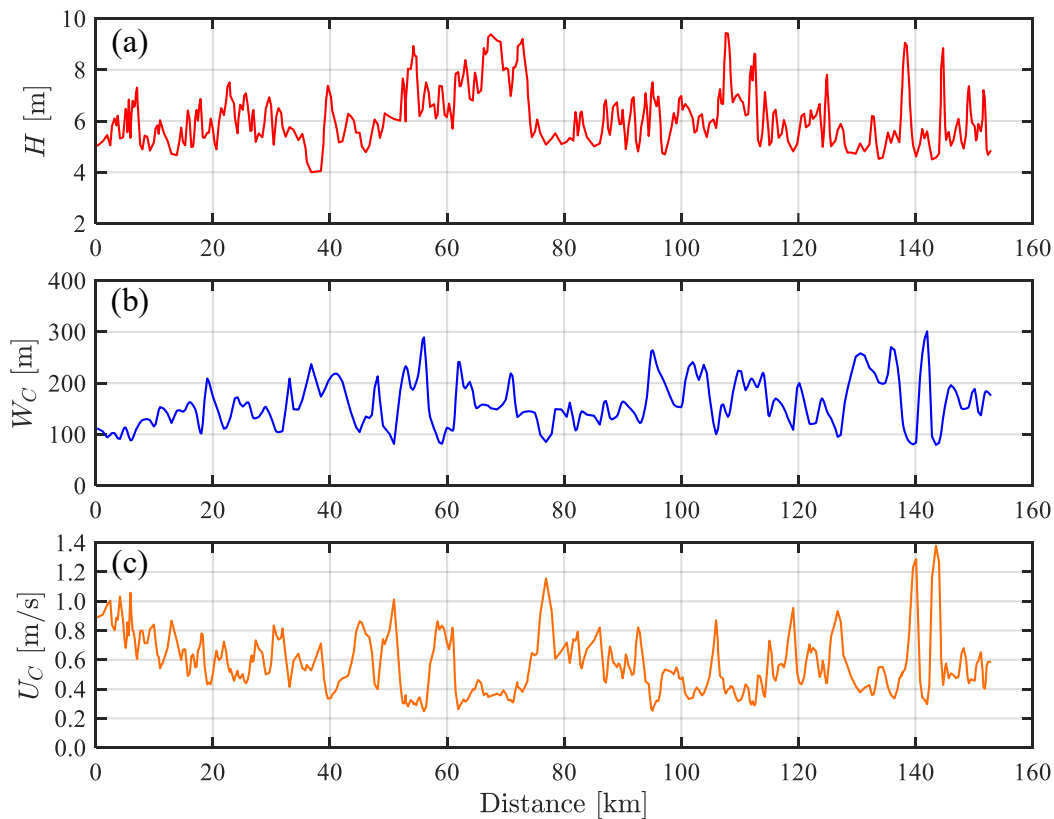


Figure 4.4. Waterway data of the selected reach with a length of 153 km.

Figure 4.5 presents the power output alongside the corresponding instantaneous fuel consumption. The results highlight the strong sensitivity of propulsion power to draught under shallow water conditions. At 40% loading, the shallowest water depth causes a 70% increase in power demand, resulting in a marked rise in fuel consumption. This effect is even more pronounced at full loading, where power requirements can become double compared to deeper water scenarios.

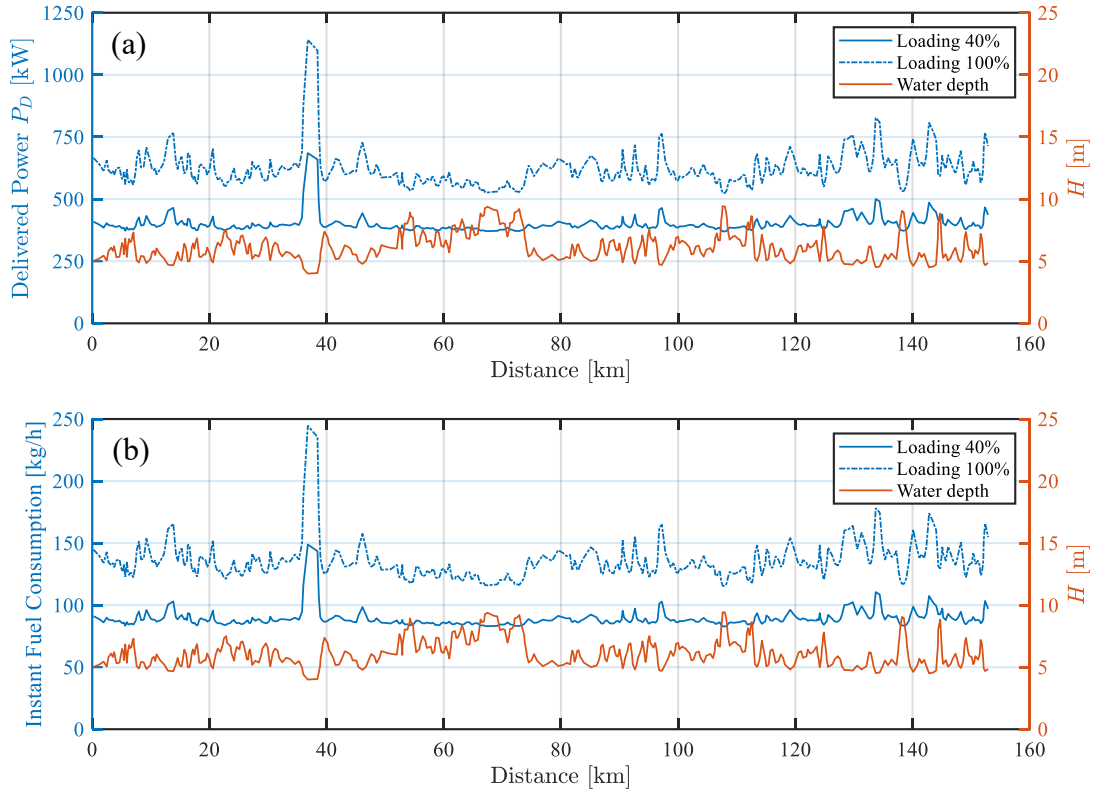


Figure 4.5. Predicted power output and fuel consumption rate based on the waterway data.

Beyond water depth, the influence of ship–bank distance on fuel consumption was examined (see Figure 4.6). Here,  $d_1$  and  $d_2$  represent the ship–bank distance as half and one-quarter of the channel width, respectively. As highlighted by the blue bounding box, resistance increases markedly when the vessel operates close to the bank. Overall, however, the bank effect has a relatively minor impact on the vessel’s fuel consumption compared with the influence of shallow water.

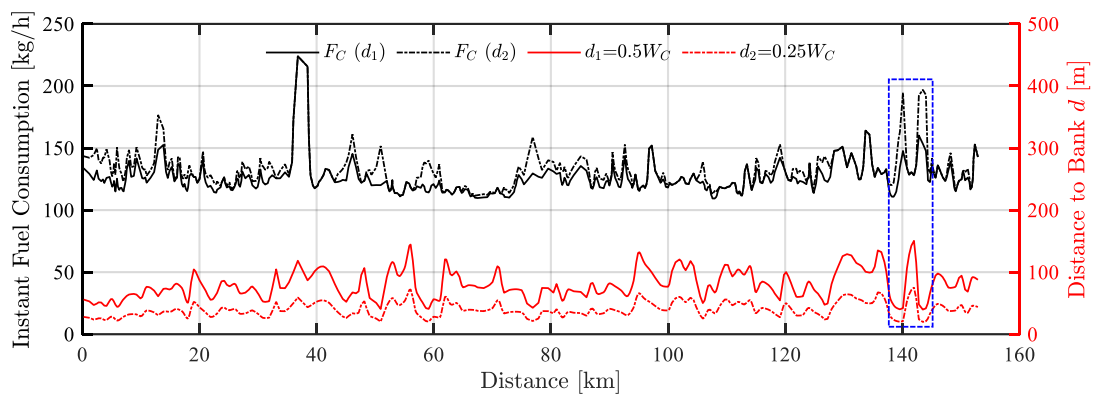


Figure 4.6. Impact of the ship–bank distance on fuel consumption rate.

## 4.2 Paper II – Manoeuvring modelling

Paper II introduces a manoeuvring model tailored for inland vessels, developed based on the 3-DoF MMG ship manoeuvring model. The main improvement of the model is to incorporate both shallow water corrections and a mathematical formulation for bank effects, enabling realistic prediction of vessel behaviour in confined environments. The main methodology and model development are presented in section 3.3.

A verification study was conducted using published hydrodynamic derivatives of a pusher-barge convoy to simulate turning manoeuvres. This was followed by a systematic investigation of bank effects on vessel trajectory without rudder input, under varying water depths, lateral distances, and propeller speeds. To assess the effectiveness of control implementation, a case study examined the rudder controller’s ability to counteract bank-induced forces while maintaining the intended course in straight channels.

### 4.2.1 Turning test validation

Validation of the manoeuvring model was carried out using experimental data from a pusher-barge model in calm water, without accounting for bank effects. The objective was to assess the model’s accuracy using hydrodynamic derivatives from publicly available literature. Turning simulations were performed at rudder angles of  $\delta = 35^\circ$  and  $\delta = 20^\circ$ , with a model speed of 0.364 m/s (equivalent to 5 knots full scale). In the original reference study by Koh and Yasukawa (2012), the fourth-order derivative  $X'_{\beta\beta\beta\beta}$  was omitted. Figure 4.7 and Figure 4.8 present selected turning results for the given rudder angles, where the red line denotes simulation results from the developed manoeuvring model. Overall, the model captures the vessel’s manoeuvring behaviour well, and it was observed that the pusher-barge exhibited enhanced turning capability from medium ( $H/T = 1.5$ ) to extremely shallow water ( $H/T = 1.2$ ). Relevant research (Liu et al., 2015; Yasukawa & Kobayashi, 1995; Yoshimura & Sakurai, 1989) indicate this phenomenon is a common characteristic of wide-beam ships, which is also exhibited by the pusher.

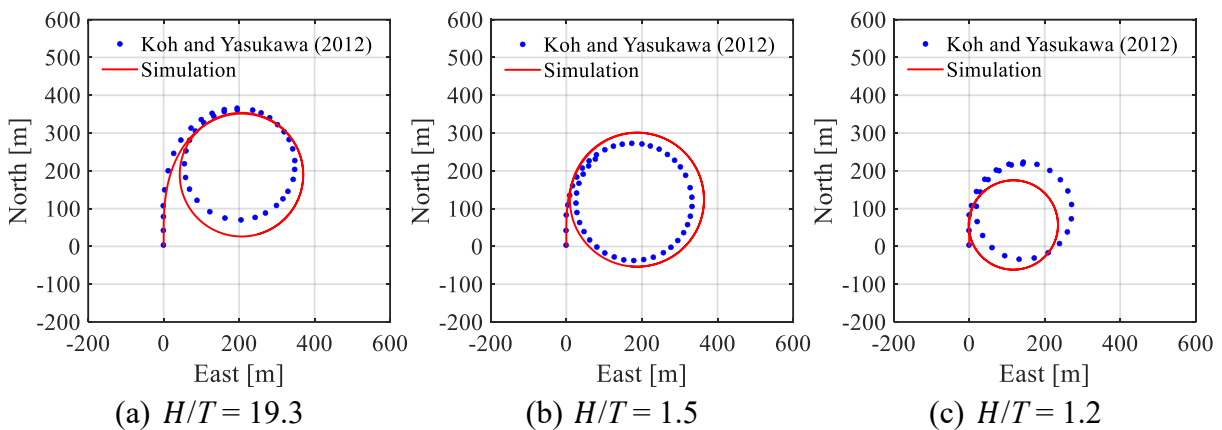


Figure 4.7. Turning simulation validation at  $\delta = 35^\circ$ .

The deviations observed in the turning circle, such as in Figure 4.8(b), may result from the empirical formula underestimating the rudder normal force or from missing parameters in the literature. The coordinates of the CoG and the relative positions of the propeller and rudder were based on assumptions, as some data were missing in the original study. Differences

between these assumed locations and those of the original ship model may lead to deviations in the computed rudder normal force.

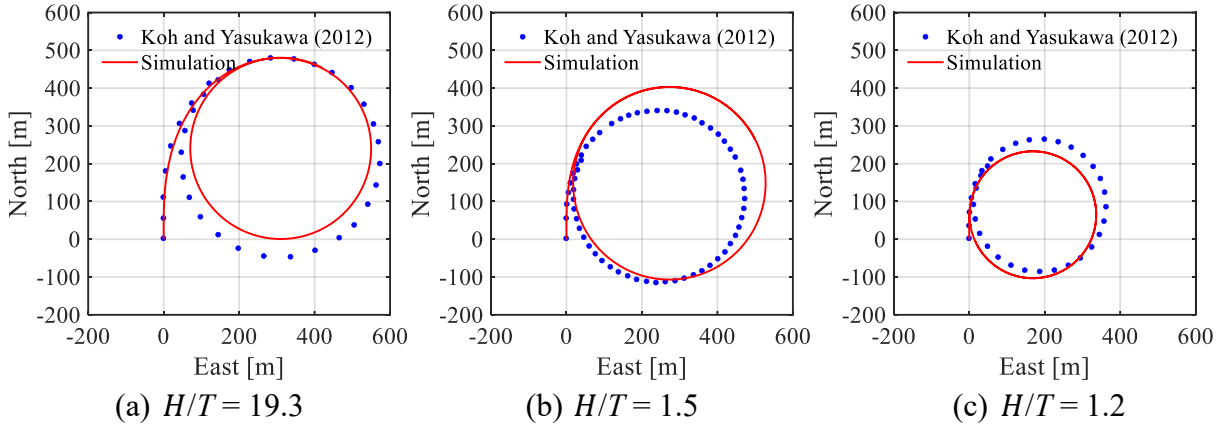


Figure 4.8. Turning simulation validation at  $\delta = 20^\circ$ .

#### 4.2.2 Bank effect simulation

To quantify the influences of bank effects on ship motion, dedicated simulations were conducted without rudder compensation. The trajectories were calculated using the manoeuvring model that includes the bank effects term regarding lateral force and moments (Zhang et al., 2024b). As shown in Figure 4.9, the vessel was modelled to navigate a straight 100 m-wide channel, with varying initial starboard-bank distances,  $y_S$ . For all scenarios, the simulation duration was fixed at 140 s. The results indicate that when sailing near the channel centre, the bank effect is minimal. However, as  $y_S$  decreases, the bow-out motion induced by asymmetric flow between the port and starboard sides becomes more pronounced, leading to noticeable course deviations. In extreme cases, such hydrodynamic effects may result in a potential risk of collision with the opposite bank, as illustrated in Figure 4.9(d).

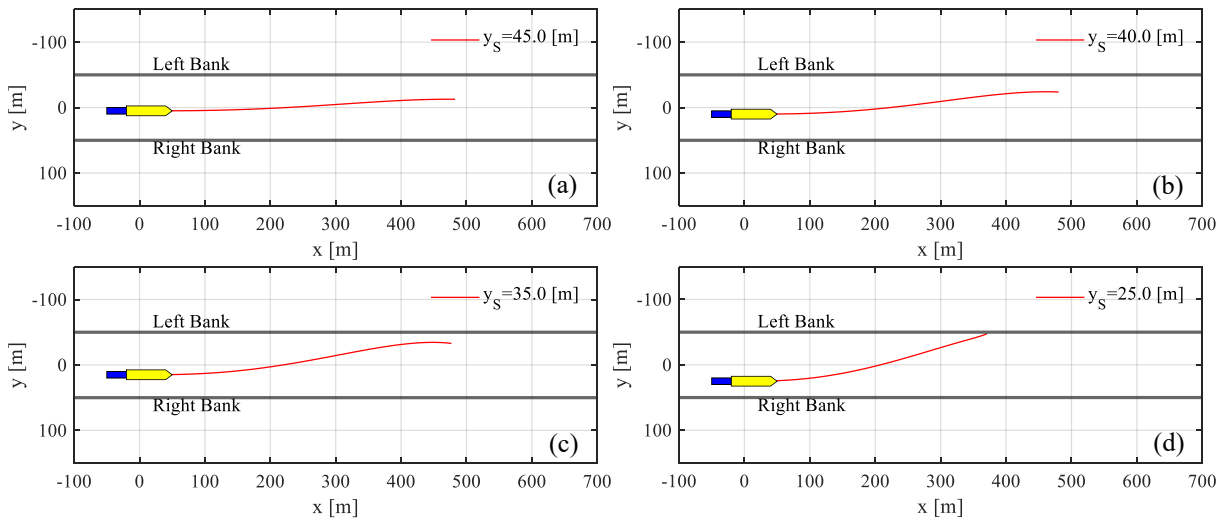


Figure 4.9. Ship trajectories under varying starboard-bank distance  $y_S$  illustrating bank effects.

It is also observed from the trajectories that, once the vessel passes the channel centreline, the left bank experiences new lateral forces and yaw moments in the opposite direction. This results

in bow-out motions from the port side, and the vessel shows zig-zag trajectories around the centreline. Such a phenomenon can be explained by the bank model in subsection 3.3.6. In Eq. (24), the nondimensional distances  $y_B$  are calculated according to the relative ship–bank distance from starboard ( $y_s$ ) and portside ( $y_p = y_s - W_C$ ). Therefore, the bank effect will be counteracted from both sides if the ship sails at the waterway centre. During near-bank operations, the direction of lateral effects depends on the relative location of each side of the banks. However, the vessel still has a high risk of collision with the left bank if the initial bow-out effect is significant, and if the initial ship–bank distance is too short, as shown in Figure 4.9 (d).

Figure 4.10 presents the ship motion under bank disturbances at varying water depths. The influence of bank effects is particularly pronounced in shallow water. The vessel experiences significant bow-out moments, especially in the extreme shallow water case ( $H/T = 1.2$ ). Additionally, reduced ship–bank distances amplify these disturbances, as shown in Figure 4.10(b).

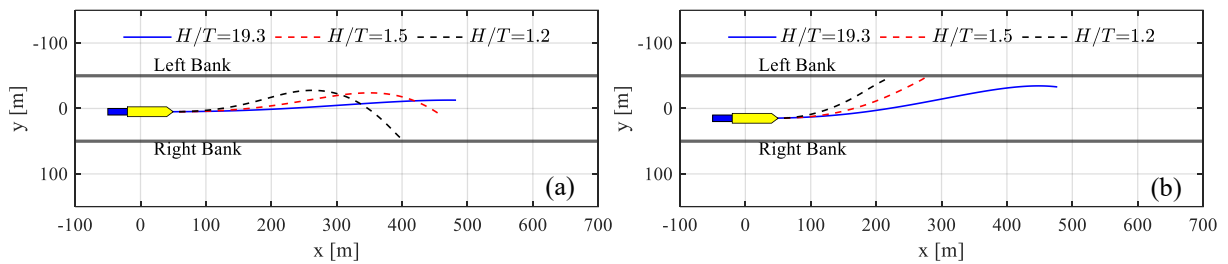


Figure 4.10. Ship trajectories with varying water depth: (a)  $y_s = 45$  m and (b)  $y_s = 35$  m.

Additionally, the influence of the operating propeller was also examined and quantified. Simulations show that higher propeller speeds increase the hydrodynamic load on the hull, thereby raising the risk of shoreline collision (see Figure 4.11). As indicated by the bank effect model in Vantorre et al. (2003), the magnitude of the hydrodynamic effect increases with propeller rpm, resulting in higher bank-induced forces and moments that influence vessel manoeuvring. As indicated in Eq. (25), the impact of propeller action on the ship–bank interaction forces and moments is decomposed into  $Y_B^P$ ,  $N_B^P$  (bollard pull conditions) and  $Y_B^{HP}$ ,  $N_B^{HP}$  (effect of propulsion combined with forward speed). Therefore, increasing the rpm will result in higher thrust, which increases the reference velocity  $V_T$  and ship speed, leading to a significant increase in both the side forces and yaw moments.

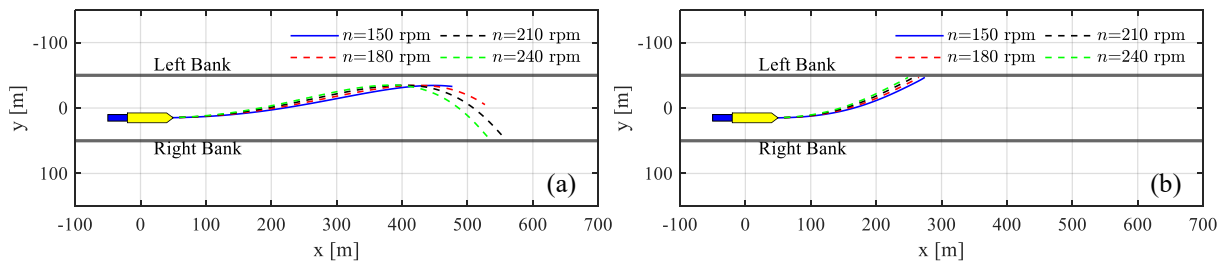


Figure 4.11. Ship trajectories showing bank effects at varying propeller speeds ( $y_s = 35$  m): (a)  $H/T = 19.3$  and (b)  $H/T = 1.5$ .

### 4.2.3 Course-keeping control simulation

Considering the presence of bank effects, safe navigation on inland waterways requires ensuring that the rudder can generate sufficient steering force and moment. This is particularly critical in

highly confined channels, where effective rudder control is essential for course-keeping and counteracting disturbances. Rudder control simulations were performed for two typical operational scenarios: (a) correcting the heading to maintain mid-channel navigation and (b) sailing along one side of the banks. Figure 4.12 presents the vessel trajectories for mid-channel navigation under river currents in different directions.

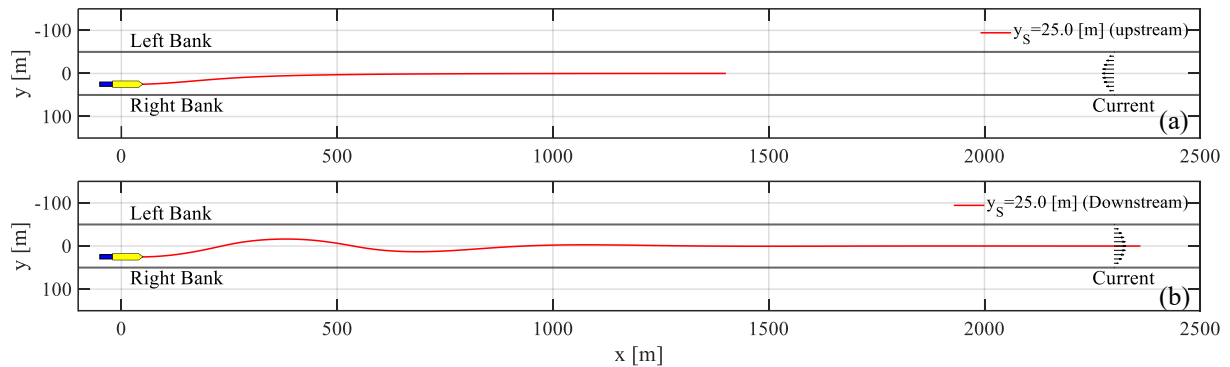


Figure 4.12. Ship trajectories for mid-channel course-keeping.

The trajectories indicate that when facing a downstream current, the vessel experienced reduced rudder inflow speed, requiring more time to realign with the target course. Since inland vessels typically reduce speed in confined waterways to mitigate risks from squat and grounding, the additional reduction in relative inflow speed caused by downstream currents further diminishes rudder effectiveness.

In the second navigation scenario, operating near the bank increases bank-induced forces and moments, making rudder control more challenging. As shown in Figure 4.13, the downstream case illustrates that the original twin-propeller twin-rudder (TPTR) configuration lacks sufficient steering capacity to counter the intensified hydrodynamic effects from the bank, and the rudder struggles to achieve stable convergence.

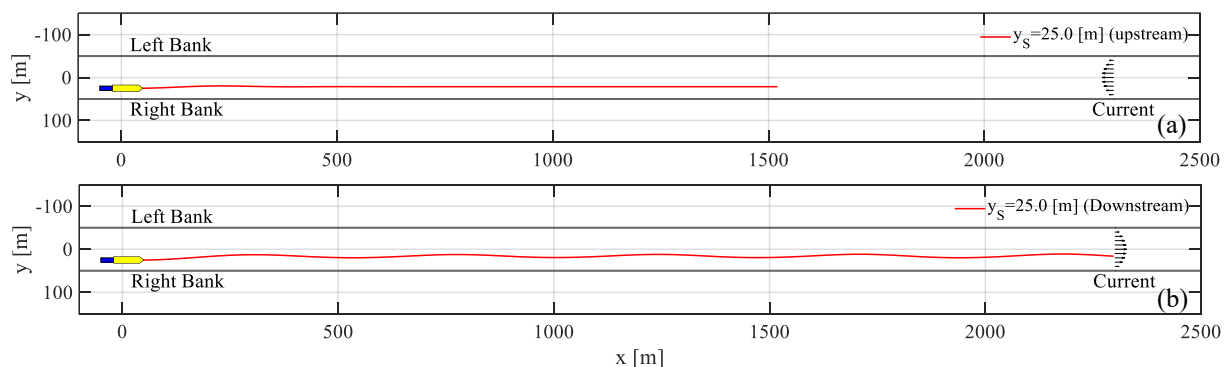


Figure 4.13. Vessel trajectories when sailing along the bank with the twin-propeller twin-rudder (TPTR) configuration.

A further analysis was conducted by upgrading the steering system from the TPTR setup to a twin-propeller quad-rudder (TPQR) arrangement, a four-propeller configuration commonly used in modern European inland vessels. As shown in Figure 4.14, the additional rudders successfully resolve the control issue, even at reduced propeller speeds during downstream operations.

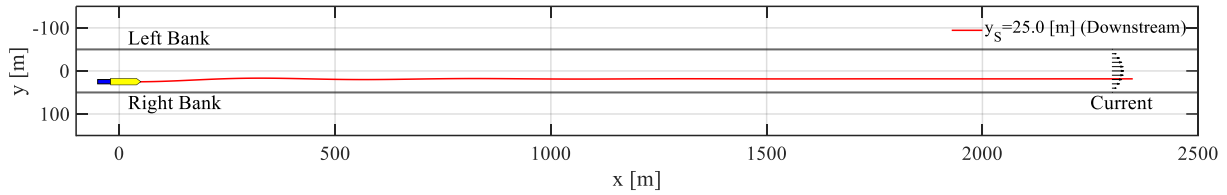


Figure 4.14. Vessel trajectory using twin-propeller quad-rudder configuration.

### 4.3 Paper III – Control design with PID

Paper III presents the control design process for inland vessels in more complex scenarios. Based on the modified MMG model from Paper II, the main contribution of control system development is to improve tracking performance in confined waterways, accounting for disturbances from shallow water, bank effects, and currents, as summarised in section 3.4. The effectiveness of the control design was evaluated under various inland waterway scenarios, including river confluences and bends. The results demonstrated that the proposed control strategy effectively mitigates hydrodynamic effects from confined waterways on ship handling and compensates for current disturbances, enabling reliable course-keeping performance for the targeted class of inland vessels.

#### 4.3.1 Operation near banks

IWVs often need to sail close to one side of a river or canal bank to allow safe passage for oncoming or overtaking vessels, particularly in narrow fairways. In such cases, the reduced ship–bank distance generates hydrodynamic interactions that can affect vessel handling. Effective rudder control is therefore essential to counter these effects and maintain the intended course. The first simulation scenario evaluates the control design during near-bank operations. With the propulsion speed fixed at 150 rpm, the vessel’s speed over ground  $U_{SOG}$  varies depending on its location along the river bend and the current direction, as shown in Figure 4.15.

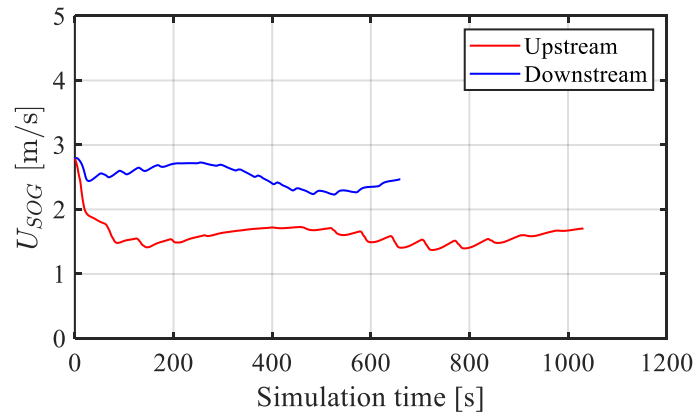


Figure 4.15. Time histories of  $U_{SOG}$  for near-bank operations.

Figure 4.16 shows the trajectories for different current directions. When sailing near a bank, the vessel experienced a pronounced bow-out moment and required a longer distance to follow the predefined path, especially in downstream conditions, as shown in Figure 4.16(b).

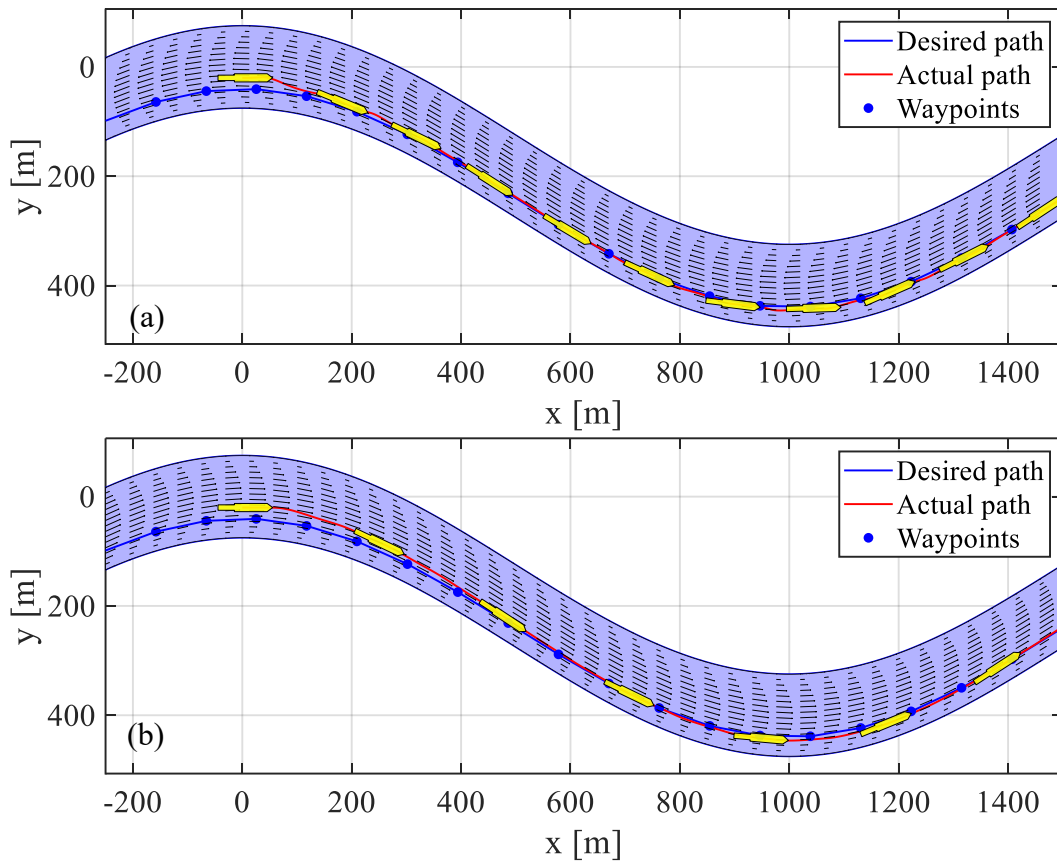


Figure 4.16. IWV trajectories while sailing along the right bank at a ship–bank distance of 35 m: (a) upstream current; (b) downstream current.

Once the target course was reached, the proposed controller effectively maintained the desired course under the two current conditions. Figure 4.17 shows the time histories of the side force acting on the vessel, indicating that the rudder control effectively counteracted forces arising from drift and bank effects.

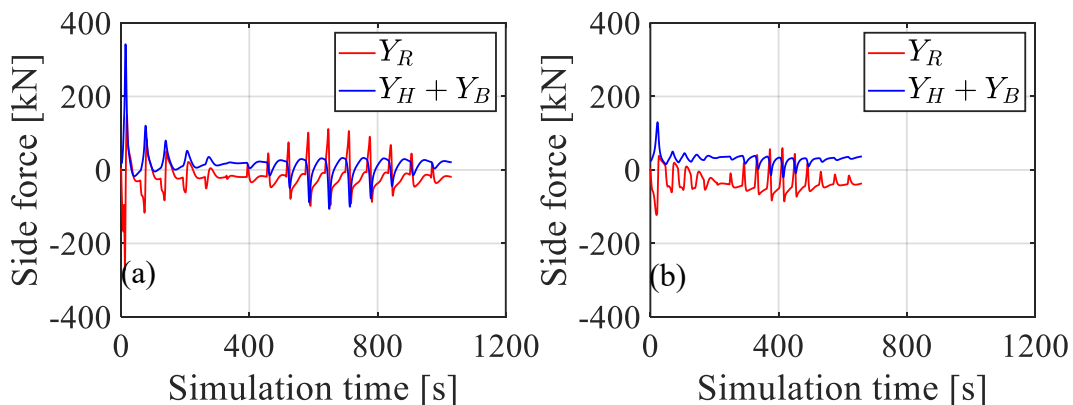


Figure 4.17. Time histories of side force acting on the vessel:  
(a) upstream current; (b) downstream current.

As shown in Figure 4.18, the results indicate that the designed PID rudder controller is generally effective in correcting the vessel’s heading and reducing XTE, particularly in river bends. It is evident that, compared with upstream conditions, downstream operation results in a larger XTE due to reduced rudder effectiveness caused by the lower inflow speed to the rudder.

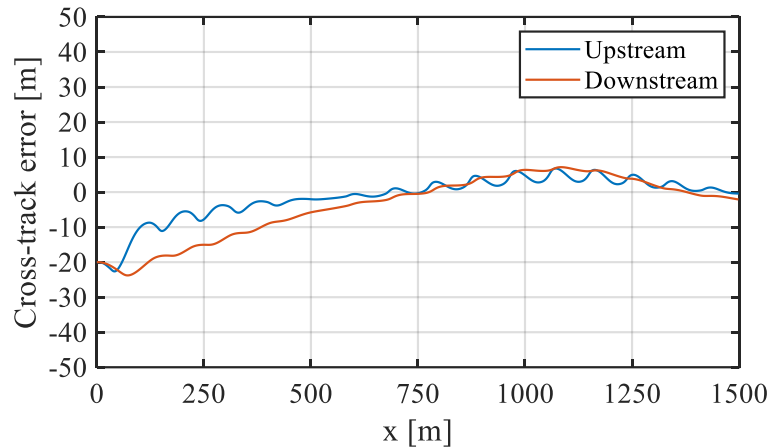


Figure 4.18. Cross-track error for near-bank operations.

### 4.3.1 Operation at the waterway confluence

In inland waterway transport, a confluence where two rivers meet serves as a key junction for traffic flow. This poses unique control challenges for vessels due to complex currents and, more importantly, the requirement for sharp turns with high-rate heading changes in limited manoeuvring space.

For the second operation scenario, a waterway confluence was constructed to test the effectiveness of the control design for path-following with sharp turns. The vessel's engine speed was reduced from 150 rpm to 100 rpm, considering the vessel's inherent response lag during turning manoeuvres. To execute a sharp turn effectively, the vessel must begin manoeuvring well in advance. Selecting a suitable turn radius is vital for navigational safety, taking into account environmental influences such as current and potential unforeseen events. Internal vessel parameters, including maximum rudder angle, dimensions, and speed also critically determine the feasible turn radius and advance distances. In this case, an advanced distance equal to 2.5 times the vessel's length was applied, based on turning test results in Paper II.

As shown in Figure 4.19, the IWV demonstrated effective trajectory tracking under different current directions, indicating that the controller can reliably adjust the vessel's heading to follow the desired path. Under upstream conditions, the current aids the vessel's turning manoeuvres, thereby reducing tracking errors. In contrast, downstream navigation presents more challenging rudder control, as the vessel is accelerated by the current, resulting in greater tracking errors. The reduced steering force during downstream operation further contributes to the pronounced course deviations.

These findings highlight the inherent limitations of the state-based PID controller in complex manoeuvring environments, where strong current–vessel interactions can substantially affect course-keeping performance. Downstream conditions, in particular, exacerbate these challenges by increasing drift and reducing rudder effectiveness. Additionally, higher vessel speeds shorten the response time available to the controller within confined manoeuvring spaces.

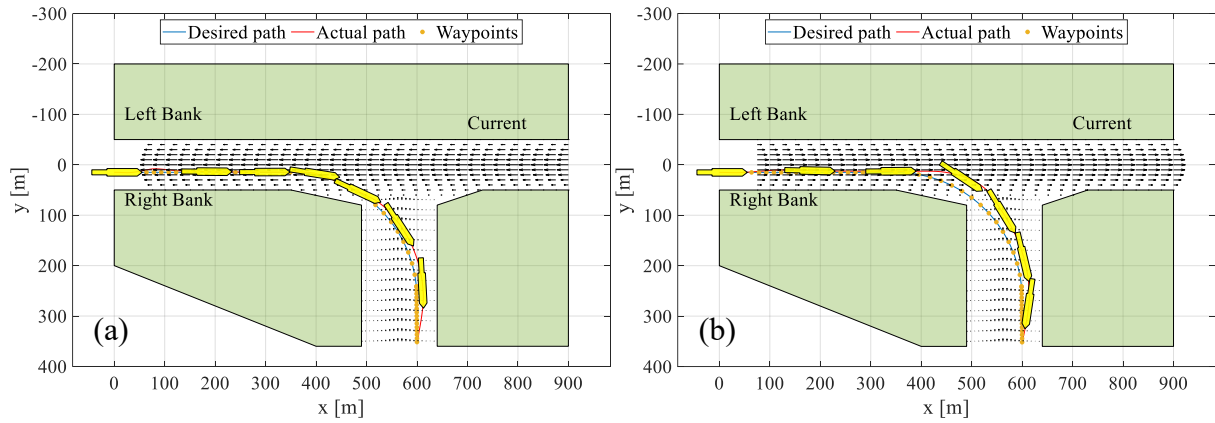


Figure 4.19. Turning result: (a) upstream current; (b) downstream current (Zhang et al., 2024a).

To address these issues, future control designs should adopt more sophisticated approaches, such as advanced MPC, which enables proactive rudder adjustments based on predicted vessel states at future time steps. By accounting for the combined effects of currents, vessel dynamics, and environmental disturbances, MPC has the potential to improve tracking performance and minimise course deviations in complex waterways, as explored further in Paper IV.

#### 4.4 Paper IV – Improved path-following with NMPC

Following the research presented in Papers II and III, Paper IV introduces an improved model-based control design. Building on the limitations of classical PID control identified previously, this study enhances control performance by incorporating advanced NMPC, aiming to minimise both course offset and control efforts. The main architecture of NMPC is summarised in subsection 3.4.4. The control design was tested under various inland water conditions, including straight channels, waterway intersections, and river meanders. Compared with conventional PID controllers, the proposed NMPC approach significantly reduces course deviations and cross-track errors across varying water depths and ship–bank distances, while also minimising rudder actuation. In addition, performance indicators tailored to IWV control are introduced to support systematic evaluation. The results confirm that NMPC effectively accounts for hydrodynamic disturbances, improving navigation stability and safety in confined waterways.

##### 4.4.1 Path following control in straight channels

The straight channel was configured with a width of  $W_C = 100$  m and a rectangular cross-section, maintaining a constant water depth of  $H/T = 1.2$  to represent an extreme shallow-water condition that could challenge steering. The current profile followed a near-parabolic distribution across the canal, with maximum velocity at the waterway centreline ( $U_{CMAX} = 0.5$  m/s). The vessel was required to maintain a constant lateral distance from the bank ( $y_S = 25$  m), a typical operational scenario in confined canals to allow safe passage for approaching or overtaking traffic. In this setting, the NMPC heading controller must counteract disturbances arising from combined hydrodynamic effects, including shallow water influence, bank effect, and currents, to track and maintain the desired course with minimal error and control effort.

Figure 4.20 shows path-following results for PID and NMPC under currents. Under upstream conditions (Figure 4.20a), both controllers followed the reference course closely. By contrast,

under downstream conditions (Figure 4.20b), heading control remained effective, but a slight course offset was observed due to reduced rudder inflow speed, resulting in lower steering force. The effect of currents is further quantified using cross-track error (Figure 4.21).

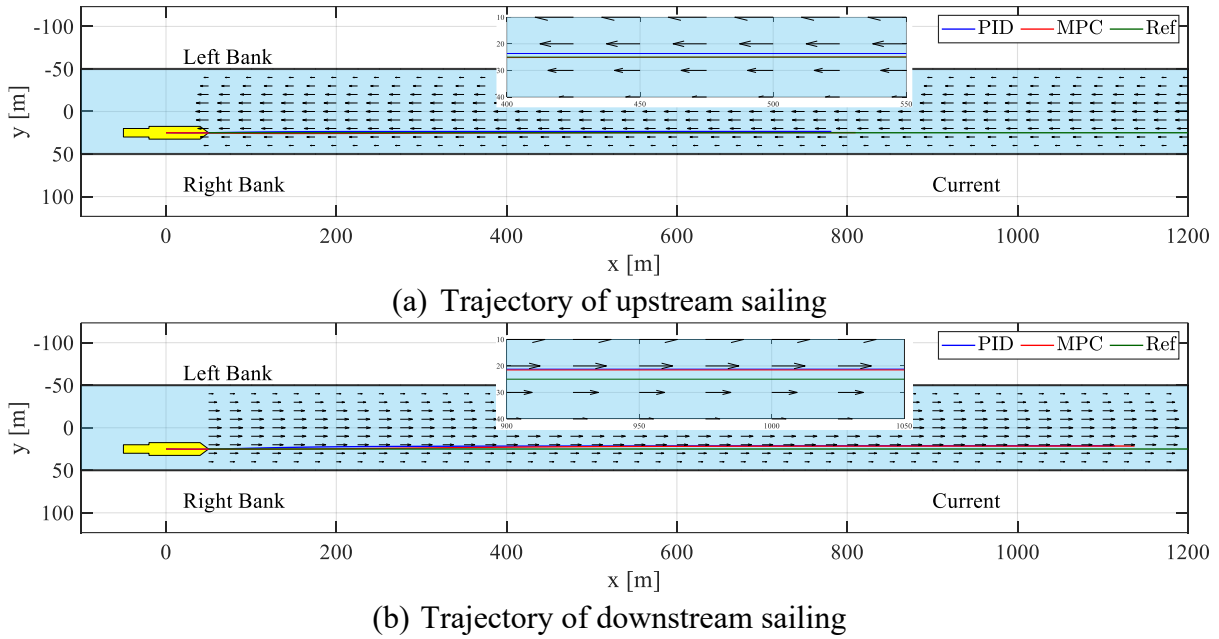


Figure 4.20. Vessel trajectories under heading control for varying current directions.

Under upstream currents, NMPC yields markedly lower tracking error and faster convergence than classical PID. Under downstream conditions, where reduced rudder inflow limits steering capability, NMPC effectively suppresses bank-induced drift and improves convergence. Overall, NMPC outperforms the standard PID method, and this scenario highlights a particularly challenging condition, where the vessel is under-actuated at very low RPM, especially under current-induced disturbances.

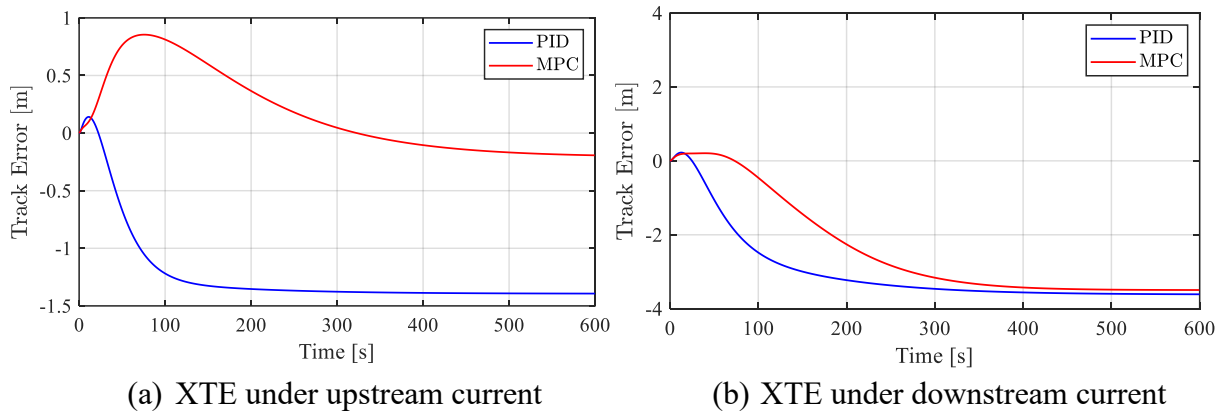


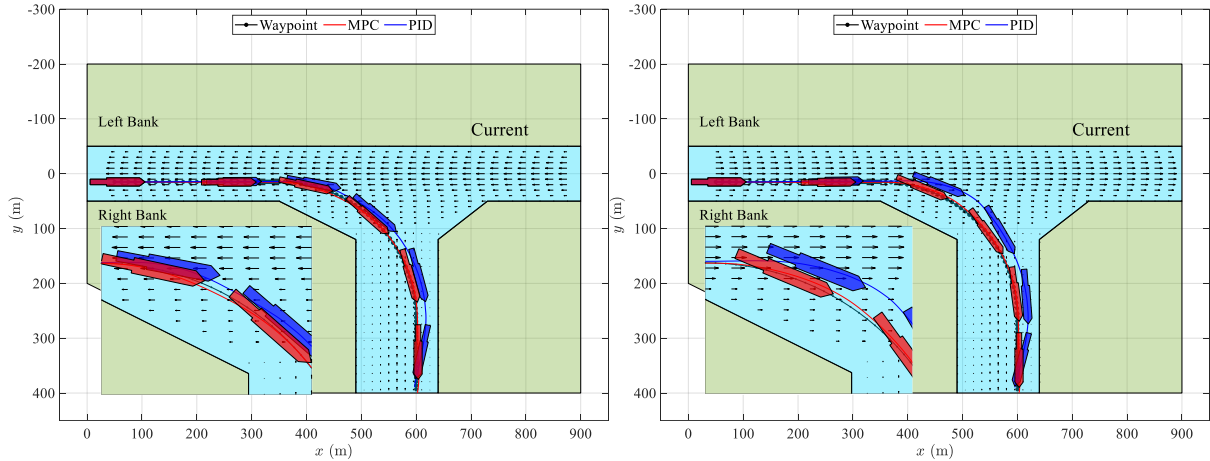
Figure 4.21. Cross-track error (XTE) for varying current directions.

#### 4.4.2 Path-following control in a waterway confluence

The second test condition represents a more operational scenario: path-following for sharp turns at waterway confluences. In this section, a T-junction waterway was configured to evaluate controller tracking performance. The main channel has a higher current speed ( $U_{CMAX} = 0.5$  m/s), and the tributary has a lower current speed ( $U_{CMAX} = 0.1$  m/s). It should be noted that

detailed confluence-flow phenomena (e.g. vortices) are neglected here, as they are beyond the scope and would require CFD simulations with accurate turbulence models.

Figure 4.22 showcases the comparison results of the two controllers. From the zoomed-in views, NMPC demonstrated markedly improved path-tracking performance. Even under downstream currents, the predictive control method can anticipate the vessel's future state and adjust the rudder in advance (see Figure 4.22b). By contrast, PID controllers exhibit significantly larger course deviations. As shown in Figure 4.23, NMPC effectively reduces the XTE under both current directions.



(a) Trajectory under upstream current

(b) Trajectory under downstream current

Figure 4.22. Comparison of trajectories at a waterway confluence under consistent shallow water conditions ( $H/T = 1.2$ ). The vessel maintains a constant propulsion speed of 100 rpm.

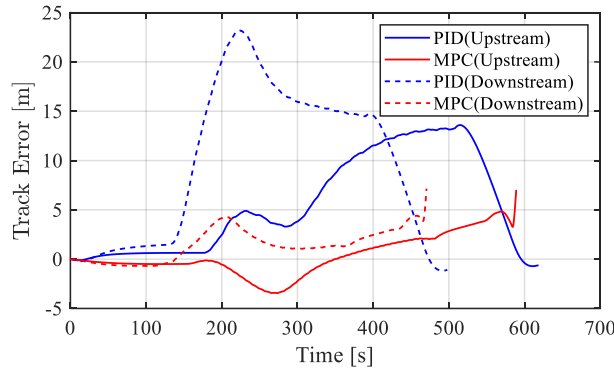


Figure 4.23. Cross-track error for path-following control at the waterway confluence.

In addition to the tracking error, the effectiveness of the two controllers was further evaluated using another key performance indicator: control effort. Figure 4.24 shows the time histories of rudder executions, where NMPC clearly outperforms PID with minimal rudder deflections along the track. By penalising control effort in the objective function, MPC produces consistently smooth rudder angles. Only a brief peak of larger deflection appears near the tributary's bank entry, where the controller must counteract newly encountered hydrodynamic disturbances to keep the vessel on course. This comparison highlights MPC's potential to minimise frequent steering adjustments, which is critical for energy conservation and maintaining the stability of autonomous systems, particularly as future inland vessels may be fully electrified.

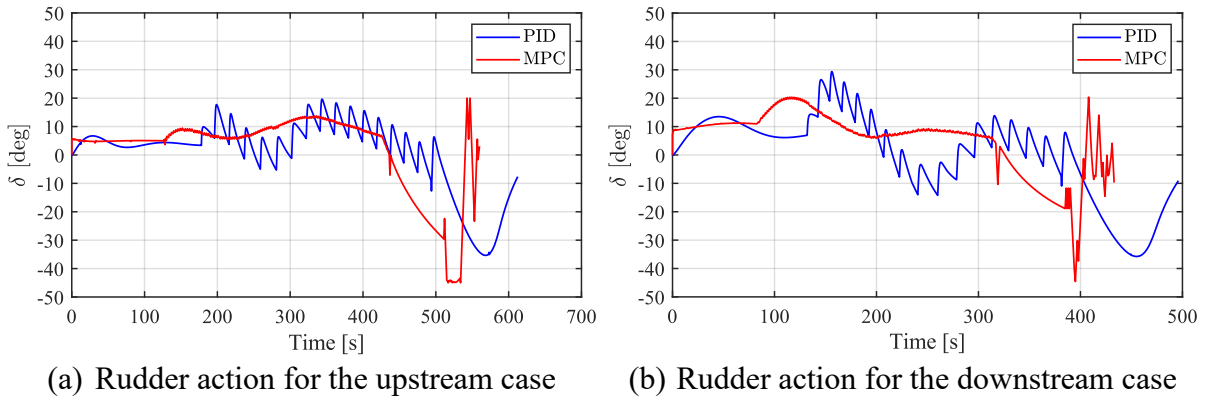


Figure 4.24. Rudder effort from model predictive control and proportional–integral–derivative controllers.

#### 4.4.3 Path following control in river bends

The third control simulation scenario involves sailing along river bends. In the previous study (Paper III), the curved channel had a rectangular cross-section. To better reflect natural inland waterways, trapezoidal cross-sections with uniform side slopes were introduced in this study. Three bank-slope configurations were evaluated, with the top width fixed at 150 m and the bottom width varying from 120 to 80 m. The maximum water depth was set to  $H/T = 1.5$  (medium shallow water) and decreased towards both banks. The detailed waterway and the corresponding cross-sectional geometry are shown in Figure 4.25.

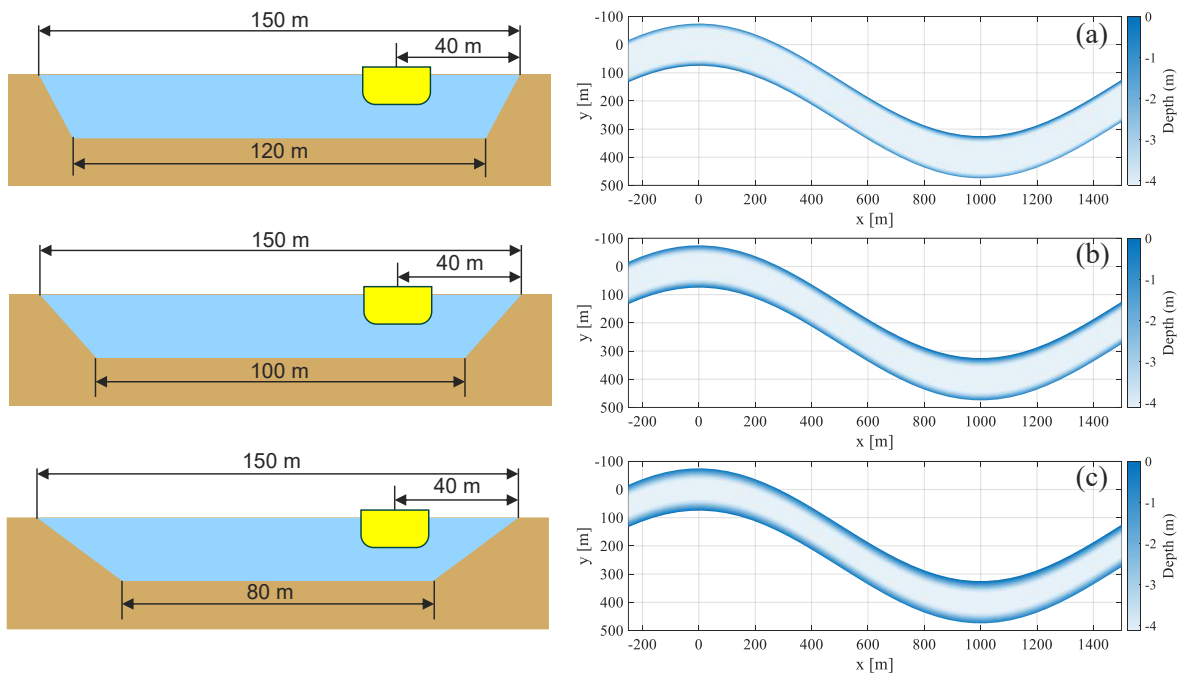


Figure 4.25. Waterways with varying cross-sectional shapes.

The vessel was required to maintain a constant distance from the bank,  $y_s = 40$  m. Reducing the bottom width increases waterway confinement and amplifies the bank effect on the hull.

Figure 4.26 shows the vessel trajectories in the channel with a relatively wider bottom. The PID controller exhibited noticeable deviations, particularly at the beginning of the simulation. Once

aligned with the track, it converged and achieved good tracking performance. In contrast, the MPC trajectory experienced a similar bow-out motion, but proactive rudder control rapidly mitigated the course deviation, as indicated by the red line.

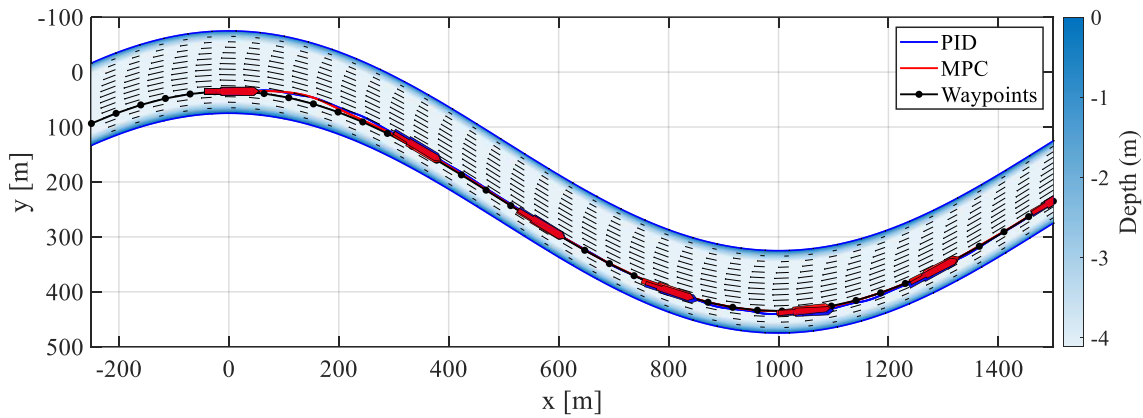


Figure 4.26. Vessel trajectories in river bends with a bottom width of  $W_{CB} = 120$  m.

As the waterway became more constrained, the channel wall generated stronger bank-induced hydrodynamic forces and moments, which affected PID tracking performance and resulted in increased cross-track error and heading deviations, as shown in Figure 4.27 and Figure 4.28.

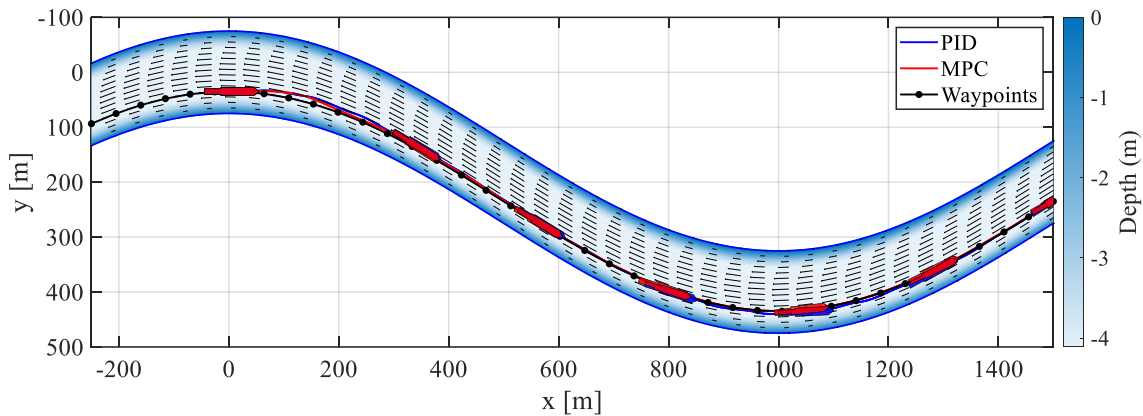


Figure 4.27. Vessel trajectories in river bends with a bottom width of  $W_{CB} = 100$  m.

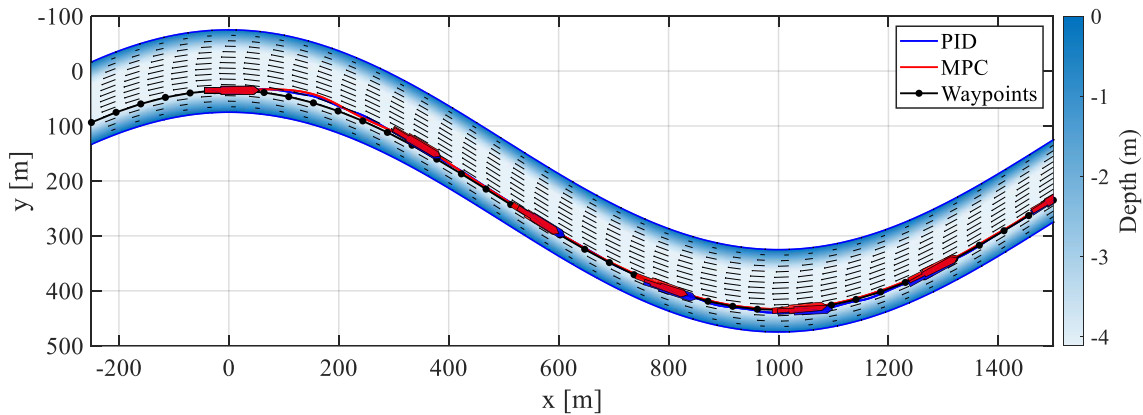


Figure 4.28. Vessel trajectories in river bends with a bottom width of  $W_{CB} = 80$  m.

It can be seen from the trajectories that compared with the classical PID, the MPC demonstrates more stable tracking performance. The quantitative assessment of cross-track error is presented in Figure 4.29, where MPC demonstrates superior performance with lower XTE. The narrower channel bottom amplifies bank effects, leading to increased tracking errors at the start; however, the heading control eventually limits deviations to a promising range (below 5 m) in all cases. By contrast, the PID controller maintains a steady cross-track error at the second bend that is nearly twice the MPC value, resulting in more frequent steering corrections and a higher risk of losing course stability.

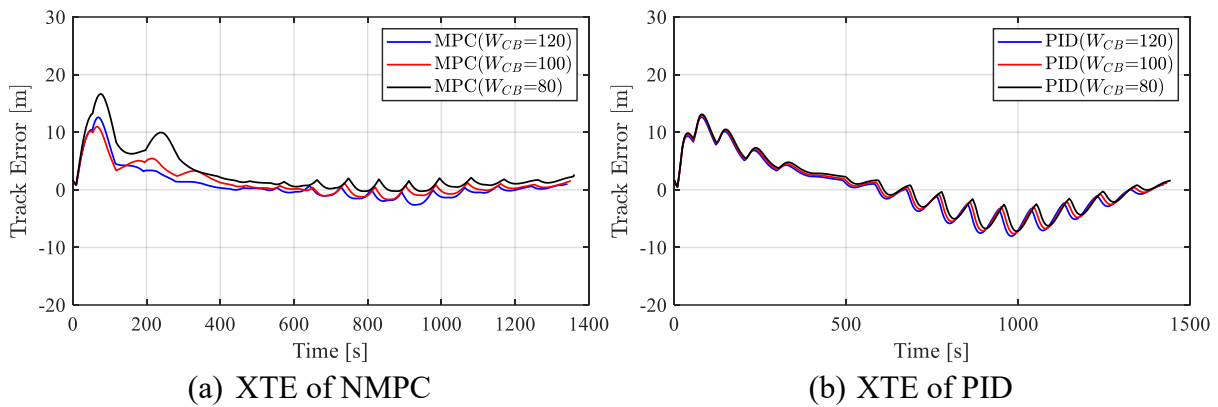


Figure 4.29. Cross-track error for model predictive control and proportional–integral–derivative controllers in river bends of varying bottom width.

Moreover, a static obstacle was added to the fairway to simulate the presence of infrastructure, such as bridge piers or terminals, and its effect on control performance. The obstacle measured 30 m in length and 15 m in width and was positioned at coordinates (1,000, 435), as shown in Figure 4.30.

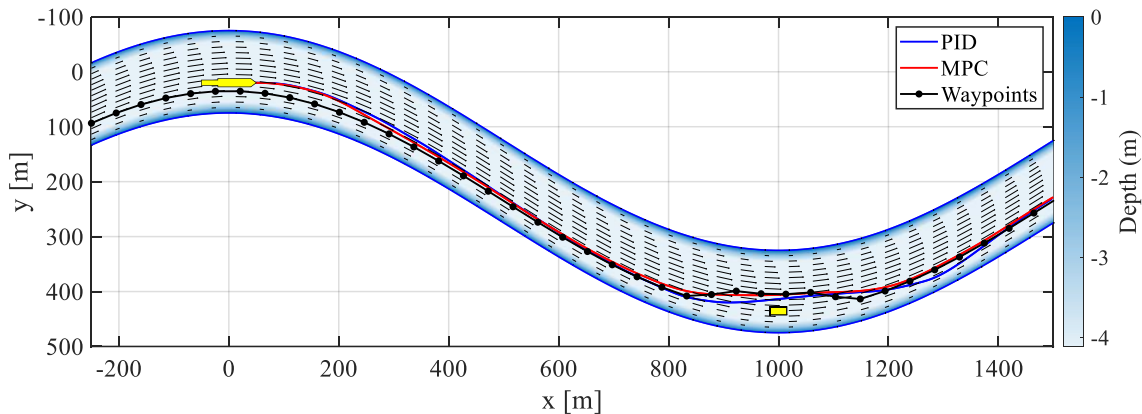


Figure 4.30. Control simulation in a river bend with a static obstacle ( $x = 1,000$  m).

It can be concluded that NMPC performs excellently in handling sharp changes in the desired route by utilising the model predictive approach. The vessel’s future motion and dynamics are well captured, providing guidance for control implementation. The key improvement is that this proactive control approach accounts for the vessel’s turning behaviour and compensates for reaction distances in advance, which is crucial for enhancing the operational safety of autonomous vessels in confined waterways.

## 4.5 Paper V – VPF development and operational analysis

Serving as the concluding part of this doctoral research project, Paper V builds on and integrates the models and methods proposed in the previous papers. To enhance shipping automation and optimise energy use, this study proposes a novel, holistic VPF tailored for inland waterway vessels, supporting both quantitative energy performance assessment and operational analysis. The VPF incorporates features such as ship energy system modelling, manoeuvring modelling, control implementation, and dynamic energy prediction, dedicated to systematic performance evaluation of autonomous inland vessels. To generate a simulation environment that captures the physical characteristics of natural rivers, a new hydraulic model was developed for the rapid and accurate representation of water currents and bathymetrical variations in meandering inland waterways, as presented in section 3.5.

To demonstrate the capabilities of the VPF, several case studies were carried out under varying operational modes, showcasing its effectiveness in robust path-following control, dynamic energy prediction, and fuel consumption optimisation. The PSO method with water depth-awareness parameter initialisation was used to optimise the fuel cost, as presented in section 3.6. In near-bank shallow water regions, the simulations show that up to 5.7% fuel savings can be achieved through speed optimisation. The results highlight that the proposed VPF can serve as a digital platform for evaluating new vessel designs and retrofitting strategies, thereby enhancing ship automation and energy efficiency in inland transport.

### 4.5.1 Model validation

The validation study was conducted in two parts: (a) energy performance model validation using full-scale trial data, and (b) hydraulic model validation using actual bathymetric measurements.

#### Energy performance model

Following the methodology outlined in Zhang et al. (2023), validation of the power prediction and fuel consumption components of the energy performance model was carried out using trial data from two inland vessels. Trials were conducted along the Yichang–Zhijiang section of the Yangtze River in China, where the average water depth was approximately 7 m. The main dimensions of the two vessels are summarised in Table 4.1.

Table 4.1. Dimensions and propulsion system of the two inland chemical tankers.

	Vessel 1	Vessel 2
Length overall [m]	99.60	105.04
Beam [m]	16.20	16.20
Draught [m]	4.40	4.80
Displacement [t]	3,000	5,000
Speed (100% MCR) [kn]	12.05	11.04
Propeller diameter [m]	2.5	2.7
Number of propellers [-]	2	2
Engine power [kW]	2 x 662	2 x 648
Engine speed [rpm]	900	900

Vessel 1 is a 3,000 DWT chemical tanker, whereas Vessel 2 is a larger 5,000 DWT vessel. Both vessels are equipped with similar diesel engines rated at a maximum speed of 900 rpm. Main engine power and fuel consumption were recorded while engine load increased from 50% to full power. Fuel consumption measurements were taken at 50%, 75%, 90%, and 100% load, with each reported rate representing the average of these measurements.

The fuel consumption rate predicted by the model was validated against measurements from three trials, as shown in Figure 4.31. The energy performance model agrees well with the measurements, particularly under the 90% engine load condition. Positive values indicate overestimation, whereas negative values indicate underestimation by the model. Across all loading conditions, the mean absolute error of the fuel consumption prediction for the two vessels is approximately 8.5%. Considering that the model was developed entirely using empirical and analytical methods with limited input data, this overall prediction demonstrates promising accuracy, with errors below 10%. Based on these results, it can be concluded that the energy performance model provides reliable estimates of the vessel’s fuel consumption.

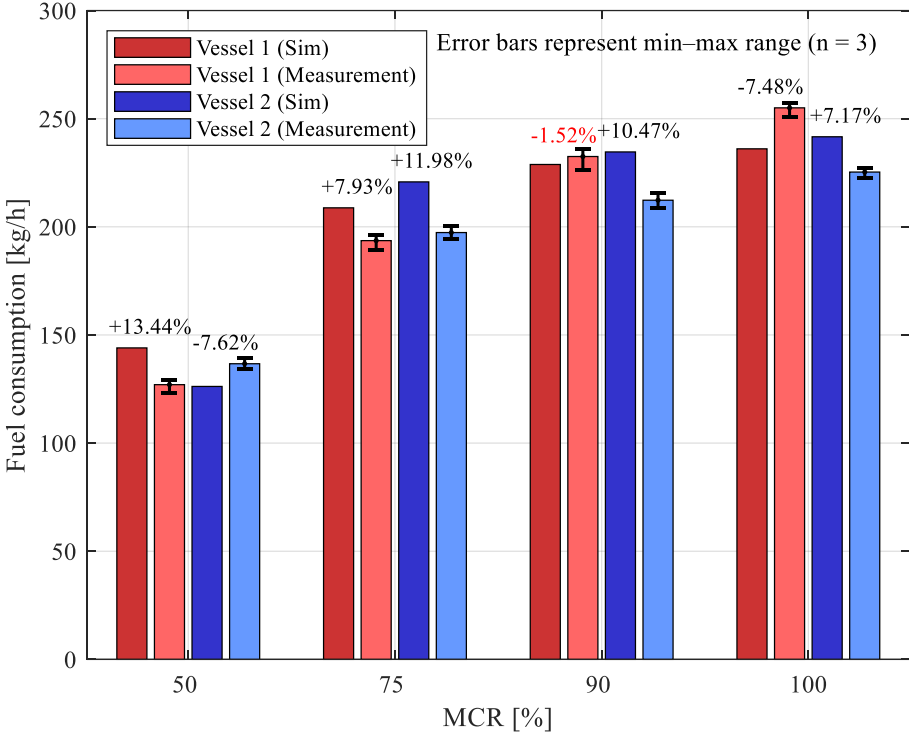


Figure 4.31. Validation of fuel consumption predictions.

**Hydraulics modelling**

To ensure the proposed hydrological formula accurately captures cross-sectional variations in river meanders, the hydraulics model was validated against field measurements from the Wabash–Embarras River confluence in the United States (Parsons et al., 2013), as shown in Figure 4.32.

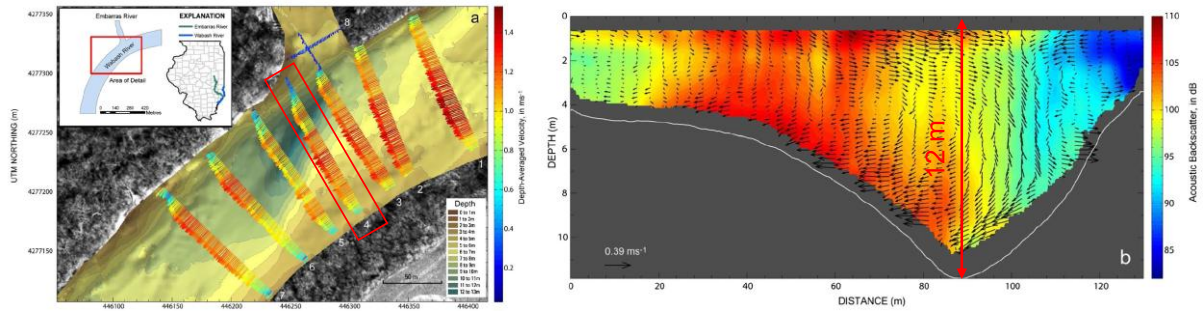


Figure 4.32. Field measurements of the Wabash–Embarras River confluence.

Taking Cross-section 4 as the reference for predicting the maximum bathymetric shift, the comparison between the hydraulic model and the measurements is presented in Figure 4.33. The selected cross-section lies approximately at the midpoint of the river bend, where the depth profile shows a pronounced shift towards the outer bank. Accordingly, the skewness factor in Eq. (7) is set to 1. The remaining parameters are the maximum cross-sectional depth,  $H_{MAX} = 12$  m, and the channel width  $2b$ , which is approximately 140 m. The results indicate that the proposed equation effectively captures the trend of cross-sectional shifting, with the predicted location of maximum depth closely matching the measurements. Deviations, particularly along the inner (left) bank, reflect the difficulty of accurately modelling riverbed slope deformation, which is governed by complex hydrodynamic and sediment transport processes and is thus beyond the scope of the current model. As shown in Figure 4.33, a distance of 20 m from the riverbank was already considered close for vessel navigation; within this operational range, the model reproduces the bathymetric profile with reasonable accuracy.

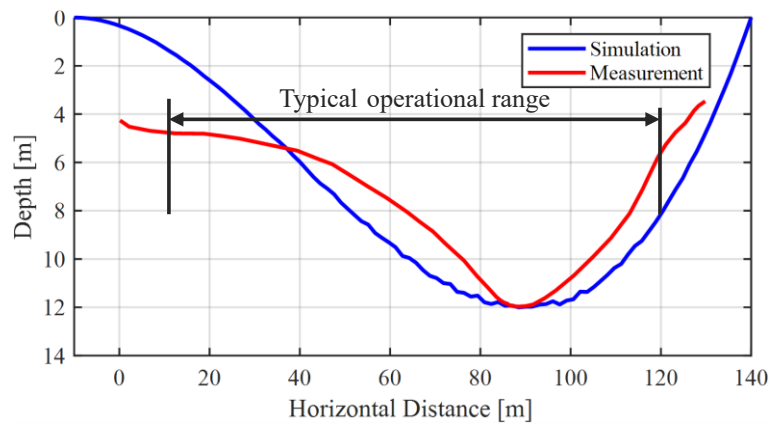


Figure 4.33. Validation of the hydraulic model using field measurements at Cross-section 4.

#### 4.5.2 Operational analysis

Operational simulations were conducted in various scenarios, including river-centre operations, path-following near infrastructure, and near-bank navigation. Vessel performance was systematically evaluated in terms of safety and energy efficiency. Vessel A, at 70% loading (2,100 DWT), was used as the reference to represent shallow water conditions. Its hydrodynamic derivatives were selected from an inland vessel of similar length and displacement (Koh & Yasukawa, 2012). The first operational case considered river-centre navigation, with a 10-km-

long river generated using the proposed hydraulic model. Although the model-based method achieved good tracking performance, computational efficiency is critical, particularly for long-duration sailings in complex environments. Based on the control designs in Papers III and IV, the classical PID was improved in an incremental form. Figure 4.34 shows the simulation results comparing the incremental PID with the conventional PID. The vessel maintained a fixed propeller speed of 250 rpm to follow the desired course against the current. The results indicate that the incremental PID improves tracking accuracy, as highlighted in the zoomed-in figure. The corresponding XTE is quantified in Figure 4.35, showing that the incremental PID effectively suppresses course offset, particularly in this meandering river with complex bathymetry and currents. These findings support using this controller for path-following simulations in other scenarios.

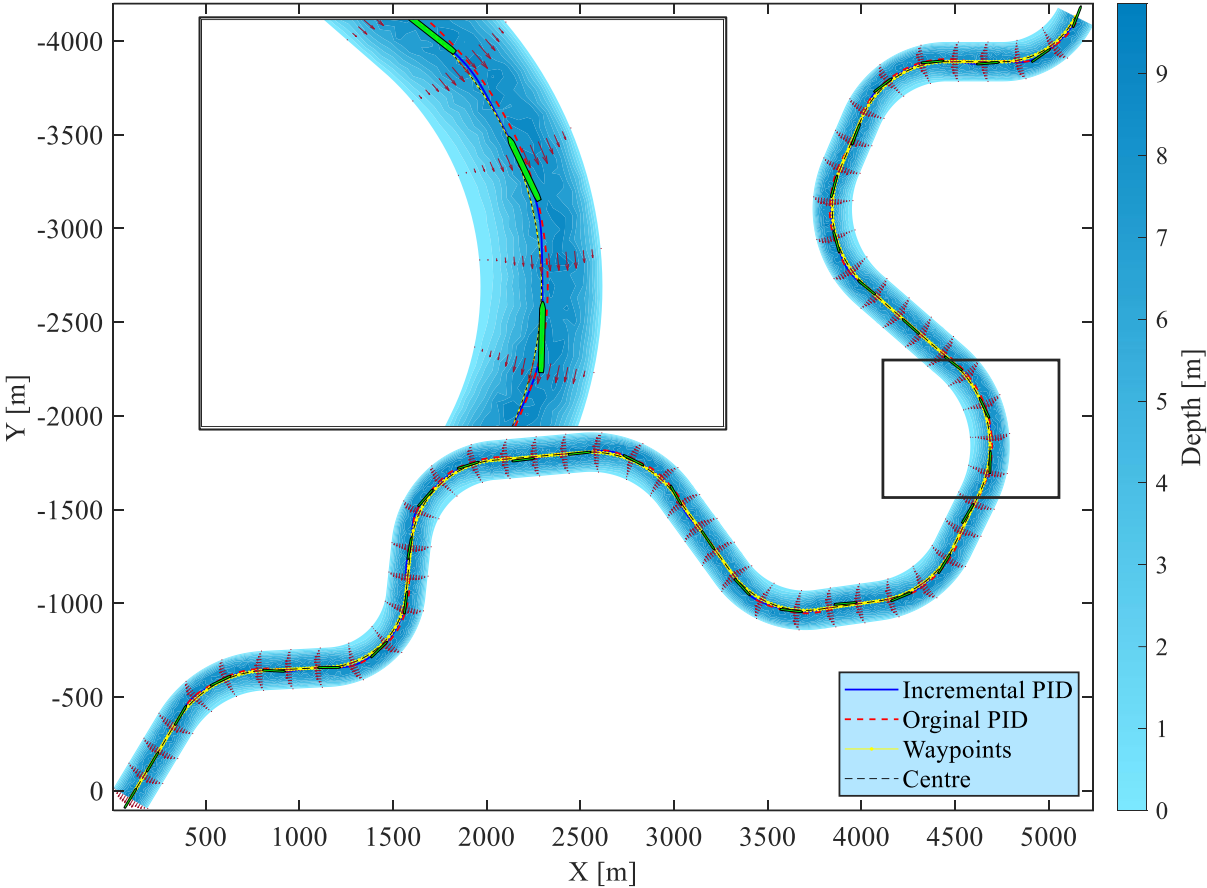


Figure 4.34. Vessel trajectories during river-centre operation.

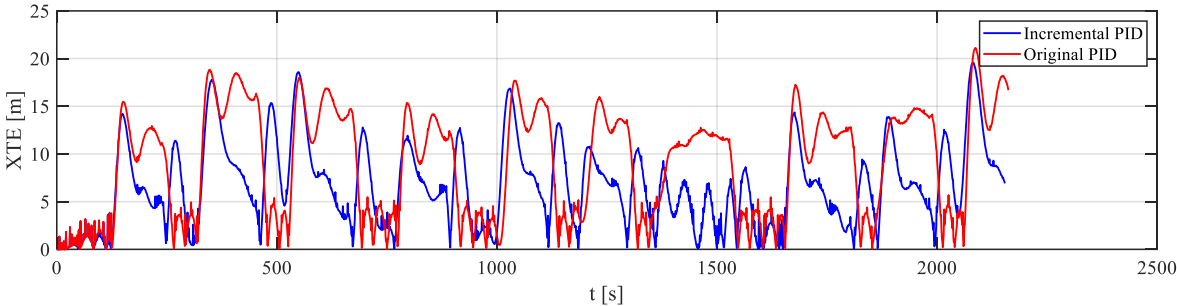


Figure 4.35. Cross-track error comparison for river-centre operation.

The second simulation case study evaluated vessel performance near built structures, such as bridge piers and river locks. To ensure safe passage through the bridge and successful stopping at the lock chamber, a speed reduction scheme was proposed as follows:

$$n = \begin{cases} 0.5n_{max}, & S_d \ll 2L(\text{pass bridge}) \\ -0.5n_{max}, & S_d \ll 3L(\text{stop at lock}) \end{cases}$$

Thus, the propeller rpm must be reduced to 50% when the distance between the vessel and the bridge is less than twice the ship’s length. Similarly, the propeller must rotate astern to bring the vessel to a stop at the lock within a defined distance. Figure 4.36 shows the control simulation in a waterway with a bridge and a lock. The bridge length is 210 m, equal to the channel width, with a 30 m span between each pier. The results indicate successful tracking, with the speed reduction effectively ensuring safe passage through the bridge (see the zoomed-in figure).

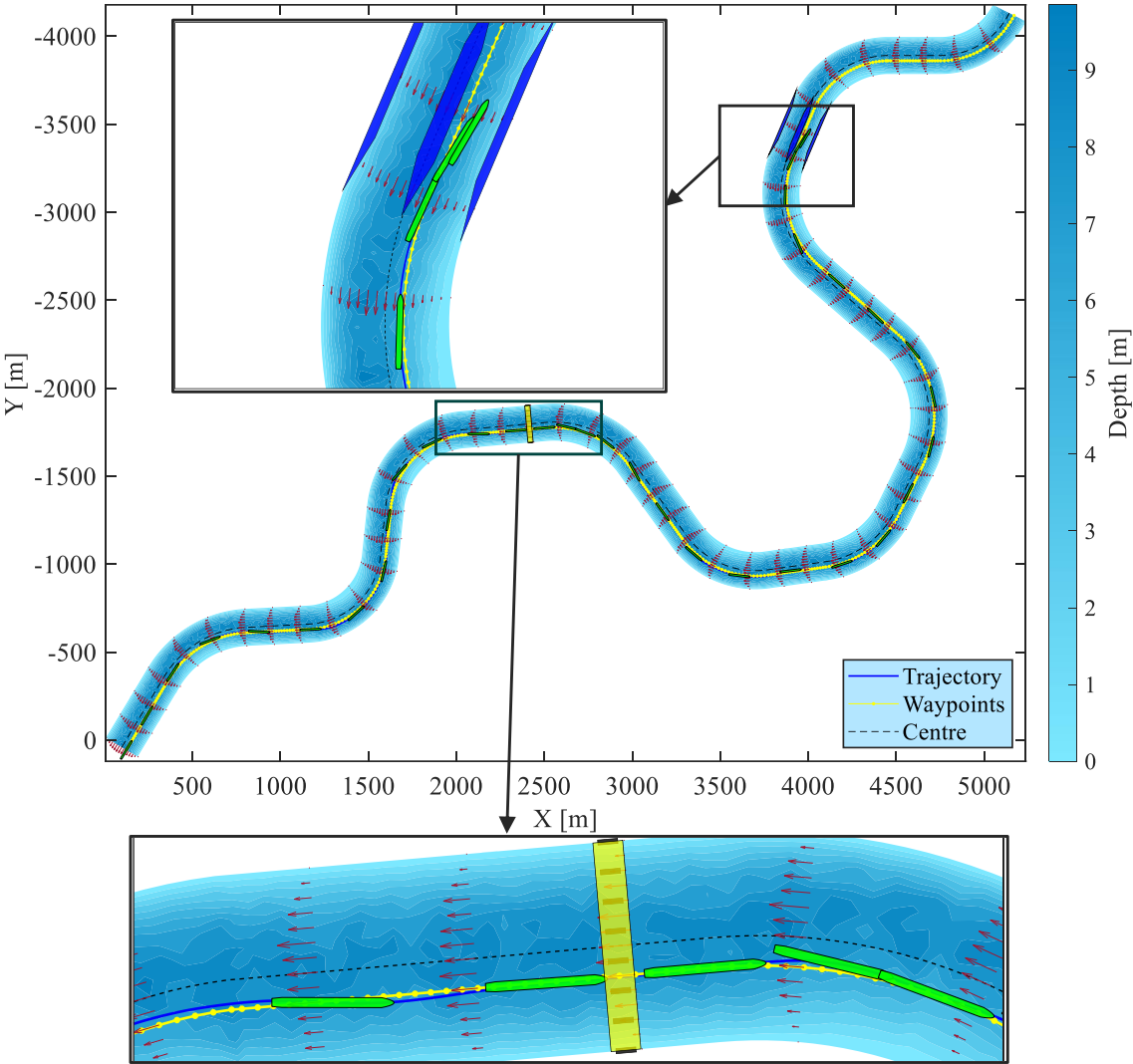


Figure 4.36. Control simulation of bridge passage and lock stop in a waterway.

As the vessel approached the lock, the propeller was reversed to stop within the lock chamber, as shown in the top bounding box. Once the speed drops below a defined threshold, rudder control becomes ineffective due to insufficient inflow, and the reversing propeller decelerates the vessel. At this stage, the objective shifts from course-keeping to achieving a complete stop,

meaning that path-following control was deactivated, which explains the course deviations at the end. This is further illustrated in Figure 4.37, where the speed and rudder histories show a clear speed reduction when approaching the bridge and lock, and a zero-rudder angle indicates heading control was deactivated at this period.

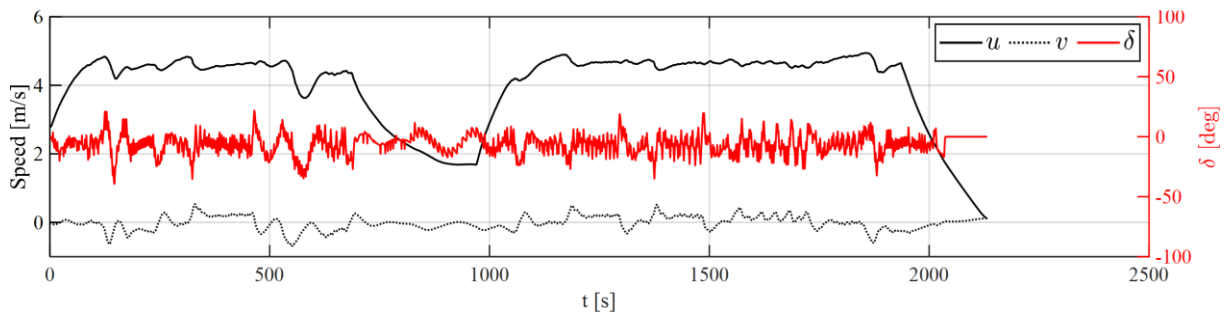


Figure 4.37. Time histories of vessel speed and rudder actions.

Lastly, the third operational case involved near-bank operations. Under this condition, the vessel is subject to more pronounced shallow water and bank effects due to the closer ship–bank distance. Figure 4.38 shows the vessel’s trajectory along a predefined course in a 15-km-long waterway, maintaining a constant 30 m ship–bank distance, corresponding to a nondimensional value of  $y'_B = 0.214$ . Overall, the vessel successfully followed the target course despite these complex disturbances. However, as it approached the inner bank in confined water, course deviations were observed in the zoomed-in figures. This highlights the impact of shallow water on vessel handling during near-bank operations and emphasises the need to account for these physical effects and disturbances in the design of onboard autonomous systems.

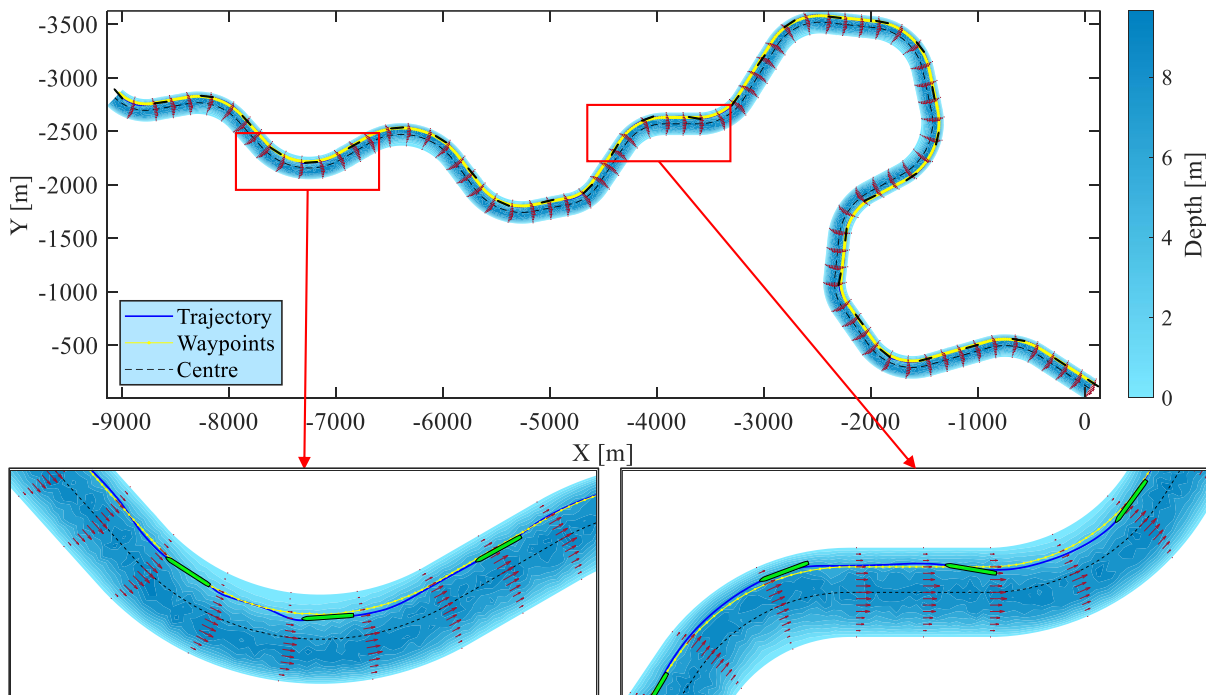


Figure 4.38. Vessel trajectory during near-bank operations.

In addition to affecting manoeuvrability, shallow water regions can also increase energy demand. Table 4.2 presents the total fuel consumption under varying ship–bank distances. The results show that current has the most significant impact on total fuel consumption, as it directly

affects sailing time. In addition, near-bank operations lead to a noticeable increase in fuel use.

Table 4.2. Fuel consumption under various ship–bank distances.

$y'_B$ [-]	Current direction [-]	Distance travelled [km]	Sailing time [min]	Maximum XTE [m]	Fuel consumption [kg]
0.214	Upstream	14.573	52.4	17.40	200.8
	Downstream	14.594	42.7	27.20	164.8
0.285	Upstream	14.574	51.7	17.17	193.5
	Downstream	14.638	42.6	24.55	162.9
0.428	Upstream	14.590	51.8	16.26	189.6
	Downstream	14.626	40.0	20.05	149.7

### 4.5.3 Energy optimisation

To enhance the energy efficiency of future autonomous vessels, this study proposed an optimisation approach to minimise fuel consumption, particularly for shallow-water near-bank operations. Based on the PSO configurations in Section 3.6, fuel optimisation in a 10-km-long waterway is presented in Figure 4.39.

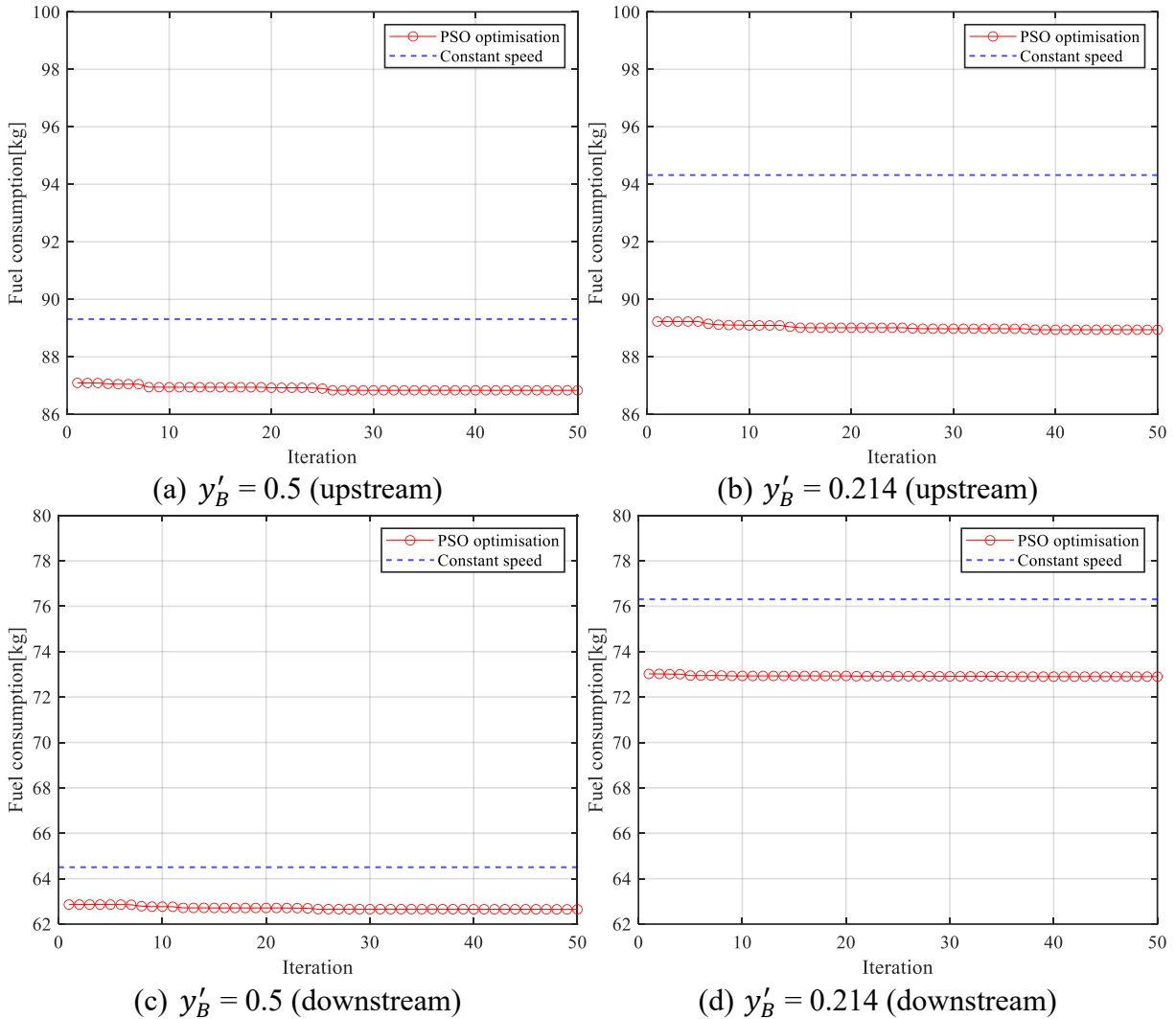


Figure 4.39. Optimisation results for varying ship–bank distances under currents.

The result indicates that operations at a fixed speed in shallow water can lead to significantly higher fuel consumption compared with sailing in deeper water near the river centre. Therefore, the optimisation algorithm has greater potential to reduce fuel consumption through speed adjustment, as shown in Figure 4.39(c) and (d).

Quantitative fuel optimisation results are summarised in Table 4.3. The PSO achieved a promising 5.8% fuel reduction in the shallow-water region while strictly following the time constraints (ETA) to ensure efficiency. The vessel experienced minor shallow-water effects in deeper water, yet an average of 2.8% fuel savings was still achieved through proper speed optimisation. The proposed energy optimisation methods have the potential to benefit future autonomous inland vessels, especially those employing fully electrified propulsion systems (Guarnieri et al., 2024; Liu et al., 2024), by lowering bunkering frequency and enhancing operational duration.

Table 4.3. Summary of particle swarm optimisation under varying ship–bank distance conditions.

$y'_B$ [-]	Operational mode [-]	Current [-]	ETA [min]	FC [kg]	Fuel savings [%]
0.5	Fix speed	Upstream	32.31	89.29	-
	PSO optimisation	Upstream	32.30	86.81	2.77
0.214	Fix speed	Upstream	30.37	94.33	-
	PSO optimisation	Upstream	30.36	88.87	5.78
0.5	Fix speed	Downstream	23.33	64.50	-
	PSO optimisation	Downstream	23.33	62.65	2.86
0.214	Fix speed	Downstream	24.42	76.30	-
	PSO optimisation	Downstream	24.42	72.89	4.47



## 5 Conclusions

This thesis presents the development of a novel, integrated voyage planning framework capable of simulating and evaluating the operational performance of arbitrary inland vessels. The framework enables comprehensive analysis of energy consumption arising from ship motion, control, and hull–waterway interactions, explicitly accounting for both hydrodynamic and hydraulic effects. The main contributions include the development of a new ship energy performance prediction model, a tailored manoeuvring model for confined waterways, systematic control design, a novel hydraulic model for bathymetry, and dynamic energy consumption analysis with optimisation schematics. This thesis emphasises the importance of accounting for disturbances from confined waters to ensure navigational safety (route feasibility) and energy efficiency. The results of this thesis provide a digital testbed that can be further extended to support the evaluation of new vessel designs and retrofitting strategies, with the aim of enhancing automation and promoting sustainable inland waterway transport. The main contributions are categorised and summarised below.

### **Ship energy performance modelling for inland vessels**

A dedicated ship energy performance model, specifically tailored for inland vessels, was developed in this thesis. This purely empirical model provides fast and accurate predictions of power and energy consumption in shallow water. The validation study demonstrates that the model predicts power with good accuracy. It was found that the mean absolute error of predicted power is 5.8% for a self-propelled inland cargo vessel and 8.7% for pusher–barge systems, based on publicly available experimental data.

The power and energy consumption calculations were validated using both full-scale numerical data from the literature and actual trial measurements of two inland chemical tankers. The results show that the model achieves promising accuracy, with an overall mean absolute error below 10% based on full-scale measurements. Requiring only limited input parameters, the model demonstrates its suitability for efficient and relatively accurate energy performance evaluations.

### **Manoeuvring modelling in confined water**

To capture ship rigid-body dynamics in shallow and confined water, a modified MMG-based manoeuvring model was proposed in this thesis. The model accounts for the unique features of inland waterways, including shallow-water and bank effects. The turning test validation shows that the model generally matches turning circles reported in the literature at 20° and 35° rudder angles under deep ( $H/T=19.3$ ), shallow ( $H/T=1.5$ ), and extremely shallow water conditions ( $H/T=1.2$ ).

In addition, it was found from the near-bank path-following control simulations that the bank effects have critical impacts on ship course stability, particularly in confined channels. The impact of ship speed was also quantified at varying rpm conditions, and it was shown from the results that the vessel has a significantly higher risk of collision with the bank at increasing speeds if no active rudder control is involved in a confined channel. The water currents can amplify such influences due to the significant differences in the incoming flow speeds of the rudder.

## **Control design: PIDs and MPC**

This thesis includes a comprehensive design of the control systems for effective vessel path-following control in confined waterways. The performances of a conventional PID controller and an advanced NMPC method were compared in this thesis. The results suggest that MPC offers excellent path-following control performances in terms of both accuracy and control effort. Owing to its predictive process, MPC can allocate rudder commands based on future ship motion, which is particularly useful for complex operational scenarios such as path-following through sharp turns or sailing in curved channels. The turning test case under river-interaction conditions shows the NMPC can achieve a remarkably low cross-tracking error within 20% compared with PID results, even though the vessel is underactuated in the downstream current.

Moreover, when the route encounters a sudden change or obstacle, NMPC can detect such changes within its prediction horizon and perform proactive rudder control to compensate for the inherent turning lag during manoeuvring, which is crucial for ensuring safe navigation in confined channels. On the contrary, the PID trajectory shows a longitudinal lag of more than 1.5 times the ship's length with obvious lateral course offsets.

Regarding control effort, it was shown from the results that NMPC produces optimal control outputs, effectively avoiding unnecessary rudder actions. In contrast, position-based PID control requires frequent rudder adjustments to maintain the reference route and heading. However, one significant drawback must be considered: the low computational efficiency of MPC, particularly its nonlinear formulations, which demand substantial computational resources in complex environments. This limitation reduces its applicability for real-time ship operation simulations, making it less suitable for long-distance voyages.

## **Operational analysis and energy optimisation**

By integrating the developed energy performance model, manoeuvring model, and control module, a holistic voyage planning framework was developed for the systematic operational analysis of inland vessels. From the literature presented in Paper V, it can be concluded that the physical environment was usually oversimplified in vessel control simulations in confined water, such as constant water depth, simple cross-sectional geometry. Therefore, a novel hydraulic model was also proposed for waterway generation, bathymetry, and current modelling, providing a physically consistent environment for vessel operation. The model was validated with field measurements from an actual river confluence in the United States. The results show that, for meandering waterways, the model yields accurate predictions of cross-sectional shifts. Consequently, the impact of riverbed morphological changes on vessel performance can be effectively captured through the framework.

Building on insights from the control design in Paper IV, an incremental PID controller was employed for operational analysis, as it provides improved tracking performance while maintaining computational efficiency. A case study demonstrates that, with the same control gain, the incremental formulation effectively reduces tracking error and rudder flapping in curved channels. The average XTE of the incremental PID is only 50% of that of the original format. Case studies further demonstrate the framework's multifunctionality for vessel performance analysis, including safety assessment when operating near infrastructure and energy consumption prediction for near-bank operations. The results suggest that, due to bathymetric changes in meandering waterways, near-bank operations, particularly near the inner bank, significantly

affect course stability and increase energy consumption because of shallow-water and bank effects.

Considering the shallow-water effect on energy efficiency, a PSO-based speed optimisation strategy was proposed. A depth-aware speed initialisation approach was adopted to improve the convergence of the PSO algorithm. It was shown that this parameter initialisation technique enables a promising 5.8% fuel saving in near-bank shallow-water regions and achieves 2.8% fuel saving in deep water regions when the vessel navigates the waterway centre.

A final conclusion from these results showcases that the VPF is a practical and crucial digital testbed for evaluating energy consumption, testing guidance-and-control designs, and comprehensively assessing the operational performance of autonomous inland vessels.



## **6 Future work**

This chapter discusses several key aspects that should be considered in future studies. The simulation framework proposed in this thesis has fulfilled its intended role as a digital testbed for inland vessels. While the framework provides a solid foundation for systematic vessel operational analysis, certain assumptions and simplifications have limited its scope. Addressing these limitations will be essential to broaden its applicability and strengthen its contribution to autonomous and intelligent inland shipping.

### **Extension of engines with comparison of different energy carriers**

This thesis focuses on inland vessels with conventional diesel engines. Future work should enhance the engine module by incorporating other types of energy carriers, such as hybrid engines, electric motors, or fuel cell systems. This enhancement would extend the framework's functionality and applicability, enabling evaluations of the energy efficiency of retrofitting strategies for existing vessels and assessments of newly designed vessels equipped with advanced electrified engines.

To support the decarbonisation of shipping, battery-powered propulsion systems have recently become a highly active research topic. They offer distinct advantages, particularly for short-duration operations, and represent a promising solution for sustainable inland shipping, which will be explored in future research as a continuation of this thesis.

### **Improved manoeuvring modelling**

The manoeuvring model presented in this thesis has limited generalisability because it relies on detailed vessel-specific coefficients, such as hydrodynamic derivatives and propeller open-water data. In addition, the model is only applicable to conventional propeller–rudder configurations. Future studies should develop a more generic manoeuvring model for shallow and confined water, which would involve creating hydrodynamic databases using experimental or CFD-based virtual captive tests across a wide range of hull types and water depths.

Moreover, the manoeuvring model should capture the characteristics of other types of steering systems, such as azimuth thrusters, tunnel thrusters, water jets, or Voith Schneider propellers, to broaden its applicability.

### **Online energy optimisation**

The energy optimisation strategy proposed in this thesis is currently limited to offline applications. More advanced methods, such as reinforcement learning or data-driven MPC, could be employed to enable online energy optimisation – for example, adjusting engine and ship speed in response to interactions between dynamic vessel states and environmental disturbances. For hybrid propulsion systems, operational optimisation could also be conducted using online algorithms to develop effective energy management strategies.

### **Digital twin for inland or coastal waterways**

The simulation framework developed in this thesis could be extended in future studies to form a more integrated digital twin that supports autonomous shipping across a broad range of

applications, including inland waterways, coastal areas, and short-sea navigation. The digital twin should be able to monitor a ship's real-time performance and optimise routes for minimum energy consumption. Achieving this will involve incorporating additional techniques, such as advanced route-planning algorithms (Chen & Mao, 2024; Chen et al., 2025), models that capture ship dynamics under wind and wave, collision-avoidance strategies, and data-driven control algorithms. In addition, future research could extend the framework by coupling it with dynamic ship–ship interaction models and traffic scenarios to analyse multi-vessel encounters in confined waterways. Besides, winter navigation is also an important topic, and the mechanics of ship–ice interactions must be analysed and incorporated into the system design. Furthermore, lightweight digital siblings could complement the full digital twin by providing task-oriented, rapid assessments, enabling rapid evaluation of vessels' operational scenarios without the computational cost of the high-fidelity model.

## References

- Abkowitz, M. A. (1964). *Lectures on ship hydrodynamics--Steering and manoeuvrability* (Report No. 5). H. S. Hydro-and Aerodynamics Laboratory.
- Åström, K. J., & Hägglund, T. (1995). *PID Controllers: Theory, Design, and Tuning*. ISA - The Instrumentation, Systems and Automation Society.
- Aztjushkov, L. (1968). Wall effect correction for shallow water model tests. *Transactions of the North-East Coast Institution of Engineers and Shipbuilders*, 85(2).
- Calleya, J. N. (2014). *Ship design decision support for a carbon dioxide constrained future* [Doctoral dissertation, University College London].
- CCNR. (2025). *CCNR roadmap for reducing inland navigation emissions*. Retrieved 4 December 2025, from <https://www.ccr-zkr.org/12090000-en.html>.
- Ch'Ng, P., Doctors, L., & Renilson, M. (1993). A method of calculating the ship-bank interaction forces and moments in restricted water. *International shipbuilding progress*, 40(421).
- Chen, C., Delefortrie, G., & Lataire, E. (2021a). Effects of water depth and speed on ship motion control from medium deep to very shallow water. *Ocean Engineering*, 231, 109102. <https://doi.org/10.1016/j.oceaneng.2021.109102>
- Chen, C., Verwilligen, J., Mansuy, M., Eloot, K., Lataire, E., & Delefortrie, G. (2021b). Tracking controller for ship manoeuvring in a shallow or confined fairway: Design, comparison and application. *Applied Ocean Research*, 115, 102823. <https://doi.org/10.1016/j.apor.2021.102823>
- Chen, L., Hopman, H., & Negenborn, R. R. (2018). Distributed model predictive control for vessel train formations of cooperative multi-vessel systems. *Transportation Research Part C: Emerging Technologies*, 92, 101-118. <https://doi.org/10.1016/j.trc.2018.04.013>
- Chen, Y., & Mao, W. (2024). An isochrone-based predictive optimization for efficient ship voyage planning and execution. *IEEE Transactions on Intelligent Transportation Systems*, 25(11), 18078-18092. <https://doi.org/10.1109/TITS.2024.3416349>
- Chen, Y., Zhang, C., Guo, Y., Wang, Y., Lang, X., Zhang, M., & Mao, W. (2025). State-of-the-art optimization algorithms in weather routing—ship decision support systems: challenge, taxonomy, and review. *Ocean Engineering*, 331, 121198. <https://doi.org/10.1016/j.oceaneng.2025.121198>
- Christodoulou Raftis, C., Vanelslander, T., & van Hassel, E. (2023). A global analysis of emissions, decarbonization, and alternative fuels in inland navigation—A systematic literature review. *Sustainability*, 15(19), 14173. <https://doi.org/doi.org/10.3390/su151914173>
- Constantine, T. (1960). On the movement of ships in restricted waterways. *Journal of Fluid Mechanics*, 9(2), 247-256. <https://doi.org/10.1017/S0022112060001080>
- Du, P., Ouahsine, A., Sergent, P., Hoarau, Y., & Hu, H. (2021). Investigation on resistance, squat and ship-generated waves of inland convoy passing bridge piers in a confined waterway. *Journal of Marine Science and Engineering*, 9(10), 1125. <https://doi.org/doi.org/10.3390/jmse9101125>
- Du, P., Ouahsine, A., Sergent, P., & Hu, H. (2020). Resistance and wave characterizations of inland vessels in the fully-confined waterway. *Ocean Engineering*, 210, 107580. <https://doi.org/10.1016/j.oceaneng.2020.107580>
- Du, Z., Negenborn, R. R., & Reppa, V. (2022). Multi-objective cooperative control for a ship-towing system in congested water traffic environments. *IEEE Transactions on Intelligent Transportation Systems*, 23(12), 24318-24329. <https://doi.org/10.1109/TITS.2022.3208328>

- Eloot, K., Verwilligen, J., & Vantorre, M. (2008). An overview of squat measurements for container ships in restricted water. Proceedings of International conference on safety and operations in canals and waterways (SOCW 2008), Glasgow, UK.
- Epps, B., Chalfant, J., Kimball, R., Techet, A., Flood, K., & Chryssostomidis, C. (2009). OpenProp: An open-source parametric design and analysis tool for propellers. Proceedings of grand challenges in modeling & simulation conference (GCMS 2009), Istanbul Turkey.
- European Commission. Retrieved 4 December 2025, from [https://climate.ec.europa.eu/eu-action/climate-strategies-targets/2050-long-term-strategy\\_en](https://climate.ec.europa.eu/eu-action/climate-strategies-targets/2050-long-term-strategy_en).
- European Commission. (2015). *2050 long-term strategy*. Retrieved 4 December 2025, from [https://climate.ec.europa.eu/eu-action/climate-strategies-targets/2050-long-term-strategy\\_en](https://climate.ec.europa.eu/eu-action/climate-strategies-targets/2050-long-term-strategy_en).
- European Commission. (2020). *MSCA-ETN-AUTOBarge*. Retrieved 4 December 2025, from <https://etn-autobarge.eu/>.
- European Commission. (2021). *NAIADES III action plan*. Retrieved 4 December 2025, from [https://transport.ec.europa.eu/transport-modes/inland-waterways/promotion-inland-waterway-transport/naiades-iii-action-plan\\_en](https://transport.ec.europa.eu/transport-modes/inland-waterways/promotion-inland-waterway-transport/naiades-iii-action-plan_en).
- European Commission. (2025a). *EU economy greenhouse gas emissions: +3.4% in Q1 2025*. Retrieved 4 December 2025, from <https://ec.europa.eu/eurostat/web/products-eurostat-news/w/ddn-20250814-1>.
- European Commission. (2025b). *Freight transport statistics - modal split*. Retrieved 4 December 2025, from [https://ec.europa.eu/eurostat/statistics-explained/index.php?title=Freight\\_transport\\_statistics\\_-\\_modal\\_split#Modal\\_split\\_of\\_freight\\_transport\\_in\\_the\\_EU](https://ec.europa.eu/eurostat/statistics-explained/index.php?title=Freight_transport_statistics_-_modal_split#Modal_split_of_freight_transport_in_the_EU).
- European Environment Agency. (2023). *Greenhouse gas emissions from transport in the EU (Infographic)*. Retrieved 4 December 2025, from <https://www.eea.europa.eu/en/analysis/maps-and-charts/greenhouse-gas-emissions-from-transport?activeTab=8a280073-bf94-4717-b3e2-1374b57ca99d>.
- Fan, A., Wang, J., He, Y., Perčić, M., Vladimir, N., & Yang, L. (2021). Decarbonising inland ship power system: Alternative solution and assessment method. *Energy*, *226*, 120266. <https://doi.org/10.1016/j.energy.2021.120266>
- Fan, A., Wang, Y., Yang, L., Tu, X., Yang, J., & Shu, Y. (2024). Comprehensive evaluation of machine learning models for predicting ship energy consumption based on onboard sensor data. *Ocean & Coastal Management*, *248*, 106946. <https://doi.org/10.1016/j.ocecoaman.2023.106946>
- Fan, A., Yan, X., Bucknall, R., Yin, Q., Ji, S., Liu, Y., Song, R., & Chen, X. (2020). A novel ship energy efficiency model considering random environmental parameters. *Journal of Marine Engineering & Technology*, *19*(4), 215-228. <https://doi.org/10.1080/20464177.2018.1546644>
- Fossen, T. I. (2011). *Handbook of marine craft hydrodynamics and motion control*. John Wiley & Sons.
- Gritskevich, M. S., Garbaruk, A. V., Schütze, J., & Menter, F. R. (2012). Development of DDES and IDDES formulations for the  $k-\omega$  shear stress transport model. *Flow, turbulence and combustion*, *88*(3), 431-449. <https://doi.org/10.1007/s10494-011-9378-4>
- Guarnieri, M., Bovo, A., Zatta, N., & Trovò, A. (2024). Design, construction and operation of a special electric vessel for water-city utilities service. *Energy*, *309*, 133110. <https://doi.org/10.1016/j.energy.2024.133110>
- Haranen, M., Pakkanen, P., Kariranta, R., & Salo, J. (2016). White, grey and black-box modelling in ship performance evaluation. Proceedings of the 1st Hull performance & insight conference (HullPIC'16), Turin, Italy.

- He, Z., Liu, C., Chu, X., Wu, W., Zheng, M., & Zhang, D. (2024). Dynamic domain-based collision avoidance system for autonomous ships: Real experiments in coastal waters. *Expert Systems with Applications*, 255, 124805. <https://doi.org/10.1016/j.eswa.2024.124805>
- Hidouche, S., Guitteyn, M., Linde, F., & Sergent, P. (2015). Ships propulsion: estimation of specific fuel consumption based on power load factor ratio. Proceedings of Hydrodynamics and simulation applied to inland waterways and port approaches., Meudon, France.
- Hu, Z. H., Jing, Y. X., Hu, Q. Y., Sen, S., Zhou, T. R., & Osman, M. T. (2019). Prediction of Fuel Consumption for Enroute Ship Based on Machine Learning. *Ieee Access*, 7, 119497-119505. <https://doi.org/10.1109/access.2019.2933630>
- Islam, H., Soares, C. G., Liu, J., & Wang, X. (2021). Propulsion power prediction for an inland container vessel in open and restricted channel from model and full-scale simulations. *Ocean Engineering*, 229, 108621. <https://doi.org/10.1016/j.oceaneng.2021.108621>
- Jiang, T. (2001). A new method for resistance and propulsion prediction of ship performance in shallow water. Proceedings of the 8th International Symposium on Practical Design of Ships and Other Floating Structures, Shanghai, China.
- Kaidi, S., Smaoui, H., & Sergent, P. (2018). CFD investigation of mutual interaction between hull, propellers, and rudders for an inland container ship in deep, very deep, shallow, and very shallow waters. *Journal of Waterway, Port, Coastal, and Ocean Engineering*, 144(6), 04018017. [https://doi.org/10.1061/\(ASCE\)WW.1943-5460.0000458](https://doi.org/10.1061/(ASCE)WW.1943-5460.0000458)
- Karagiannidis, P., & Themelis, N. (2021). Data-driven modelling of ship propulsion and the effect of data pre-processing on the prediction of ship fuel consumption and speed loss. *Ocean Engineering*, 222, 108616. <https://doi.org/10.1016/j.oceaneng.2021.108616>
- Kennedy, J., & Eberhart, R. (1995). Particle swarm optimization. Proceedings of International Conference on Neural Networks (ICNN'95), Perth, WA, Australia.
- Kijima, K., & Nakiri, Y. (1990). Prediction method of ship manoeuvrability in deep and shallow waters. Proceedings of International Conference on Marine Simulation and Ship Manoeuvrability 1990 (MARSIM & ICSM 90), Tokyo, Japan.
- Koh, K., & Yasukawa, H. (2012). Comparison study of a pusher-barge system in shallow water, medium shallow water and deep water conditions. *Ocean Engineering*, 46, 9-17. <https://doi.org/10.1016/j.oceaneng.2012.03.002>
- Koh, K. K., Yasukawa, H., & Hirata, N. (2008). Hydrodynamic derivatives investigation of unconventionally arranged pusher-barge systems. *Journal of Marine Science and Technology*, 13(3), 256-268. <https://doi.org/10.1007/s00773-008-0030-5>
- Lackenby, H. (1963). The effect of shallow water on ship speed. *Shipbuilder and Marine Engineer*, 70, 446-450.
- Lang, X., Wu, D., & Mao, W. (2024). Physics-informed machine learning models for ship speed prediction. *Expert Systems with Applications*, 238, 121877. <https://doi.org/10.1016/j.eswa.2023.121877>
- Lataire, E. (2014). *Experiment based mathematical modelling of ship-bank interaction* [Doctoral dissertation, Ghent University].
- Lataire, E., Vantorre, M., & Delefortrie, G. (2012). A prediction method for squat in restricted and unrestricted rectangular fairways. *Ocean Engineering*, 55, 71-80. <https://doi.org/10.1016/j.oceaneng.2012.07.009>
- Lataire, E., Vantorre, M., & Delefortrie, G. (2018). The influence of the ship's speed and distance to an arbitrarily shaped bank on bank effects. *Journal of offshore mechanics and arctic engineering*, 140(2), 021304. <https://doi.org/10.1115/1.4038804>

- Lataire, E., Vantorre, M., & Eloot, K. (2009). Systematic model tests on ship-bank interaction effects. Proceedings of the 3rd International conference on Ship manoeuvring in shallow and confined water: bank effects (MARSIM'09), Ghent, Belgium.
- Launder, B. E., & Sharma, B. I. (1974). Application of the energy-dissipation model of turbulence to the calculation of flow near a spinning disc. *Letters in heat and mass transfer*, 1(2), 131-137.
- Li, Z., Du, P., Ouahsine, A., & Hu, H. (2021). Ship Hydrodynamics of Several Typical Scenes During Inland Waterway Transport. Proceedings of 2021 International Conference on Agriculture Science and Water Resource,
- Linde, F. (2017). *3D modelling of ship resistance in restricted waterways and application to an inland eco-driving prototype* [Doctoral dissertation, Université de Technologie de Compiègne].
- Linde, F., Ouahsine, A., Huybrechts, N., & Sergent, P. (2017). Three-Dimensional Numerical Simulation of Ship Resistance in Restricted Waterways: Effect of Ship Sinkage and Channel Restriction. *Journal of Waterway Port Coastal and Ocean Engineering*, 143(1), Article 06016003. [https://doi.org/10.1061/\(asce\)ww.1943-5460.0000353](https://doi.org/10.1061/(asce)ww.1943-5460.0000353)
- Liu, J., Hekkenberg, R., Quadvlieg, F., Hopman, H., & Zhao, B. (2017). An integrated empirical manoeuvring model for inland vessels. *Ocean Engineering*, 137, 287-308. <https://doi.org/10.1016/j.oceaneng.2017.04.008>
- Liu, J., Hekkenberg, R., Rotteveel, E., & Hopman, H. (2015). Literature review on evaluation and prediction methods of inland vessel manoeuvrability. *Ocean Engineering*, 106, 458-471. <https://doi.org/10.1016/j.oceaneng.2015.07.021>
- Liu, J., Quadvlieg, F., & Hekkenberg, R. (2016). Impacts of the rudder profile on manoeuvring performance of ships. *Ocean Engineering*, 124, 226-240. <https://doi.org/10.1016/j.oceaneng.2016.07.064>
- Liu, S., Wang, Y., Liu, Q., Panchal, S., Zhao, J., Fowler, M., Fraser, R., & Yuan, J. (2024). Thermal equalization design for the battery energy storage system (BESS) of a fully electric ship. *Energy*, 312, 133611. <https://doi.org/10.1016/j.energy.2024.133611>
- Mahipala, D., & Johansen, T. A. (2023). Model predictive control for path following and collision-avoidance of autonomous ships in inland waterways. Proceedings of the 31st Mediterranean Conference on Control and Automation (MED '23), Limassol, Cyprus.
- Menter, F. R. (1992). *Improved two-equation k-omega turbulence models for aerodynamic flows* (NASA-TM-103975). N. A. R. Center.
- Mermiris, D., Vassalos, D., Dodworth, K., Sfakianakis, D., & Mermiris, G. (2011). Dynamic energy modelling – a new approach to energy efficiency and cost-effectiveness in shipping operations. Paper presented at International Conference on Technologies, Operations, Logistics and Modelling for Low Carbon Shipping, Glasgow, Scotland, UK.
- Millward, A. (1989). The effect of water depth on hull form factor. *International shipbuilding progress*, 36(407).
- Mucha, P., el Moctar, O., Dettmann, T., & Tenzer, M. (2017). Inland waterway ship test case for resistance and propulsion prediction in shallow water. *Ship technology research*, 64(2), 106-113. <https://doi.org/10.1080/09377255.2017.1349723>
- Mucha, P., el Moctar, O., Dettmann, T., & Tenzer, M. (2018). An experimental study on the effect of confined water on resistance and propulsion of an inland waterway ship. *Ocean Engineering*, 167, 11-22. <https://doi.org/10.1016/j.oceaneng.2018.08.009>
- Nomoto, K., Taguchi, T., Honda, K., & Hirano, S. (1957). On the steering qualities of ships. *International shipbuilding progress*, 4(35), 354-370.
- Norrbin, N. (1976). Bank effects on a ship moving through a short dredged channel. Proceedings of 10 th Symposium on Naval Hydrodynamics, Cambridge, Massachusetts, US.

- Norrbin, N. (1985). Bank clearance and optimal section shape for ship canals. Proceedings of the 26th PIANC international navigation congress, Brussels, Belgium.
- Odgaard, A. J. (1989). River-meander model. I: Development. *Journal of Hydraulic Engineering*, 115(11), 1433-1450. [https://doi.org/10.1061/\(ASCE\)0733-9429\(1989\)115:11\(1433\)](https://doi.org/10.1061/(ASCE)0733-9429(1989)115:11(1433))
- Ogawa, A., & Kasai, H. (1978). On the mathematical model of manoeuvring motion of ships. *International shipbuilding progress*, 25(292), 306-319. <https://doi.org/https://doi.org/10.3233/ISP-1978-2529202>
- Parkes, A. I., Sobey, A. J., & Hudson, D. A. (2018). Physics-based shaft power prediction for large merchant ships using neural networks. *Ocean Engineering*, 166, 92-104. <https://doi.org/10.1016/j.oceaneng.2018.07.060>
- Parsons, D. R., Jackson, P., Czuba, J. A., Engel, F., Rhoads, B. L., Oberg, K., Best, J. L., Mueller, D., Johnson, K., & Riley, J. (2013). Velocity Mapping Toolbox (VMT): A processing and visualization suite for moving-vessel ADCP measurements. *Earth Surface Processes and Landforms*, 38(11), 1244-1260. <https://doi.org/10.1002/esp.3367>
- Paulig, N., & Okhrin, O. (2024). Robust path following on rivers using bootstrapped reinforcement learning. *Ocean Engineering*, 298, 117207. <https://doi.org/10.1016/j.oceaneng.2024.117207>
- Perera, L. P., & Mo, B. (2017). Machine intelligence based data handling framework for ship energy efficiency. *IEEE Transactions on Vehicular Technology*, 66(10), 8659-8666. <https://doi.org/10.1109/TVT.2017.2701501>
- Pompée, P.-J. (2015). About modelling inland vessels resistance and propulsion and interaction vessel-waterway key parameters driving restricted/shallow water effects. Proceeding of Smart Rivers 2015, Buenos Aires, Argentina.
- Raven, H. (2012). A computational study of shallow-water effects on ship viscous resistance. Proceedings of the 29th Symposium on Naval Hydrodynamics, Gothenburg, Sweden.
- Raven, H. (2016). A new correction procedure for shallow-water effects in ship speed trials. Proceedings of the 13th International Symposium on PRACTical Design of Ships and Other Floating Structures (PRADS'2016), Copenhagen, Denmark.
- Rhoads, B. L. (2020). *River dynamics: Geomorphology to support management*. Cambridge University Press.
- Rotteveel, E., Hekkenberg, R., & van der Ploeg, A. (2017). Inland ship stern optimization in shallow water. *Ocean Engineering*, 141, 555-569. <https://doi.org/10.1016/j.oceaneng.2017.06.028>
- Sano, M., Yasukawa, H., & Hata, H. (2014). Directional stability of a ship in close proximity to channel wall. *Journal of Marine Science and Technology*, 19(4), 376-393. <https://doi.org/10.1007/s00773-014-0271-4>
- Schlichting, O. (1934). Ship resistance in water of limited depth-resistance of sea-going vessels in shallow water. *Jahrbuch der STG*, 35, 127-148.
- Tao, W., Zhu, M., Chen, S., Cheng, X., Wen, Y., Zhang, W., Negenborn, R. R., & Pang, Y. (2022). Coordination and optimization control framework for vessels platooning in inland waterborne transportation system. *IEEE Transactions on Intelligent Transportation Systems*, 24(12), 15667-15686. <https://doi.org/10.1109/TITS.2022.3220000>
- Tillig, F., Ringsberg, J., Mao, W., & Ramne, B. (2017). A generic energy systems model for efficient ship design and operation. *Proceedings of the Institution of Mechanical Engineers, Part M: Journal of Engineering for the Maritime Environment*, 231(2), 649-666. <https://doi.org/10.1177/1475090216680672>

- Vantorre, M., Delefortrie, G., Eloot, K., & Lforce, E. (2003). Experimental investigation of ship-bank interaction forces. Proceedings of International Conference on Marine Simulation and Ship Maneuverability (MARSIM' 03), Kanazawa, Japan.
- Waltz, M., Paulig, N., & Okhrin, O. (2025). 2-level reinforcement learning for ships on inland waterways: Path planning and following. *Expert Systems with Applications*, 274, 126933. <https://doi.org/10.1016/j.eswa.2025.126933>
- Wang, K., Yan, X., Yuan, Y., & Li, F. (2016). Real-time optimization of ship energy efficiency based on the prediction technology of working condition. *Transportation Research Part D: Transport and Environment*, 46, 81-93. <https://doi.org/10.1016/j.trd.2016.03.014>
- Xu, D., Huang, Y., Zhou, X., & Xu, H. (2023). Path following control for large inland ships in a restricted waterway using the nonlinear terminal sliding mode method. *Ocean Engineering*, 284, 115159. <https://doi.org/10.1016/j.oceaneng.2023.115159>
- Yamazaki, D., Ikeshima, D., Sosa, J., Bates, P. D., Allen, G. H., & Pavelsky, T. M. (2019). MERIT Hydro: a high-resolution global hydrography map based on latest topography dataset. *Water Resources Research*, 55(6), 5053-5073. <https://doi.org/10.1029/2019WR024873>
- Yan, X., Wang, K., Yuan, Y., Jiang, X., & Negenborn, R. R. (2018). Energy-efficient shipping: An application of big data analysis for optimizing engine speed of inland ships considering multiple environmental factors. *Ocean Engineering*, 169, 457-468. <https://doi.org/10.1016/j.oceaneng.2018.08.050>
- Yang, B., Kaidi, S., & Lefrançois, E. (2022). Numerical investigation of the parameters that may seriously impact the ship control lability in restricted bending channels. *Ocean Engineering*, 266, 112735. <https://doi.org/10.1016/j.oceaneng.2022.112735>
- Yang, Y., & el Moctar, O. (2024). A mathematical model for ships maneuvering in deep and shallow waters. *Ocean Engineering*, 295, 116927. <https://doi.org/10.1016/j.oceaneng.2024.116927>
- Yang, Y., & el Moctar, O. (2025). A Fourier-based model for dynamic ship–ship interactions during overtaking in deep and shallow waters. *Applied Ocean Research*, 154, 104378. <https://doi.org/10.1016/j.apor.2024.104378>
- Yasukawa, H., & Kobayashi, E. (1995). Shallow water model experiments on ship turning performance. Proceedings of Mini Symposium on Ship Manoeuvrability, Fukuoka, Japan.
- Yasukawa, H., & Yoshimura, Y. (2015). Introduction of MMG standard method for ship maneuvering predictions. *Journal of Marine Science and Technology*, 20, 37-52. <https://doi.org/10.1007/s00773-014-0293-y>
- Yoshimura, Y. (1986). Mathematical model for the manoeuvring ship motion in shallow water. *Journal of the Kansai society of naval architects*(200).
- Yoshimura, Y., & Sakurai, H. (1989). Mathematical model for the manoeuvring ship motion in shallow water (3rd report: manoeuvrability of a twin-propeller Twinrudder ship). *Journal of the Kansai Society of Naval Architects, Japan*, 211, 115-126.
- Yuan, Z., Liu, J., Zhang, Q., Liu, Y., Yuan, Y., & Li, Z. (2021). Prediction and optimisation of fuel consumption for inland ships considering real-time status and environmental factors. *Ocean Engineering*, 221, 108530. <https://doi.org/10.1016/j.oceaneng.2020.108530>
- Zeng, Q. (2019). *A method to improve the prediction of ship resistance in shallow water* [Doctoral dissertation, Delft University of Technology].
- Zeng, Q., Hekkenberg, R., Thill, C., & Hopman, H. (2020). Scale effects on the wave-making resistance of ships sailing in shallow water. *Ocean Engineering*, 212, 107654. <https://doi.org/10.1016/j.oceaneng.2020.107654>

- Zeng, Q., Thill, C., & Hekkenberg, R. (2018). A benchmark test of ship resistance in extremely shallow water. Proceedings of the 4th International Conference on Maritime Technology and Engineering (MARTECH 2018), Lisbon, Portugal.
- Zeng, Q. S., Hekkenberg, R., & Thill, C. (2019). On the viscous resistance of ships sailing in shallow water. *Ocean Engineering*, *190*, 106434. <https://doi.org/10.1016/j.oceaneng.2019.106434>
- Zentari, L., el Mocta, O., Lassen, J., Hallmann, R., & Schellin, T. E. (2022). Experimental and numerical investigation of shallow water effects on resistance and propulsion of coupled pusher-barge convoys. *Applied Ocean Research*, *121*, 103048. <https://doi.org/10.1016/j.apor.2022.103048>
- Zentari, L., Tödter, S., el Moctar, O., Neugebauer, J., & Schellin, T. E. (2023). Experimental and numerical investigation of the gap flow between a pusher and a barge in deep and shallow water. *Applied Ocean Research*, *132*, 103466. <https://doi.org/10.1016/j.apor.2023.103466>
- Zhang, C., Dhyani, A., Ringsberg, J. W., Thies, F., Negenborn, R. R., & Reppa, V. (2025a). Nonlinear model predictive control for path following of autonomous inland vessels in confined waterways. *Ocean Engineering*, *334*, 121592. <https://doi.org/10.1016/j.oceaneng.2025.121592>
- Zhang, C., Dhyani, A., Ringsberg, J. W., Thies, F., Reppa, V., & Negenborn, R. R. (2024a). Manoeuvring modelling and control design of autonomous vessels on inland waterways. Proceedings of the 43rd International Conference on Offshore Mechanics and Arctic Engineering (OMAE 2024), Singapore.
- Zhang, C., Ma, Y., Thies, F., Ringsberg, J. W., & Xing, Y. (2024b). Towards autonomous inland shipping: a manoeuvring model in confined waterways. *Ships and Offshore Structures*, 1-13. <https://doi.org/10.1080/17445302.2024.2358284>
- Zhang, C., Ringsberg, J. W., & Thies, F. (2023). Development of a ship performance model for power estimation of inland waterway vessels. *Ocean Engineering*, *287*, 115731. <https://doi.org/10.1016/j.oceaneng.2023.115731>
- Zhang, C., Vergara, D., Zhang, M., Nikolaos, T., & Mao, W. (2025b). A machine learning method to evaluate head sea induced weather impact on ship fuel consumption. *Energy*, *328*, 136533. <https://doi.org/10.1016/j.energy.2025.136533>
- Zhang, C., Zhang, C., Thies, F., Mao, W., & Ringsberg, J. W. (2025c). A voyage planning framework for energy performance analysis of autonomous inland waterway vessels. *Energy*, 137906. <https://doi.org/10.1016/j.energy.2025.137906>
- Zheng, H., Negenborn, R. R., & Lodewijks, G. (2016). Predictive path following with arrival time awareness for waterborne AGVs. *Transportation Research Part C: Emerging Technologies*, *70*, 214-237. <https://doi.org/10.1016/j.trc.2015.11.004>
- Zheng, Q.-Q., Zhang, Y., Guo, W.-J., Tian, H.-W., & He, L.-J. (2024). Solving energy-efficient lock group co-scheduling problem with ship lift and approach channel using a collaborative adaptive multi-objective algorithm. *Expert Systems with Applications*, *242*, 122712. <https://doi.org/10.1016/j.eswa.2023.122712>
- Ziegler, J. G., & Nichols, N. B. (1942). Optimum settings for automatic controllers. *Transactions of the American society of mechanical engineers*, *64*(8), 759-765.
- Zou, L., & Larsson, L. (2013). Computational fluid dynamics (CFD) prediction of bank effects including verification and validation. *Journal of Marine Science and Technology*, *18*(3), 310-323. <https://doi.org/10.1007/s00773-012-0209-7>